

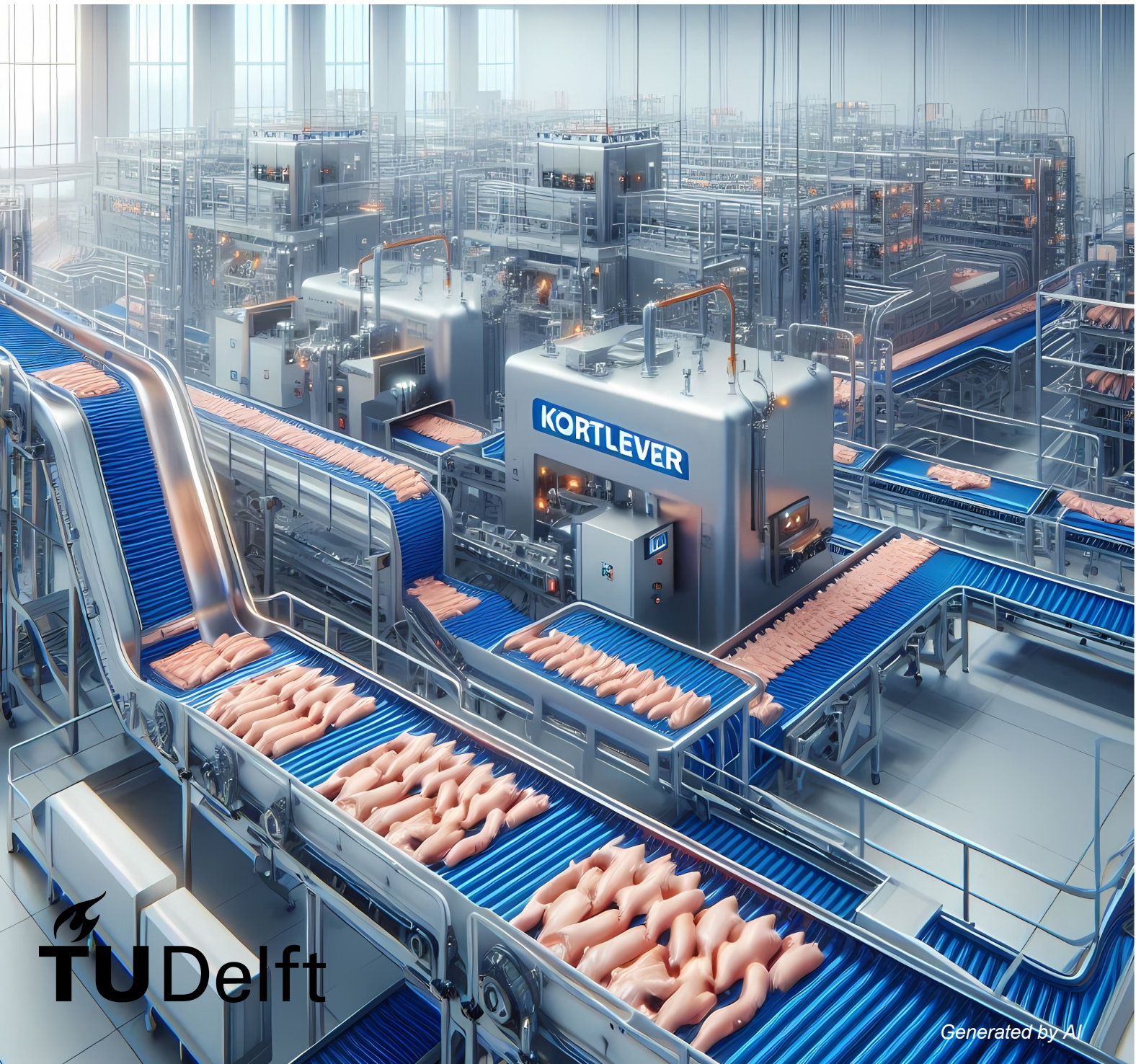
October 10, 2024

# From Bulk to Belt

A simulation driven approach to automating chicken fillet processing

Matthias Vink - 5154499

MASTER THESIS



# From Bulk to Belt

A simulation driven approach to  
automating chicken fillet processing

By

M. Vink

## MASTER THESIS

IN PARTIAL FULFILMENT OF THE REQUIREMENTS FOR THE DEGREE OF

**Master of Science**  
in Mechanical Engineering

at the Department Maritime and Transport Technology of Faculty Mechanical, Maritime and  
Materials Engineering of Delft University of Technology  
to be defended publicly on Thursday, October 17, 2024, at 10:00 AM

**Student number:** 5154499

**MSc track:** Multi-Machine Engineering

**Report number:** 2024.MME.8988

**Supervisor:** Dr. ir. J. Jovanova

**Thesis committee:**

Prof. dr. ir. D.L. Schott, TU Delft committee Chair, Mechanical Engineering

Dr. Y. Wu, TU Delft committee member, Civil Engineering and Geosciences

Ir. W. Kortlever, company Supervisor, Technisch Bureau Kortlever

**Date:** Oktober 17, 2024

An electronic version of this thesis is available at <http://repository.tudelft.nl/>.

It may only be reproduced literally and as a whole. For commercial purposes only with written authorization of Delft University of Technology. Requests for consult are only taken into consideration under the condition that the applicant denies all legal rights on liabilities concerning the contents of the advice.

# Abstract

The escalating global demand for poultry products, coupled with the challenges of securing personnel for the often arduous tasks in poultry processing plants, has underscored the urgent need for automation in this sector. The inherent variability and delicate nature of poultry products, like chicken fillets, pose significant hurdles for traditional automation solutions. This research seeks to address this challenge by employing simulation-aided design to develop an automated solution for singulating and orienting chicken fillets. The study investigates existing technologies in poultry and other food industries and develops a practice-oriented Discrete Element Method (DEM) model to simulate chicken fillet behaviour. The model's efficacy is validated through a series of tests, including damping, bending, sliding, sensitivity analyses and real-life experiments. The insights gained from these simulations inform the design of an automated solution, which is then iteratively refined and visualised in the DEM software. The proposed solution successfully demonstrates the potential of simulation-assisted design to automate complex tasks within the poultry processing industry, paving the way for increased efficiency, productivity, and reduced reliance on manual labour. The research also underscores the importance of considering the unique characteristics of poultry products in developing effective automation solutions, highlighting the need for further exploration into advanced modelling techniques and material and interfacing equipment behaviour analysis.

# Contents

<b>1</b>	<b>Introduction</b>	<b>1</b>
1.1	The State of Automation in the Food Industry . . . . .	1
1.2	Research Gap . . . . .	2
1.3	Case Study . . . . .	3
<b>2</b>	<b>Conceptual Design</b>	<b>5</b>
2.1	Design Methodology . . . . .	5
2.2	Functions and Requirements . . . . .	5
2.3	Concepts . . . . .	6
2.4	Chapter Conclusions . . . . .	9
<b>3</b>	<b>Chicken Fillet Modelling</b>	<b>10</b>
3.1	Current State-of-the-art Modelling of Flexible Objects . . . . .	10
3.2	Discrete Element Method . . . . .	11
3.3	Generating the particle representation of a Fillet . . . . .	11
3.3.1	The Bonded Particle Model . . . . .	13
3.3.2	Model Input Parameters . . . . .	15
3.4	Testing the Models . . . . .	16
3.4.1	Configuration Tests . . . . .	16
3.4.2	Sensitivity Analysis . . . . .	19
3.5	Compression test . . . . .	20
3.6	Chapter Conclusions . . . . .	21
<b>4</b>	<b>Model Simulation Results</b>	<b>22</b>
4.1	Configuration Tests . . . . .	22
4.1.1	Sub-particle selection . . . . .	22
4.1.2	Damping . . . . .	22
4.1.3	Bending . . . . .	23
4.1.4	Sliding . . . . .	24
4.2	Sensitivity Analysis . . . . .	25
4.2.1	Impact Speed Stability . . . . .	25
4.2.2	Angle Stability . . . . .	25
4.2.3	Scaling Stability . . . . .	27
4.3	Compression Test . . . . .	27
4.4	Chapter Conclusions . . . . .	28
<b>5</b>	<b>Concept Evaluation</b>	<b>30</b>
5.1	DEM implementations . . . . .	30
5.2	Evaluations . . . . .	31
5.2.1	Hinged Plates Concept Evaluation . . . . .	32
5.2.2	Mailbox Bulk Concept Evaluation . . . . .	34
5.2.3	Leveller Concept Evaluation . . . . .	35
5.3	Detailing the Design . . . . .	37
5.4	Chapter Conclusions . . . . .	40
<b>6</b>	<b>Validation Experiments</b>	<b>41</b>
6.1	Mailbox Bulk . . . . .	41
6.2	Squeeze Roller . . . . .	44
6.3	Discussion . . . . .	44
6.3.1	Insights Gained in this study . . . . .	45
6.3.2	Limitations of this Study . . . . .	45
<b>7</b>	<b>Conclusions and Recommendations</b>	<b>47</b>
7.1	Conclusions . . . . .	47
7.2	Recommendations . . . . .	48

<b>Bibliography</b>	<b>49</b>
<b>A Scientific paper</b>	<b>52</b>
<b>B Model Parameters</b>	<b>53</b>
B.1 Model Testing Parameters . . . . .	53
<b>C Design of experiments testmatrixes</b>	<b>54</b>
C.1 Stiffness variations . . . . .	54
<b>D Morphological Chart</b>	<b>55</b>
D.1 Existing Technology Filter . . . . .	56
D.2 Simple Solutions Filter . . . . .	57
D.3 Chosen Concepts . . . . .	58

# List of Figures

1.1	The amount of installed robots per industry in the United States [3]. . . . .	1
1.2	The portioning production step with the portion cutter of Marelec [11]. . . . .	3
1.3	Two different but similar fillet orientation processes in two Plukon factories. . . . .	4
2.1	A summary of the design methodology used in this research. . . . .	5
2.2	Some of the existing technology considered in this study. . . . .	6
2.3	The concept sketch of the concept with hinged plates along with a partial 3D implementation. . . . .	7
2.4	The sketch of the concept with a mailbox bulk along with a partial 3D implementation. . . . .	8
2.5	The concept sketch of the concept with a mailbox bulk along with a partial 3D implementation. . . . .	9
3.1	The model representing flexible stems developed by Guan et al. . . . .	10
3.2	A chicken fillet compared with a particle model representation of a chicken fillet. . . . .	12
3.3	Several models of chicken fillet, with meta-particles generated with sub-particle radii ranging from 7-3 mm. . . . .	13
3.4	Preventing undesired bonds from forming. . . . .	14
3.5	The contact radius limit increases Using two different particle types. . . . .	14
3.6	An stl mesh next to its generated meta-particle. . . . .	14
3.7	Some mechanical properties of chicken breast compared to plant-based alternatives [38]. . . . .	15
3.8	The Poisson's ratio of chicken nugget crumb and crust over temperature [39]. . . . .	15
3.9	The maximum friction coefficients of hydrogel tissue on steel for normal hydrogel and hydrogel with DMSO added to it [40], the $\mu_{max}$ value without DMSO, 0.4, was used in this study. . . . .	16
3.10	A 2D schematic of the basic bounce test performed to test damping and the influence of shear stiffness. . . . .	17
3.11	The bend test, comparing the model with a real-life experiment, and the vectors for automatic calculation by the model are also shown. . . . .	18
3.12	The sliding test, comparing the model with a real-life experiment. . . . .	19
3.13	A surface drop test, dropping 90 fillets, 15 of each variant, from a height of 500mm. . . . .	19
3.14	The compression test setup. . . . .	21
4.1	The stability over impact velocities and computational times of the 5 different flexible models of Figure 3.3 . . . . .	22
4.2	The energy graphs of a particle without tangential stiffness (green) and with tangential stiffness (blue). The blue and green lines overlap in the first part of the plot, and thus, only the blue line is visible. . . . .	23
4.3	The time it takes to dampen 90, 95 and 99% of the total energy under different stiffness configurations. . . . .	23
4.4	The stability of the model for different combinations, the stable-unstable boundary is also clearly visible. Darker green means the model is more stable, while red means it is unstable . . . . .	23
4.5	The bend angle of the models for different stiffness combinations. . . . .	24
4.6	The sliding angle of different fillet models, the test was run for all sub-particle sizes mentioned in Figure 3.3, but there were no noticeable differences between the sizes. . . . .	24
4.7	The sliding angles of a dry and wet chicken fillet on a stainless steel surface in real life. . . . .	25
4.8	The stability of the model for different stiffness combinations under different impact velocities. The colours visualise the percentage of intact bonds for that position in the DOE space. The two 3D graphs show the same plot and contain all points for which 50% or more bonds remained intact. . . . .	25
4.9	A visualisation of some of the drop orientations. . . . .	26

4.10	The stability of the model dropped on a floor at two m/s velocity under all possible angles. The thresholds mean that for all the plotted points, less than that percentage of the bonds are still intact. . . . .	26
4.11	Three 2D views of the 75% threshold plot. . . . .	27
4.12	The behaviour of the model when scaling between 0.25x - 10x. . . . .	27
4.13	The stress strain curve resulting from the compression test. . . . .	28
4.14	The force-displacement curves of a chicken fillet tested at different compression speeds. The tests were performed in the same order as the legend. . . . .	28
5.1	The fillet model configuration and the concept configuration influence the concept solution's behaviour. . . . .	30
5.2	The hinged plates concept. . . . .	31
5.3	The mailbox bulk concept. . . . .	31
5.4	The leveller concept. . . . .	32
5.5	Hinged plates, pyramid splitters, and 3-lane belt. . . . .	33
5.6	Bread orienter. . . . .	33
5.7	Scooper. . . . .	33
5.8	Mailbox bulk. . . . .	34
5.9	Shaker and guiding rails. . . . .	34
5.10	Sideflip and multilane belt. . . . .	35
5.11	Universal leveller. . . . .	35
5.12	Speed transitions. . . . .	36
5.13	Flipping plate. . . . .	36
5.14	The eight possible fillet orientations when leaving the guiding rail section. . . . .	37
5.15	The combined concept, the blue components are conveyors. . . . .	37
5.16	The CAD model of the concept. . . . .	38
5.17	The mailbox bulk. . . . .	38
5.18	The universal leveller. . . . .	38
5.19	The takt and aligning section. . . . .	39
5.20	The rejection crate and flipping plates. . . . .	39
5.21	The centring and orienting units. . . . .	40
6.1	The experiment setup. . . . .	41
6.2	The smaller version of the mailbox bulk. . . . .	42
6.3	The mailbox bulk test with chicken fillets. . . . .	42
6.4	The mailbox bulk test with chicken fillets compared to the same setup in the DEM software. . . . .	43
6.5	The squeeze roller assembled on the testing conveyor. . . . .	44
6.6	The squeeze roller interacting with chicken fillets. . . . .	44
D.1	The morphological chart used in the design process. . . . .	55
D.2	All the existing technologies. . . . .	56
D.3	Some additional simple solutions. . . . .	57
D.4	The three concepts highlighted on the reduced morphological chart. . . . .	58

# List of Tables

1.1	Foodstuff characteristics and the challenges they pose on automation [12] . . . . .	2
3.1	The different size variants of the model in mm . . . . .	12
3.2	The varying parameters of the damping test. . . . .	17
3.3	The varying parameters of the bending test. . . . .	18
3.4	The varying parameters of the sliding test. . . . .	18
3.5	The varying parameters of the impact speed test. . . . .	19
3.6	The varying parameters of the angle speed test. . . . .	20
3.7	The size of the block of fillet in mm. . . . .	20
5.1	The main pros and cons of the mailbox plates concept. . . . .	32
5.2	The main pros and cons of the mailbox bulk concept. . . . .	34
5.3	The main pros and cons of the leveller concept. . . . .	35
5.4	The scores of the three concepts. . . . .	36
B.1	The EDEM input parameters used in this study, these are used unless mentioned otherwise. . . . .	53
C.1	The stiffness levels used in the design of experiments . . . . .	54

# Chapter 1

## Introduction

As the global population continues to grow and many countries develop rapidly, the global demand for poultry products also continues to surge. The demand for poultry meat is expected to experience substantial growth of over 120% in the coming decades [1], [2]. At the same time, finding personnel willing to perform repetitive and heavy pick-and-place tasks in poultry processing has become increasingly difficult. The cold operating temperature of most of these plants further contributes to these harsh working conditions. Furthermore, the COVID-19 pandemic highlighted the vulnerability of this sector, with many abattoirs and plants having to close due to disease outbreaks. To meet this escalating demand and personnel problem, the poultry processing industry is increasingly turning to automation and robotics to improve efficiency, productivity, and overall operational capabilities, reducing the dependency on human labour.

### 1.1 The State of Automation in the Food Industry

Although robotics and general automation are rapidly being implemented across various industries, especially in the automotive sector, the food industry is falling behind. This is evident by the number of annual installations of industrial robots in the industry (Figure 1.1).

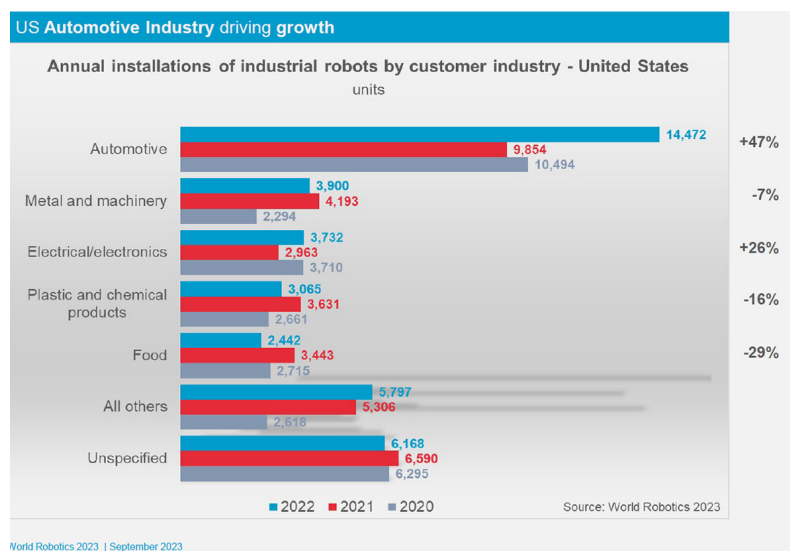


Figure 1.1: The amount of installed robots per industry in the United States [3].

The potential for robotic systems in the poultry industry was first discussed in 1993 by Daley et al. [4]. They highlighted the need to develop advanced grippers and vision systems. In 2003, Chua et al. highlighted that many companies in the food industry viewed automation as essential for their survival [5]. However, they also pointed out the limitations of existing end effectors in handling flexible and irregularly shaped food products [5].

Despite advancements in grippers for food handling [6] [7] and high-speed delta robots for pick-and-place operations since then [8], automation in the poultry industry remains challenging. Although success has been achieved in simple processes such as palletising packaged food and portioning [9] [10] [11], automating more complex operations involving raw chicken has proven challenging.

Table 1.1: Foodstuff characteristics and the challenges they pose on automation [12]

Characteristic	Effect on automation	Example
Naturally soft or fragile	Loss of grip probable, Likely damaged under pressure	Tomatoes, berries, figs, cheeses, eggs
Slippery surfaces	Loss of grip by slippage	Cut-up fruits, peeled vegetables, meat and poultry
Non-rigid or semi-rigid	Likely damaged under pressure	Apricots, cheeses, pastries, meat and poultry
Irregular shapes and sizes	Likely affect surface grip. Systems will require visual systems for IR to assess each item and use decision-making to handle it	All-natural foodstuffs are irregular in shapes and sizes
Uneven surfaces	Can cause difficulties grabbing the object	Avocados, meat and poultry

A primary challenge for implementing automatic solutions lies in the inherent variability of food products. Furthermore, the high costs and downtime associated with installing new automated lines are significant barriers [13]. Table 1.1 summarises the main challenges facing engineers presented by different characteristics of foodstuffs.

These challenges inherent to food processing are particularly evident in chicken fillet processing, where the variability in size, shape, and texture demands a highly adaptable automation solution. Traditional automation systems designed for uniform products often fail to handle the delicate and unpredictable nature of chicken fillets, leading to increased waste and lower production efficiency. Chicken fillets also require careful handling to avoid damages that could render the product unsellable.

Much of the required automation technology is already in existence; however, due to the aforementioned inherent properties of chicken fillets, successful implementation remains challenging [14]. Furthermore, when automated solutions are conceptualised, it is difficult to evaluate potential performance and predict the behaviour of chicken fillets in these systems due to the absence of knowledge and modelling methods of machine-chicken fillet interactions. This makes developing and implementing automated solutions complex and expensive.

Simulations provide a solution for this problem; simulation-aided design offers a promising approach to accelerate the development of automated solutions. By creating virtual environments to evaluate concepts and optimise designs, the need for costly physical prototypes can be reduced [15]. For such an approach to be feasible, it is essential that a model is realised within a practical timeframe. This study will discuss the creation of a sufficiently accurate chicken fillet model for concept evaluation by focusing on creating an adequate representation rather than a perfectly calibrated one.

## 1.2 Research Gap

The increasing demand for automation in the food industry highlights a technological void that demands urgent attention. Innovative solutions that are capable of handling the inherent flexibility of food products are required. Compared to other industries, this sector's relatively slow development and implementation of automation can be partly attributed to the challenges of modelling irregular objects, such as chicken fillets, among others, due to the absence of knowledge of the engineering properties of fillets. As of now, existing research on flexible object modelling has either focused on simple beam-like objects or, when tackling more complex shapes, has yielded relatively rigid models. Additionally, no modelling methods for simulating chicken fillets and machine-fillet interactions exist. Moreover, developing an accurate model of a complex product such as chicken fillets is time-consuming, which makes it impractical to do during the design process.

This research seeks to address both of these gaps by developing a practice-orientated model to simulate chicken fillets and subsequently employing simulation-aided design to devise a reliable and efficient automated solution to singulate chicken fillets from bulk and place them in a specific orientation on a conveyor. The aim is to replace human workers currently performing repetitive pick-and-place tasks in the demanding environment of poultry processing plants. The central research question that guides this study is the following:

## How can simulation-aided design be leveraged to develop automation solutions that accommodate the flexibility and variety of chicken fillets?

With the following subquestions:

1. How can the process of orienting and singulating chicken fillets be automated?
2. How can the behaviour, complex shape and flexible nature of single and bulk chicken fillets be simulated in a virtual environment?
3. How can simulations of chicken fillets be used to evaluate the performance of concept solutions?
4. How can the chicken fillet model be validated?

### 1.3 Case Study

The situation at a chicken fillet processing plant will be the case study for this research. While already quite well automated, this process still incorporates repetitive manual tasks.

Chicken fillet processing initiates from bulk storage; from there, the fillets are singulated and oriented. Then, several cut actions are performed on these fillets by a portion cutter, resulting in a portion of a specific weight, some strips and potentially a remainder, illustrated in Figure 1.2. The orientation of the fillet is very important for these cuts, as the knife of the portion cutter is in a fixed location. The precise orientation of the fillet before entering the portion cutter is essential to maintain the visual quality of the portion and attain the best yield. Moreover, to ensure the weight of the portions is correct, it is important that no air is present between the fillet and the conveyor belt, as then the portion cutter will scan the weight distribution incorrectly.

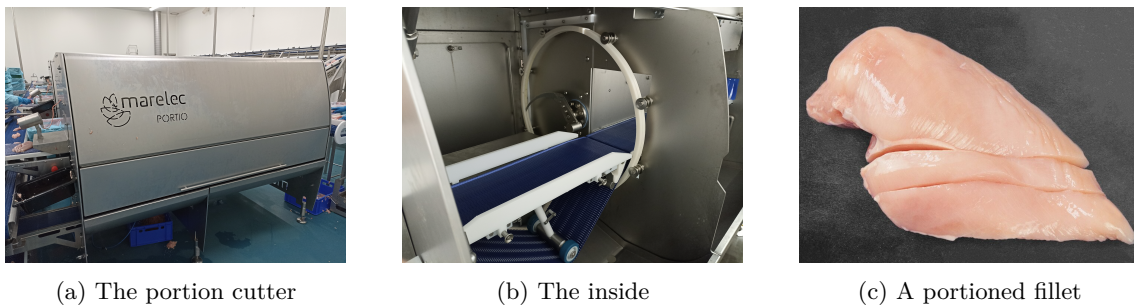


Figure 1.2: The portioning production step with the portion cutter of Marelec [11].

Currently, the placement of fillets on the conveyor preceding the portion cutter is manually executed through human pick-and-place actions. Each operator places between 40 and 50 fillets per minute onto the belt, ensuring that:

- The fillet is singulated.
- It is oriented correctly on the belt.
- The fillet is not folded up, and no air gaps exist between the fillet and the conveyor.

Figure 1.3a illustrates fillets placed on the belt by a human operator. This manual task is labour-intensive, monotonous, and performed in a cold environment, justifying the need for an automated solution. Figure 1.3b demonstrates a similar process at an alternate chicken fillet processing facility, where fillets must be placed 'upside down' in slots on the belt. Despite minor procedural differences, the fundamental tasks of singulating and orienting remain consistent. While this study does not concentrate on these variations, a versatile solution capable of accommodating slight procedural differences across different facilities is highly desirable.

This chapter discussed the need for automation and the background of the research of the study. The next chapter will discuss the design methodology of the research. Chapter 3 will then discuss the chicken fillet model in detail. The results of various model tests will subsequently be covered in Chapter 4, and the model will be deployed in Chapter 5 from concept evaluation to detailing. Experiments and tests that were performed to validate the model and concepts are discussed

in Chapter 6. But first, Chapter 2 delve into the concept design for the problem described in Section 1.3.



(a) Placed fillets in Nijkerk.

(b) Placed fillets in Goor.

Figure 1.3: Two different but similar fillet orientation processes in two Plukon factories.



- Singulate the fillet.
- Ensure that a specific side of the fillet is facing up.
- Ensure a specific rotation of the fillet on the belt.
- Ensure the fillet is not bunched up and has no air underneath it.

Along with these functions, there are several requirements that the solution must fulfil; they are a detailed description of how the solution should operate. The following requirements are defined for the design of the solution, the solution must:

- Process at least 50 fillets per minute.
- Meet hygienic design standards.
- Avoid damaging the fillets.
- Operate fully autonomously.
- Operate in a cold and wet environment.

## 2.3 Concepts

Several potential solutions for the above functions were identified and organised into a morphological chart. Because the process of singulating is very complex, the function of singulating the fillet was divided into three sub-functions: bulk  $\rightarrow$  layer, layer  $\rightarrow$  line, and line  $\rightarrow$  singulated, moving from 3D to 2D to 1D to single fillets. The morphological chart can be seen in Figure D.1.

A few selections were made on the morphological chart to narrow down the solution space. Firstly, emphasis was placed on selecting existing technology from the chart since these are already tried and tested methods and are often readily available. Some of the existing technology considered in this study can be seen in Figure 2.2. To supplement this, some remaining simple and practical solutions were selected; these are often cheap and easy to clean, which is beneficial. Some more sub-solutions were excluded for various reasons. Three distinct concepts (blue, green, and yellow) were subsequently developed from the remainder and can be found in Figure D.4. Notably, these concepts are mechanical solutions, as complete robotic solutions for the problem have already been developed [16]. Mechanical solutions are also often much simpler, resulting in a cheaper product that is easier to clean. The filtering steps and concept formulations are detailed in Appendix D.

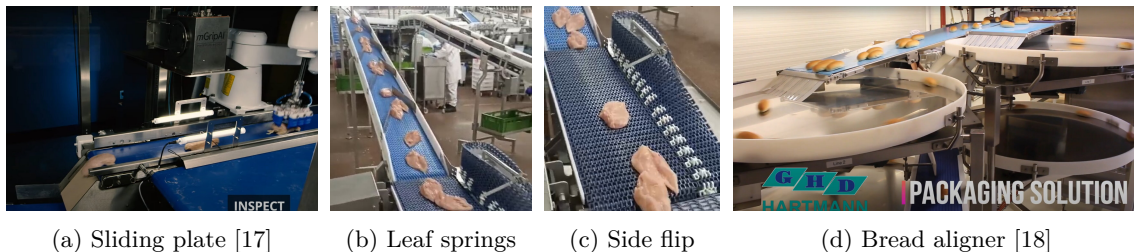
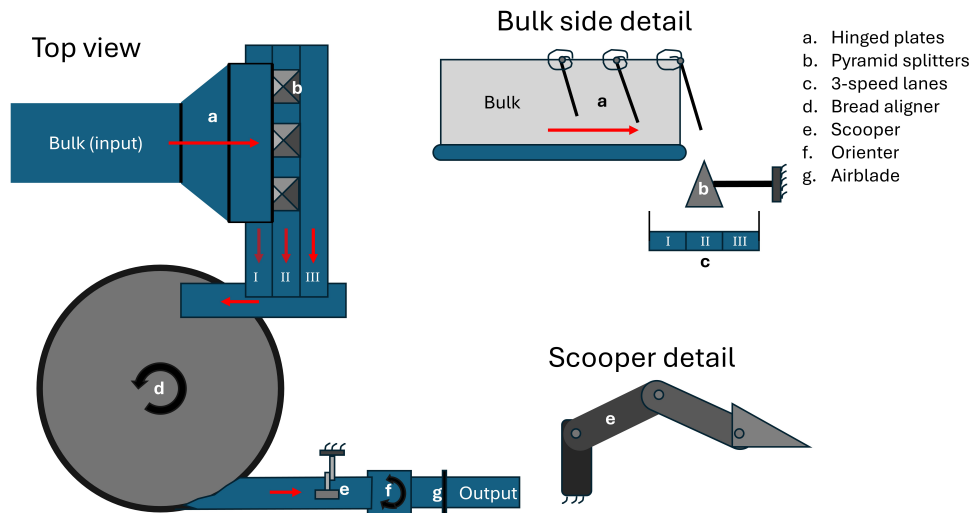


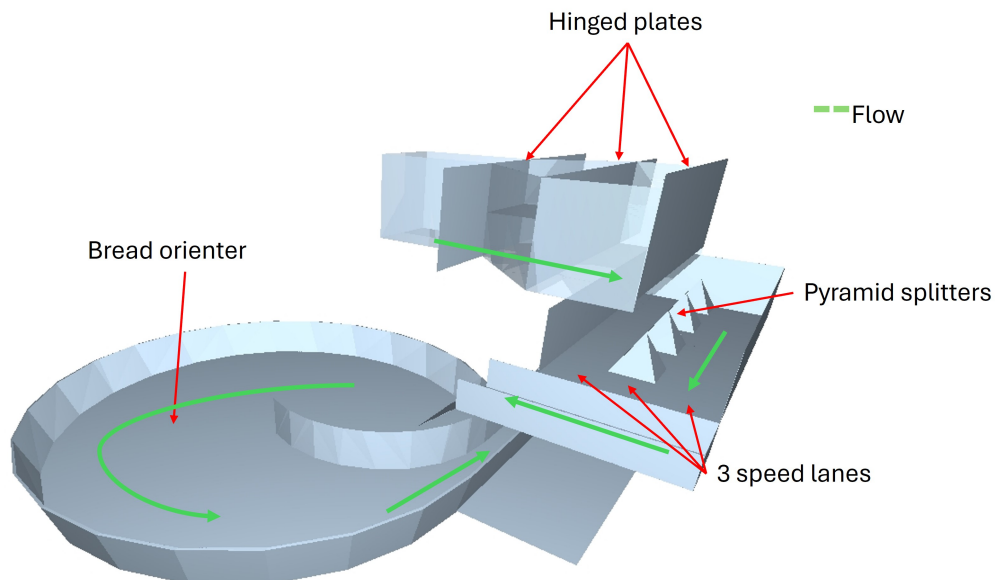
Figure 2.2: Some of the existing technology considered in this study.

### **The Hinged plates Concept: hinged plates, split multilane drop with a bread aligner, scooper, orienter conveyor and airblade**

The first concept developed, depicted in Figure 2.3, comprises of five parts. Section a consists of a series of three steel plates that are hinged and connected to a torsion spring. The second plate is a bit longer than the first, and the third one is longer, so roughly one fillet fits through the final opening. This height difference ensures the singulation in the 3D - 2D stage is done gradually. The pyramid splitters, section b, ensure the entire three-lane belt is populated with fillets. These three lanes are then controlled to provide a constant flow of fillets onto the transverse conveyor and to the bread aligner, section d. This big spinning plate aligns the fillets to the edge and ensures they are really singulated. A scooper then picks up and flips over the fillet if necessary (e), and a servo-actuated conveyor then places them into the desired orientation. Finally, the fillets pass under an airblade that squeezes them to the conveyor, removing any air gaps.



(a) Concept sketch; the red arrows depict the direction of fillet flow

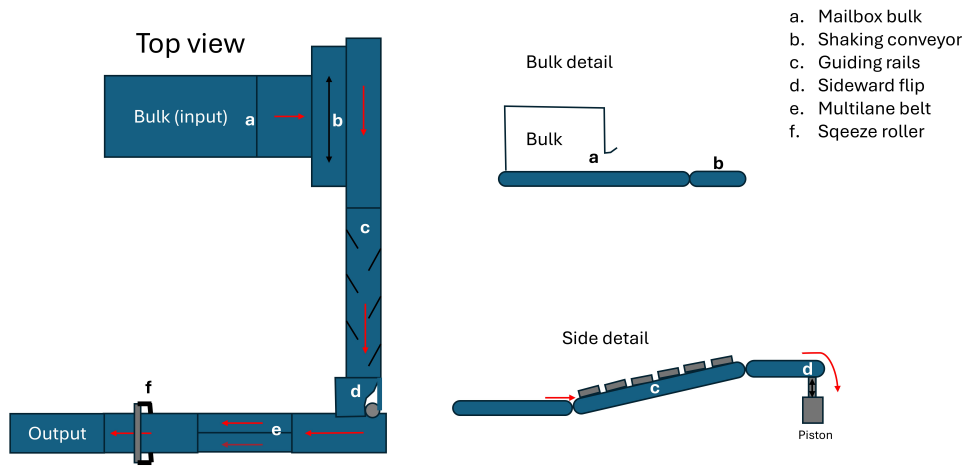


(b) 3D model; the green arrows depict the direction of fillet flow

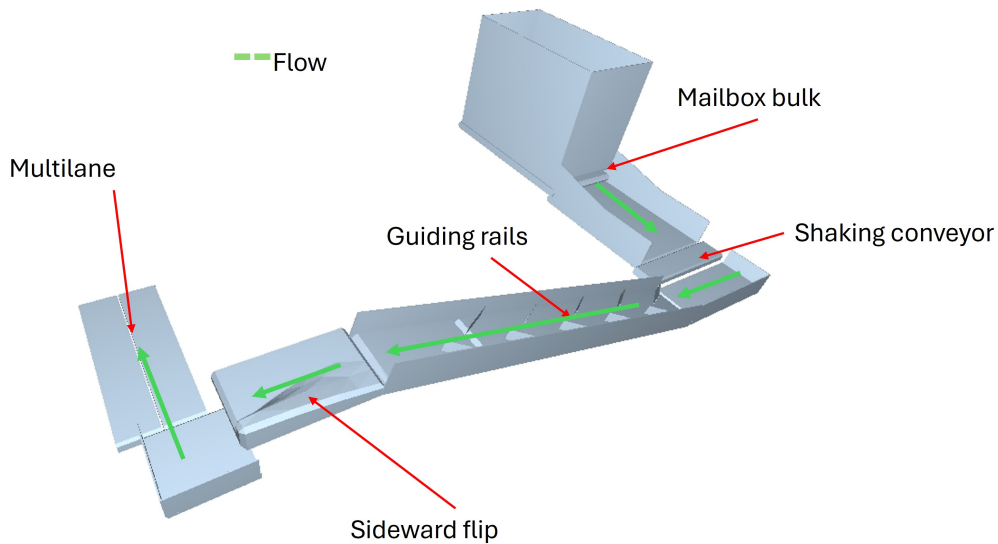
Figure 2.3: The concept sketch of the concept with hinged plates along with a partial 3D implementation.

**The Mailbox bulk Concept: mailbox, shaking conveyor with guiding rails, a sideways flip, multilane belt and a squeeze roller**

Figure 2.4 shows the yellow concept. Part a, the mailbox, is a bulk box on a conveyor with a fixed slit opening. This setup ensures that only one fillet can fit underneath in height, creating the 2D layer. The shaking conveyor (b) then ensures the layer gets gradually deposited onto the transverse conveyor. The guiding rails in section c ensure all fillets are aligned parallel to the conveyor and in a row. After which, if necessary, the fillet is flipped over sideways by a conveyor section that can twist (Figure 2.2c). These then move onto a 2-lane belt where roughly half of the fillet is on the first and the other half on the second belt. The belts are controlled at different speeds so that the orientation of the fillet can be adjusted. Finally, the fillets pass under a squeeze roller that removes any air remaining underneath.



(a) Concept sketch; the red arrows depict the direction of fillet flow



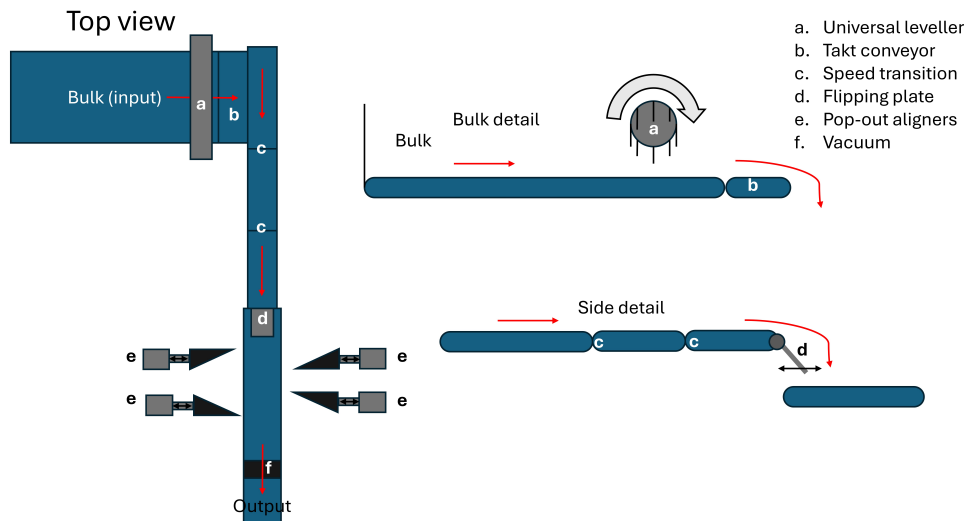
(b) 3D model; the green arrows depict the direction of fillet flow

Figure 2.4: The sketch of the concept with a mailbox bulk along with a partial 3D implementation.

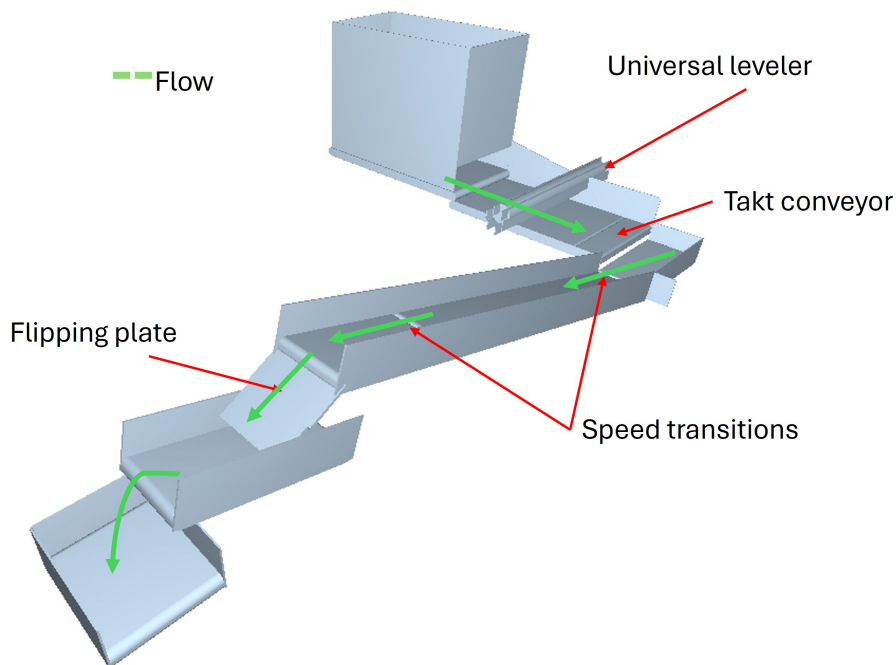
**The Leveller Concept: a universal leveller, takt conveyor, speed transitions with a flipping plate, pop-out aligners and a vacuum**

The final designed concept, illustrated in Figure 2.5, firstly utilises a Kortlever universal leveller to reduce the 3D bulk of fillets to a 2D layer in part a. This machine employs rotating blades on a cylinder to sweep material back, creating a consistent height layer. The layer is then transferred to a takt conveyor, a short, high-acceleration conveyor that pulls a 1D line of fillets from the layer at fixed intervals in section b. Subsequent increasing-speed belt transitions pull the line apart, singulating the fillets (c).

Following this, the fillets pass over a sliding plate in section d. If the correct side of the fillet is already facing up, the plate acts as a slide. If not, the plate rotates out of the way, creating a drop and allowing the fillet to flip over. Shaped pop-out aligners, in two sets for left and right fillets, then push the fillets into the desired orientation (e). Finally, part f is a vacuum section that ensures the fillets are pulled flat onto the belt, removing any air underneath.



(a) Concept sketch; the red arrows depict the direction of fillet flow



(b) 3D model; the green arrows depict the direction of fillet flow

Figure 2.5: The concept sketch of the concept with a mailbox bulk along with a partial 3D implementation.

## 2.4 Chapter Conclusions

This chapter discussed the design methodology of this research that was used to create a solution for the problem discussed in Section 1.3. It then defined the various functions and requirements that any solution must fulfil. Subsequently, three concept solutions were defined using a morphological chart, using various pre-existing technologies. These concepts show how chicken fillets could be singulated from bulk and subsequently oriented automatically.

However, determining how these concepts will perform under real-life conditions is difficult, making it practically impossible to make a well-informed concept decision. Therefore, Chapter 3 will discuss the creation of a chicken fillet DEM model to evaluate the performance of these three concepts.

# Chapter 3

## Chicken Fillet Modelling

This chapter covers the methods employed for modelling chicken fillets, focussing on creating a sufficient representation for concept evaluation. Section 3.1 covers the current state-of-the-art in flexible modelling. Section 3.3 then discusses how the shape of chicken fillets is recreated in DEM. The particle bonding and parameter configuration is then discussed in Section 3.3.1 and Section 3.3.2. Section 3.4 then details the testing procedures employed to refine the model and analyse its sensitivity. Finally, Section 3.5 describes a compression test on real chicken fillets to gain more insight into the material characteristics of chicken fillets.

### 3.1 Current State-of-the-art Modelling of Flexible Objects

In this practice-oriented study, a model's primary function is facilitating concept evaluation rather than perfectly replicating chicken fillet behaviour. Therefore, the focus is on developing a sufficiently accurate and visually realistic model rather than calibrating all parameters. This approach prioritises time efficiency, enabling the rapid creation of a model that can be effectively utilised for preliminary analysis, design exploration, and decision-making within a reasonable timeframe. It is crucial to incorporate their inherent flexibility to effectively model chicken fillets. Discrete Element Method (DEM) software has been utilised in various studies to simulate the flexibility of objects.

Numerous publications have focused on modelling flexible stem-like shapes using DEM. For example, Guan et al. employed the bonded contact model in Altair@*EDEM*<sup>TM</sup> to simulate the behaviour of rape stem [19]. Similar research includes Schramm and Tekeste's wheat straw model, Zhong et al.'s simulation of wet fibres, and Patel et al.'s model of paddy straw [20], [21], [22]. Xu et al. expanded on this concept by modelling entire flexible rice plants during harvest and calibrating various parameters [23].

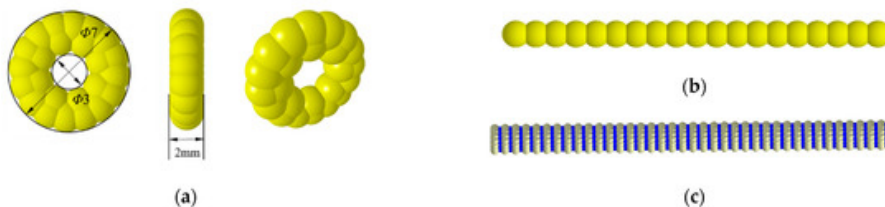


Figure 3.1: The model representing flexible stems developed by Guan et al.

Despite these significant advancements in modelling flexible items, these studies predominantly focus on relatively simple, isotropic stems, often represented by a single line of solid sub-particles (as illustrated in Figure 3.1).

Li et al. advanced the modelling of complex objects by developing a rapid prototyping model capable of generating intricate shapes for various organic items [24]. Using the bonded particle model to connect particles, they simulated corncobs, garlic, wheat kernels, and wheat ears. To validate their algorithm, they conducted compression tests, comparing simulated and experimental forces at failure, demonstrating their methods' viability. However, their analysis employed relatively high stiffness values, implying relatively small deformations. Gilvari et al. similarly calibrated a model of biomass pellet breakage, comparing the outcomes of two distinct bonded contact models [25], with similar limitations in the magnitude of deformation.

Alternative models of flexible objects include the Shafiei and Barthelat scaled skin model, constructed from linked cubes of varying shapes using sets of springs to test different scale arrangements [26]. Mathias et al. employed stacked linked triangle surfaces to model flexible surfaces, validating their model through a beam bend test [27].

In contrast to the objects of these studies, chicken fillets present a unique challenge due to their high flexibility and complex 3D non-isotropic nature, rendering accurate modelling of their behaviour far more intricate. Moreover, certain parameters exhibit considerable variability depending on the specific circumstances. Notably, fresh fillets are remarkably slippery and free-flowing, while prolonged exposure to air induces stickiness due to the formation of specific proteins on their surface.

## 3.2 Discrete Element Method

The discrete element method (DEM) was employed to simulate chicken fillets. DEM is a numerical simulation technique designed to model the behaviour of materials composed of distinct, interacting particles [28] [29] [30] [31] [32]. An object within DEM is represented as a single particle or an assemblage of small particles, each possessing unique properties such as size, shape, mass, and material characteristics. This method calculates the motion and interactions (e.g., collisions, bonding, and forces) among these particles over time through predefined timesteps. Equation (3.1) show the method's force equations of two colliding particles. Where  $E^*$  and  $G^*$  are the equivalent Youngs, shear moduli,  $R^*$  is the equivalent radius, and  $\delta_n$  and  $\delta_t$  are the normal and tangential particle overlap. These particle contacts also include damping terms, Equation (3.2) and (3.3) show how the damping forces are calculated, here  $m^*$  is the equivalent mass,  $e$  is the coefficient of restitution and  $v^{rel}$  the relative particle velocity. DEM is particularly advantageous for simulating granular materials, flexible objects, or systems subject to significant deformations and breakage, such as soils, powders, or, specifically, in this case, chicken fillets.

$$F_n = \frac{4}{3}E^*\sqrt{R^*}\delta_n^{\frac{3}{2}} \quad \text{and} \quad F_t = -8G^*\sqrt{R^*}\delta_n\delta_t \quad (3.1)$$

$$F_n^d = -2\sqrt{\frac{5}{6}} \cdot \frac{-\ln(e)}{\sqrt{\ln^2(e) + \pi^2}} \cdot \sqrt{2mE^*\sqrt{R^*}\delta_n} \cdot \vec{v}_n^{rel} \quad (3.2)$$

$$F_t^d = -2\sqrt{\frac{5}{6}} \cdot \frac{-\ln(e)}{\sqrt{\ln^2(e) + \pi^2}} \cdot \sqrt{8mG^*\sqrt{R^*}\delta_n} \cdot \vec{v}_t^{rel} \quad (3.3)$$

The discrete element method was selected because of its ability to easily create and configure complex shapes, such as chicken fillets, as well as for its ability to simulate bulk material behaviour, which is crucial for many processes involving chicken fillets [23] [33] [34]. The Altair®*EDEM<sup>TM</sup>* software was selected to simulate the behaviour of chicken fillets. This is a high-performance simulation software for granular and bulk material simulation based on the discrete element method (DEM) [35]. Altair®*EDEM<sup>TM</sup>* was selected because of its speed and precision in simulation, ease of use, and compatibility with other software to run co-simulations with, for example, multibody dynamics. Another reason for selecting this specific software was the researcher's prior experience with the software, which allowed a quick implementation.

Chicken fillets are inherently sticky, so the Hertz-Mindlin contact model with JKRv2 was selected to model this. The Hertz-Mindlin model calculates contact forces based on the particle overlap and is known for its accuracy and efficiency. The JKRv2 model accurately implements the JKR theory; it creates adhesion forces based on interfacial surface energy to model adhesion between the fillets and geometries and is suitable for particles using a contact radius.

## 3.3 Generating the particle representation of a Fillet

As a starting point for the model, a 3D STL model of a chicken fillet was obtained from Sketchfab [36]. Several models were generated from this mesh. A basic algorithm was developed to fill the mesh with a simple raster of specified-sized particles. These particles are then bonded using the built-in bondingV2 model to create flexible meta-particles consisting of a specific number of sub-particles. Figure 3.3 shows several fillet models considered in this study.

To account for the varying sizes of chicken fillets, the base model was non-homogeneously scaled slightly, resulting in three distinct size variants. Each size variant was then mirrored to represent both left and right chicken fillets, yielding six different fillet types.

Table 3.1: The different size variants of the model in mm

	Length	Width	Thickness
1	144	72	40
2	172	72	32
3	176	72	40

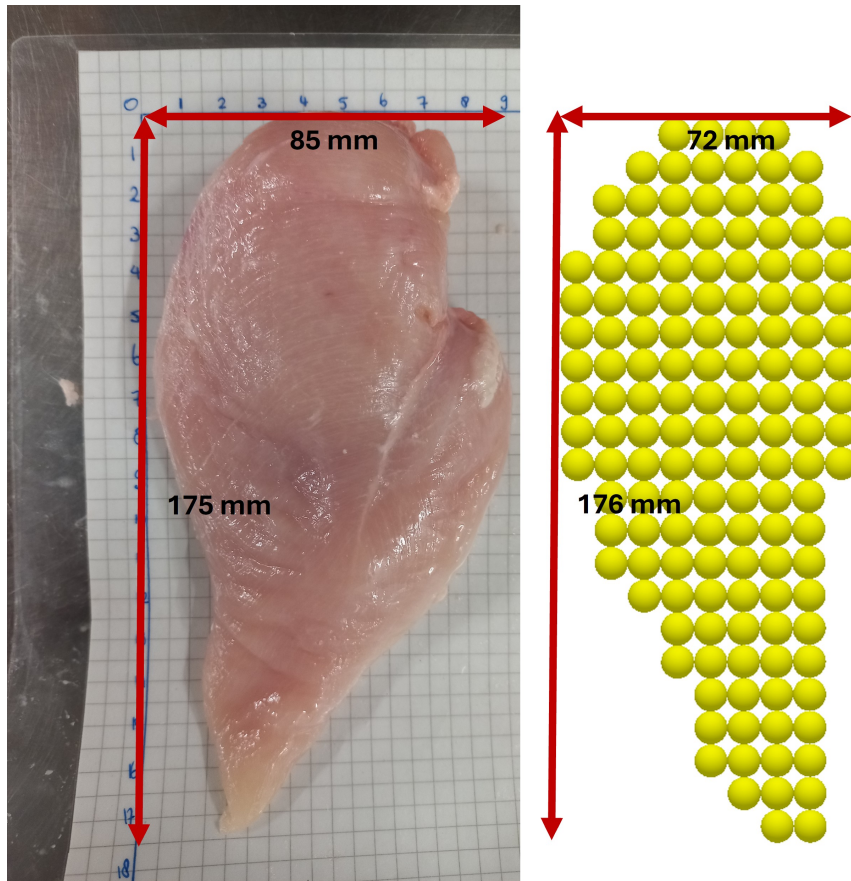


Figure 3.2: A chicken fillet compared with a particle model representation of a chicken fillet.

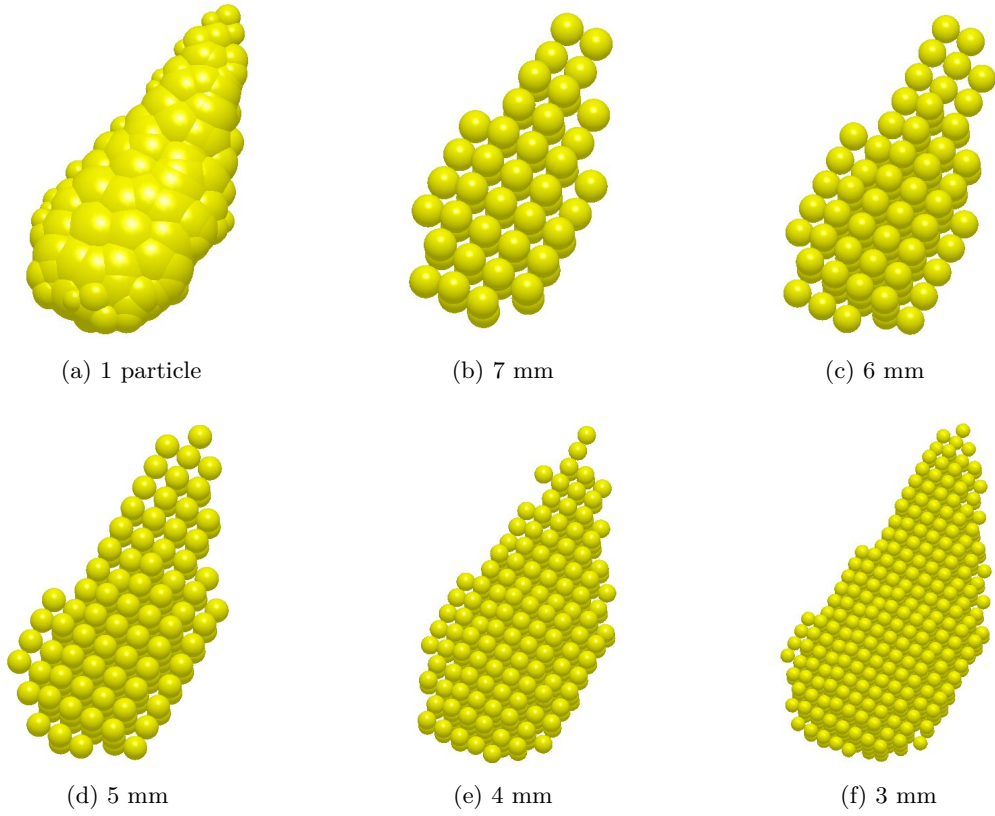


Figure 3.3: Several models of chicken fillet, with meta-particles generated with sub-particle radii ranging from 7-3 mm.

To evaluate the differences between the model variants described in Figure 3.3, 50 of each variant were dropped on a horizontal surface at speeds ranging from 0-10 m/s. After impact, the amount of intact bonds and the computational time were measured.

### 3.3.1 The Bonded Particle Model

The DEM bonding model links particles based on a virtual contact radius. If the contact radii of two particles overlap during generation, a bond is formed between them (see Figure 3.4a). When bonded, forces are transmitted between the particles using the equations of Potyondy and Cundall [37]. When a bond is formed, the normal and shear forces on the particles are calculated by Equation (3.4) and 3.5. Where  $v_{n,t}$  are the normal and tangential velocities of the particle,  $S_{n,t}$  the bond stiffnesses,  $R_b$  the particle radius multiplied by the bonded disk scale and  $\delta_t$  the timestep. In particular, these equations do not include any damping terms, so another damping method was developed, as will be discussed in Section 3.4.1. These bonds can break during simulation in two ways: by exceeding the defined critical stress or by separating the particles beyond their overlapping contact radii.

$$\delta F_n = v_n S_n \pi R_b^2 \delta_t \quad (3.4)$$

$$\delta F_t = v_t S_t \pi R_b^2 \delta_t \quad (3.5)$$

Modelling significant flexibility, as in chicken fillets, requires low stiffness values. However, large deflections can cause bond failure due to particle separation. A larger sub-particle size can be used to mitigate this, resulting in a larger contact radius. However, this leads to an inaccurate 3D representation of the fillets and increased surface roughness. Alternatively, increasing the contact radius also allows for more deformation, but this is limited as it can result in undesired bonding, creating a stiff truss structure. When using only one particle type, this limit is  $R\sqrt{2}$  as explained in Figure 3.4.

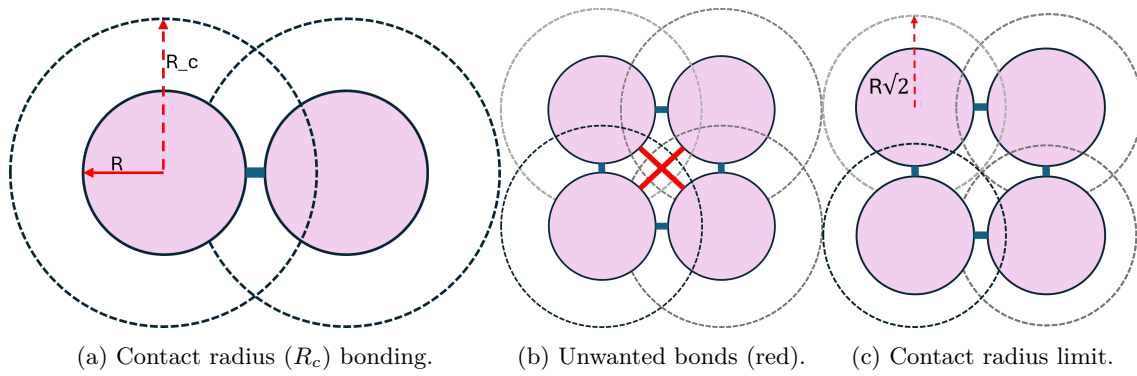


Figure 3.4: Preventing undesired bonds from forming.

To increase this contact radius limit, multiple different particle types were used. An example of this can be seen in Figure 3.5, where the two types are placed in a grid so that type A only directly borders type B. If only a bond between type A and B is defined and not for A-A or B-B, the contact radius limit increases to  $R\sqrt{3}$ . This could, in theory, be scaled up to more and more particle types but would require a more complex particle placement algorithm. In this research, only two different particle types were used, as seen in Figure 3.6.

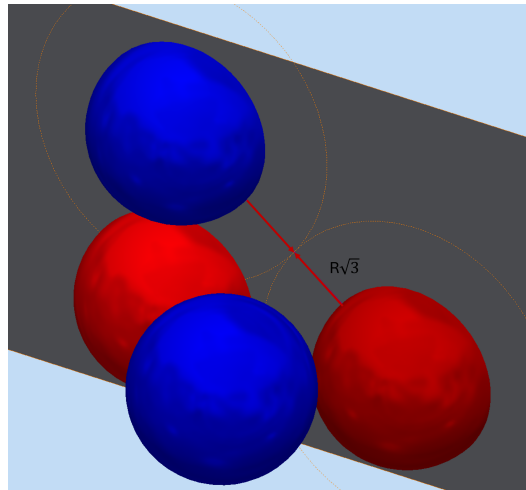


Figure 3.5: The contact radius limit increases Using two different particle types.

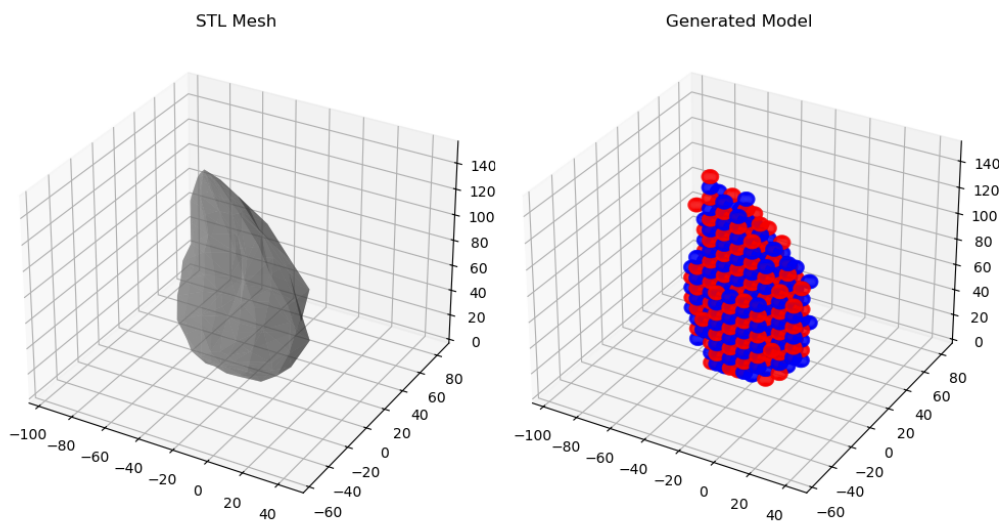


Figure 3.6: An stl mesh next to its generated meta-particle.

### 3.3.2 Model Input Parameters

The mechanical properties and other parameters must be defined to simulate chicken fillets. Because there is very little available documentation on the properties of chicken fillets, and to speed up the development of the model, the best available values will be used for many parameters.

Ko et al. analysed some of the mechanical properties of chicken breasts, comparing them with plant-based alternatives, evaluating the hardness and Young's moduli, as well as their stress-strain curves [38]. The results of their study can be found in Figure 3.7. The Young's modulus they found for chicken, 0.37 MPa, will be used throughout this study.

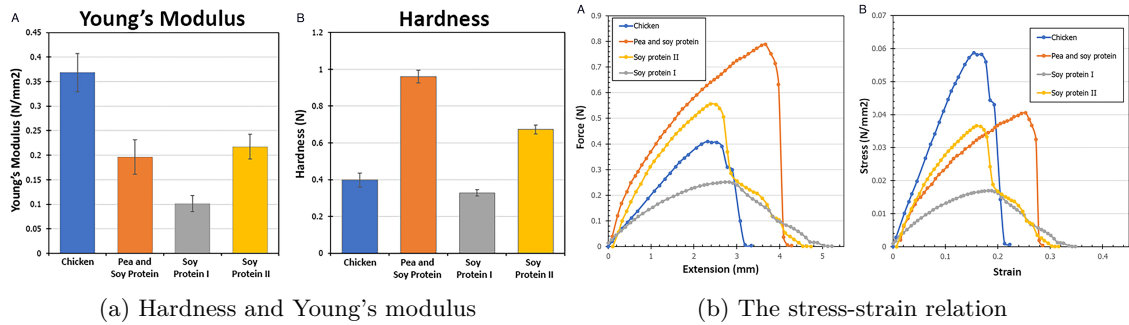


Figure 3.7: Some mechanical properties of chicken breast compared to plant-based alternatives [38].

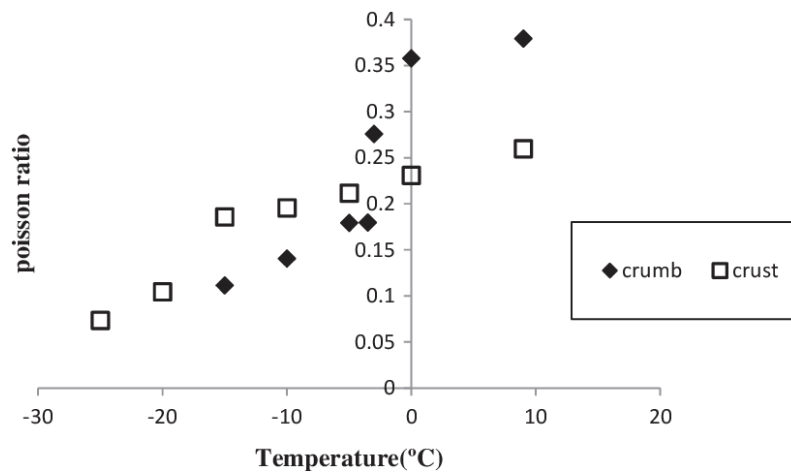


Figure 3.8: The Poisson's ratio of chicken nugget crumb and crust over temperature [39].

Jahanbakhshian et al. researched the Poisson ratio of chicken nugget crumbs and crust based on temperature, which can be seen in Figure 3.8. Chicken nugget crumbs are partially made from chicken fillets, so their value can function as a starting base for the model. The temperature in chicken fillet processing plants must be around 8 degrees, so a Poisson ratio of 0.37 was selected from the graph [39].

Friction coefficients of the interactions between, for example, chicken fillets and steel, product and machine, are also crucial to creating an accurate simulation. These remain unknown at the point of writing this report. However, Kosukegawa et al. performed a study that analyses the friction between soft tissue such as hydrogel and stainless steel. Although this is not the same, the surface characteristics of the hydrogel are the closest resemblance available to those of chicken fillets, so their results were used as a starting point for simulation. The results of their study are found in Figure 3.9 [40].

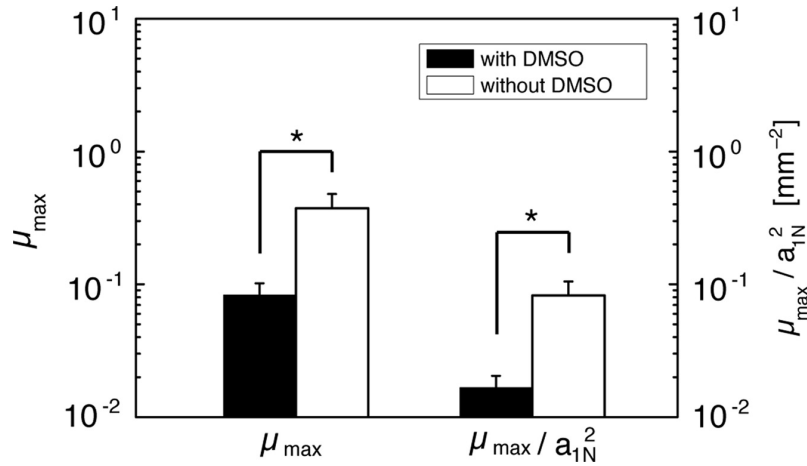


Figure 3.9: The maximum friction coefficients of hydrogel tissue on steel for normal hydrogel and hydrogel with DMSO added to it [40], the  $\mu_{max}$  value without DMSO, 0.4, was used in this study.

To configure the adhesion of chicken fillets, the model requires an interfacial surface energy value. Silva et al. measured the critical surface tension of chicken breasts and found it was 54.56 mN/m [41]. While this is not the same as interfacial surface energy, the parameter is related to this value and can be used as an approximation, which is sufficient for the purpose of this model. No rolling friction model was used because, in reality, fillets mostly show sliding behaviour. Also, the coefficients of restitution were set to a minimal value to represent the extreme damping behaviour of chicken fillets on impact.

Various test simulations were performed to configure the bond stiffness parameters and find a parameter set that provided adequate stability, flexibility, and damping. Chicken fillets inherently have very high damping properties due to their soft and pliable nature, and the bonding parameters significantly influence the damping of the model. The bondingV2 model does not include any damping terms in the bond equations, which resulted in very bouncy fillets as energy was transferred back and forth between bonds, causing oscillations. To combat this bounciness, a very low tangential stiffness could be used to force energy to be transferred via sub-particle interactions, which do include damping terms. However, very low tangential stiffness values made the model unstable, causing the meta-particle to explode, so a balance had to be struck. Torque feedback was turned off to increase the flexibility of the meta-particles; as a result, the bonded disk scale had no effect other than simply multiplying the two stiffness values, and thus, it was left at 1. The final parameter selection was made based on the angle of bending, stability, and damping, as well as the visual assessment.

## 3.4 Testing the Models

Several tests were performed to validate and refine the model and calibrate its parameters. Additionally, a few sensitivity analyses were performed to examine the model's limits and stability. Altair Hyperstudy was used to create the design of experiments for these simulations [42]. The details of these tests will be discussed in this section. The variable parameters will be discussed with each test, and all other constant model parameters can be found in Appendix B.

### 3.4.1 Configuration Tests

A series of tests were executed to configure the model and its parameters to more accurately represent the mechanical behaviour of chicken fillets. These encompassed damping, bending, and sliding assessments to align model predictions with empirical observations. The Altair®Hyperstudy software was selected to perform simulations en masse and explore the design space. The bounds for the stiffness parameters under examination were iteratively estimated. Parameters that exceeded the upper threshold induced a model that exhibited excessive rigidity, thereby significantly diverging from the observed behaviour of chicken fillets. In contrast, parameters near the lower threshold produced an insufficiently stiff and inherently unstable model, often falling apart. Given the extensive range of these parameters, a discrete logarithmic distribution consisting of 28 distinct

levels was employed to ensure equitable representation of the lower orders of magnitude within the Design of Experiments (DOE). These values can be found in Appendix C.

### Damping tests

In this test, initially, a basic meta-particle consisting of eight sub-particles was dropped from a distance onto a horizontal surface to test how fast the energy would dampen. This test aimed to gain insight into how the stiffness parameters of the model can be configured to dampen its energy as quickly as possible. A schematic image of it can be seen in Figure 3.10.

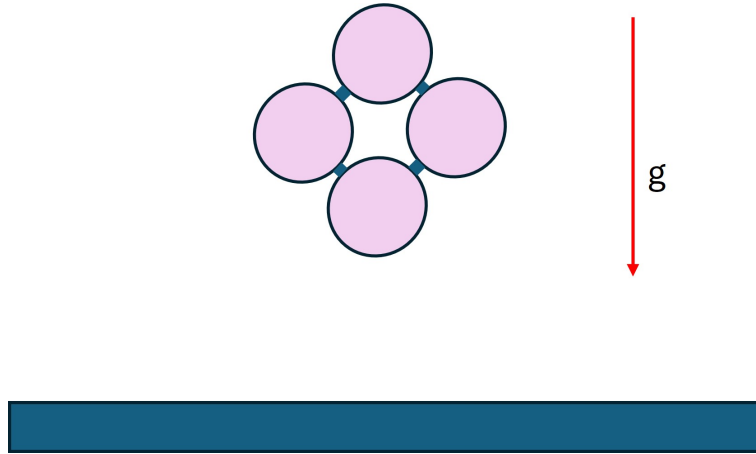


Figure 3.10: A 2D schematic of the basic bounce test performed to test damping and the influence of shear stiffness.

This test was then replicated with the fillet-shaped meta-particles, 15 of each of the six types dropped at random orientations from a height of 500mm onto a horizontal surface. The time to dampen the energy, the so-called settle time, was analysed for a range of normal and shear stiffnesses by 784 simulations in a full factorial analysis. This time was calculated as the time between impact and the moment a specific percentage of the energy was remaining. An overview of the varying parameters can be seen in Table 3.2.

Table 3.2: The varying parameters of the damping test.

Parameter	Min value	Max value	unit
Normal stiffness	1e5	1e8	N/m <sup>3</sup>
Tangential stiffness	1e4	1e7	N/m <sup>3</sup>

### Bending test

A bending test was performed to ensure that the meta-particles have adequate flexibility and to analyse the influence of the bond stiffness parameters on this flexibility. The bending of some real chicken fillets from the local store was compared with the bending of a modelled fillet to configure the stiffness values. The local fillets were smaller than the fillets Plukon processes, 16x9x2cm, and thus a custom test fillet was created for this test to start. The test was also run with the six variants described in Section 3.3; their bend angles were measured, and the average angle was calculated. The angle was automatically calculated by hyperstudy to allow for an easy analysis. Figure 3.11a explains how the angle was calculated. The first vector was obtained by taking the x and z positions at the top at the final timestep where a particle was present between the two parallel lines. At this timestep, the maximum x coordinate and the minimum z coordinate were also extracted, defining the second vector. The angle between these two vectors was then calculated using Equation (3.6). A full factorial analysis was performed with 784 simulations for both experiment The limits of the varying parameters can be found in Table 3.3 and the full test matrix in Appendix C. Images of the tests can be seen in Figure 3.11.

$$\alpha = \cos^{-1} \frac{a \cdot b}{|a| \cdot |b|} \quad (3.6)$$

Table 3.3: The varying parameters of the bending test.

Parameter	Min value	Max value	unit
Normal stiffness	1e5	1e8	N/m <sup>3</sup>
Tangential stiffness	1e4	1e7	N/m <sup>3</sup>

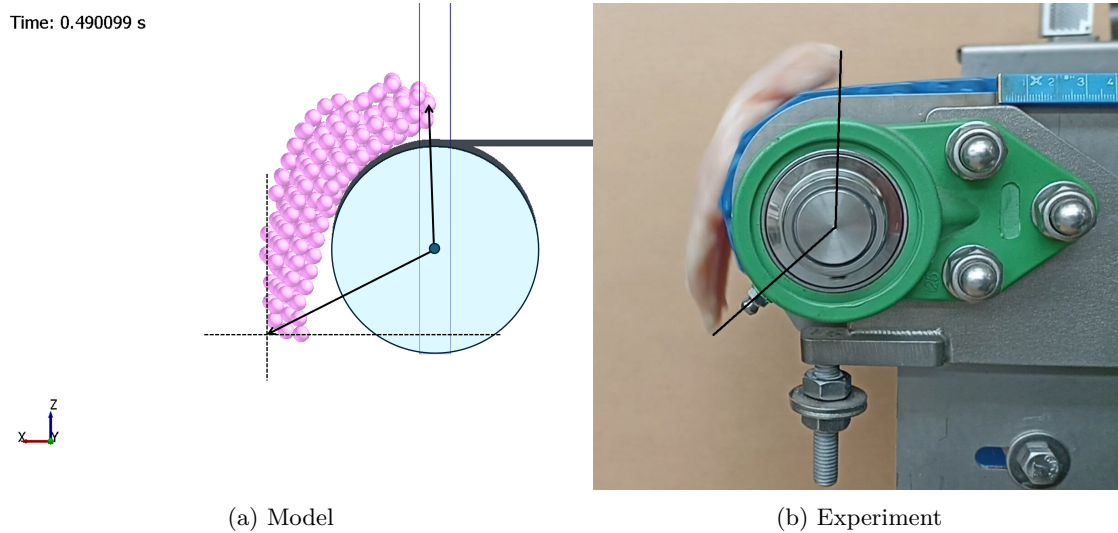


Figure 3.11: The bend test, comparing the model with a real-life experiment, and the vectors for automatic calculation by the model are also shown.

### Sliding test

Because no earlier studies at the time of writing researched the sliding behaviour of chicken fillets on steel, a sliding test was performed. This test determined the sliding angle of real chicken fillets and their modelled counterparts on a stainless steel surface. This angle is influenced by the friction coefficient and adhesion between the fillets and steel, both of which are model parameters.

The experimental setup involved a one-meter-long plate lifted from one side until the fillet started to slide. The angle at this point was recorded, and the process was repeated five times. Subsequently, the fillet was briefly submerged in water, and the test was repeated, completing five more submersion cycles and testing.

To investigate the impact of the friction coefficient and surface energy on the sliding angle, 50 simulations were conducted for each particle configuration described in Figure 3.3. The Hammersley distribution was employed to ensure good parameter space coverage while minimising the total number of simulations. The parameter ranges used in these simulations can be found in Table 3.4, and Figure 3.12 illustrates the experimental setup.

Table 3.4: The varying parameters of the sliding test.

Parameter	Min value	Max value	unit
Friction coefficient	0	1	-
Interfacial surface energy	0	0.25	J/m <sup>2</sup>

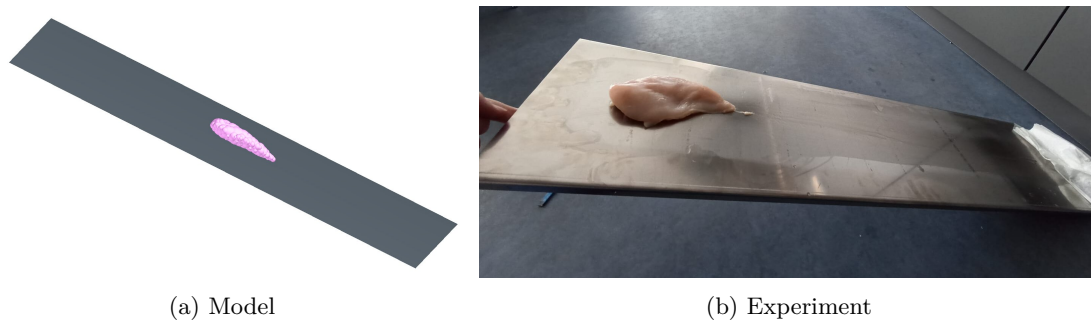


Figure 3.12: The sliding test, comparing the model with a real-life experiment.

### 3.4.2 Sensitivity Analysis

Several additional simulation tests were conducted to evaluate the robustness and response of the model under varying conditions. The analysis aimed to assess how changes in input parameters affect the model's performance, providing insights into its overall stability, reliability and predictive capabilities. These tests are all surface drop tests under different conditions, an example of which can be seen in Figure 3.13.

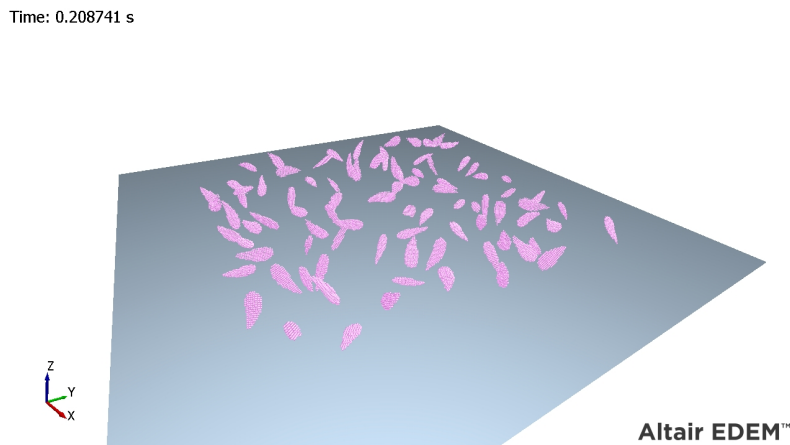


Figure 3.13: A surface drop test, dropping 90 fillets, 15 of each variant, from a height of 500mm.

#### Impact speed

The model's stability was assessed under varying impact speeds and stiffness configurations. These tests were performed to investigate if any specific stiffness configurations are more stable than others and cope with larger impact velocities. A series of simulations were conducted using the setup of Figure 3.13. However, instead of the drop height of 500mm, an initial velocity was given to the fillets. They were dropped in random orientations, and the number of intact bonds was reported at the end of each simulation. The test was run with initial velocities of up to 10 m/s. This bound was chosen because chicken fillets usually do not drop for more than a meter in factory conditions. A Hammersley distribution with 5000 data points was employed to efficiently explore the 3D DOE space and ensure comprehensive coverage of parameter variations within a limited number of simulations. This high amount was chosen because the parameters span large ranges across multiple orders of magnitude and to capture the border region where the model becomes unstable more accurately.

Table 3.5: The varying parameters of the impact speed test.

Parameter	Min value	Max value	unit
Velocity	0	10	m/s
Normal stiffness	10e5	10e7	N/m <sup>3</sup>
Tangential stiffness	10e4	10e6	N/m <sup>3</sup>

### Angle drop

To assess the stability of the model under varying impact angles, the surface drop test of Figure 3.13 was re-run. But this time, the fillets were dropped in a specific orientation. The 3D DOE space, containing all possible orientations, was sampled using a Hammersley distribution. A total of 5000 simulations were performed to ensure good coverage. The amount of intact bonds was measured throughout every simulation to determine how many had broken. The range of the angles can be found in Table 3.6.

Table 3.6: The varying parameters of the angle speed test.

Parameter	Min value	Max value	unit
Yaw $\psi$	0	$2\pi$	rad
Pitch $\theta$	0	$2\pi$	rad
Roll $\phi$	0	$2\pi$	rad

### Scaling

A scaling test was performed to analyse the stability of the modelled fillets when they are bigger or smaller. In this experiment, the surface drop test of Figure 3.13 was recreated, dropping the fillets in random orientations. But this time, all fillets were scaled by a factor between 0.25x and 10x in intervals of 0.25, so 40 simulations in total. The time to dampen the energy and the stability in terms of how many bonds are still intact are recorded for every simulation. The scales were applied upon particle generation, so the sub-particle radii were scaled, but the total number of particles remained the same.

## 3.5 Compression test

A compression test was performed to validate the Young's modulus of the literature and gain insight into the material behaviour of chicken fillets. The test was performed using a rectangular block of chicken fillet cut from the centre part of a whole fillet. The size of the block can be found in Table 3.7. To ensure the hygiene of the test setup, the fillet block remained inside a sealed plastic bag during the test. To minimise the bags' influence on the test results, they were filled with enough air to give the fillet room to deform.

The test was repeated on the same fillet block three times, and the force-deformation curves were recorded each time. The compression was done at a 1 mm/min speed and limited to 5N to avoid completely destroying the cubes. From the resulting curve, the Young's modulus was calculated Equation (3.7).

$$E = \frac{F \cdot L}{A \cdot \Delta L} \quad (3.7)$$

Table 3.7: The size of the block of fillet in mm.

Length	35
Width	35
Height	10

Additionally, some compression tests were performed on a different whole fillet, depicted in Figure 3.14b. These tests were performed at different compression speeds to determine if that affected the response of the fillet. The fillet was repositioned between the tests to ensure it was in contact with the press at the start of every test.



(a) Small block

(b) Fillet

Figure 3.14: The compression test setup.

### 3.6 Chapter Conclusions

This chapter discussed the steps of the creation of a chicken fillet model. While previous studies focussed on simulating rigid or very simple flexible shapes like stems, it showed that DEM software can also be used to recreate the much more complex shape of a chicken fillet by creating a particle representation based on sub-particles. The particle representation can be configured to represent actual chicken fillet behaviour using a combination of input parameter values from literature and several real-life experiments and model tests. When arranging the fillet shape with several different particle types, the contact radii of the bonded particles can be increased significantly. This enhances the flexibility of the model, making it more realistic. Several sensitivity analysis tests were also defined to test the limits of the model and its behaviour under varying circumstances. The results of all these configuration and sensitivity tests will be discussed in detail in Chapter 4, and the final selection of simulation parameters used for developing concepts can be found in Appendix B.

# Chapter 4

## Model Simulation Results

This chapter will discuss the results of all the model tests and experiments described in Chapter 2. Section 4.1 will discuss the results of the tests to configure the model. The results of the sensitivity analyses will be covered in Section 4.2, and the findings of the compression tests will be discussed in Section 4.3.

### 4.1 Configuration Tests

This section will cover the results of the various tests that were performed to configure and refine the model.

#### 4.1.1 Sub-particle selection

The results from the sub-particle selection tests can be found in Figure 4.1. Only a sub-particle radius of 3mm is significantly less stable than the others, as is evident from the dark blue line in Figure 4.1a. Meanwhile, the computational time does not improve significantly when the sub-particle radius is larger than 5mm, as can be seen in Figure 4.1b. Therefore a sub-particle radius of 4mm was selected as it gives the most accurate fillet shape representation while still being very stable and having a reasonable computational time.

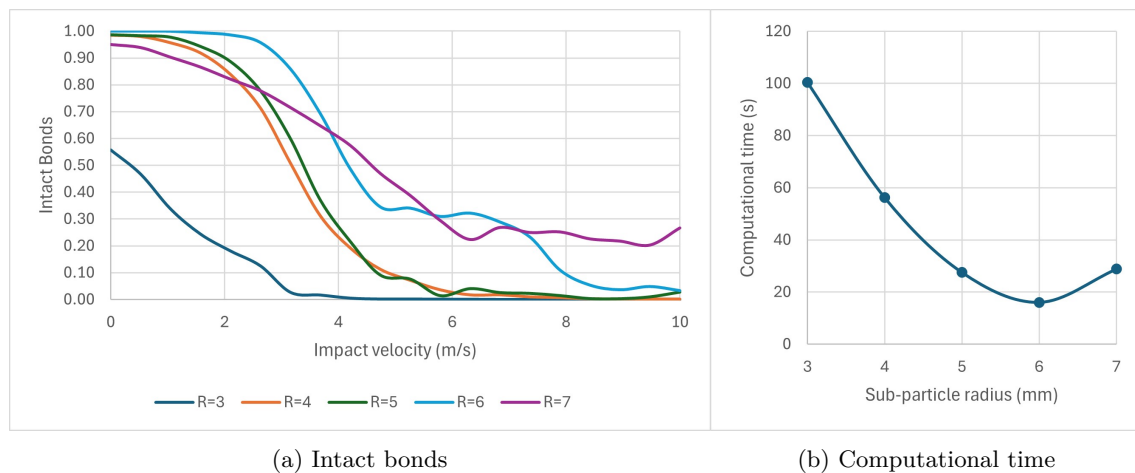


Figure 4.1: The stability over impact velocities and computational times of the 5 different flexible models of Figure 3.3

#### 4.1.2 Damping

The results of the basic damping test are found in Figure 4.2. The potential and kinetic energy of the particle dampen significantly faster when the bonds do not have tangential stiffness, as is evident from Figure 4.2a and 4.2b. As the bonding equations do not include damping terms, it was expected that a low tangential bond stiffness would result in better damping as the forces must then pass down through particle contacts and less through bond stretching. However, the total energy, which includes any energy stored in the particle bonds, spiralled out of control, causing instability and making the meta-particle explode. This instability could not be solved by significantly lowering the timestep and even remaining for a timestep to 1e-10s.

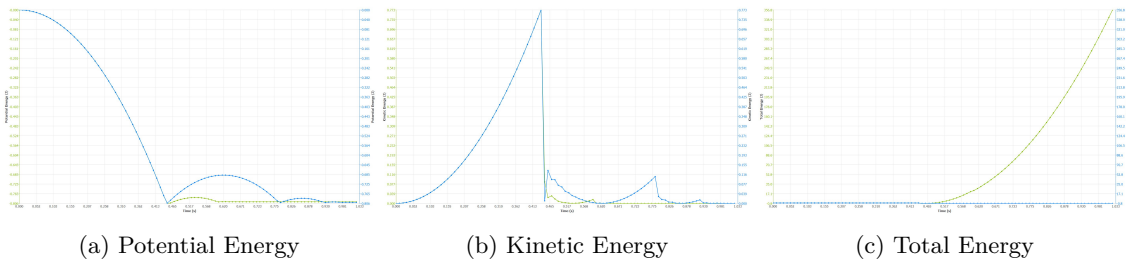


Figure 4.2: The energy graphs of a particle without tangential stiffness (green) and with tangential stiffness (blue). The blue and green lines overlap in the first part of the plot, and thus, only the blue line is visible.

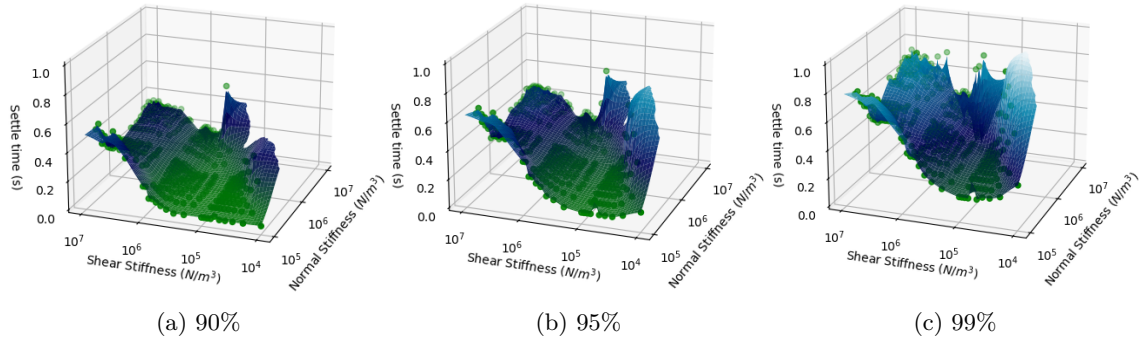


Figure 4.3: The time it takes to dampen 90, 95 and 99% of the total energy under different stiffness configurations.

Figure 4.3 shows the settling time of the model for a range of stiffness combinations. The distinct valley shape indicates that the damping is optimal when both stiffness values are roughly equal. Additionally, as is most clearly visible in Figure 4.3c, lower stiffness values result in faster dissipation of the energy.

A section on the right side of the plots in Figure 4.3 is empty; this is because the model became unstable in this region. This instability is visualised in Figure 4.4, which shows how many bonds remained intact during the damping test simulations. Figure 4.4a also indicates that the model is the most stable when the normal and shear stiffness values are roughly equal. Increasing one of the two parameters reduces stability or even leads to instability.

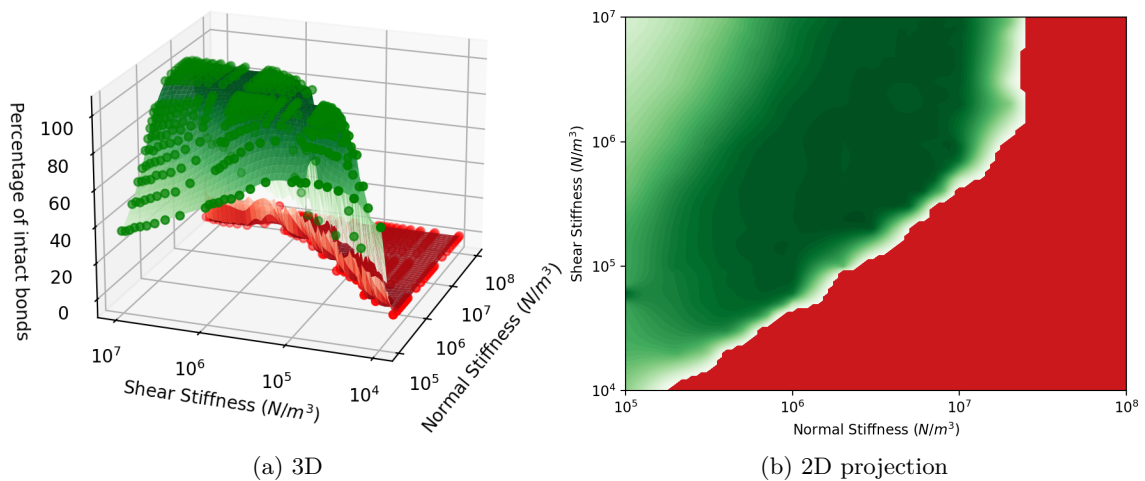


Figure 4.4: The stability of the model for different combinations, the stable-unstable boundary is also clearly visible. Darker green means the model is more stable, while red means it is unstable

### 4.1.3 Bending

The results from the bending tests can be seen in Figure 4.5. As was expected, higher stiffnesses resulted in lower angles as the model was more rigid. Both types of stiffness seem to influence the

bend angle about equally. The unstable region that was also present in the damping test can also be seen and is roughly the same. Interestingly, the custom test fillet has a small island of stable stiffness combinations that is absent for the larger model. Besides that, there is no significant difference between the bending of the custom test fillet (Figure 4.5a) and the larger model fillets (Figure 4.5b). The bending angle of the real fillet was approximately 130 degrees, so to replicate this with the model, very low stiffness values need to be used.

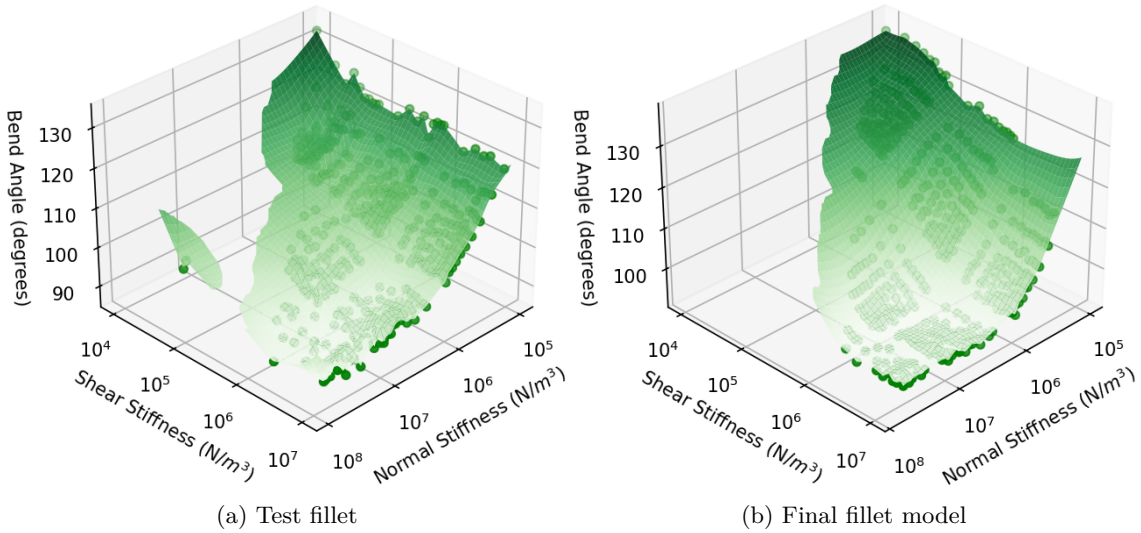


Figure 4.5: The bend angle of the models for different stiffness combinations.

#### 4.1.4 Sliding

Figure 4.6 shows the results of the simulations of the sliding test. The coefficient of friction was expected to linearly influence the sliding angle. However, the interfacial surface energy of the JKR<sub>V2</sub> model does not influence the angle at all. Additionally, the coefficient of friction has a higher impact on the sliding angle of the solid fillet than that of the flexible fillets, resulting in higher sliding angles. The sub-particle size did not influence the sliding angle either.

The results of the real sliding experiment can be found in Figure 4.7. The error bars in the plot show a high level of uncertainty in the angle measurements. Also, submerging the fillet in water before the test did not affect the angle.

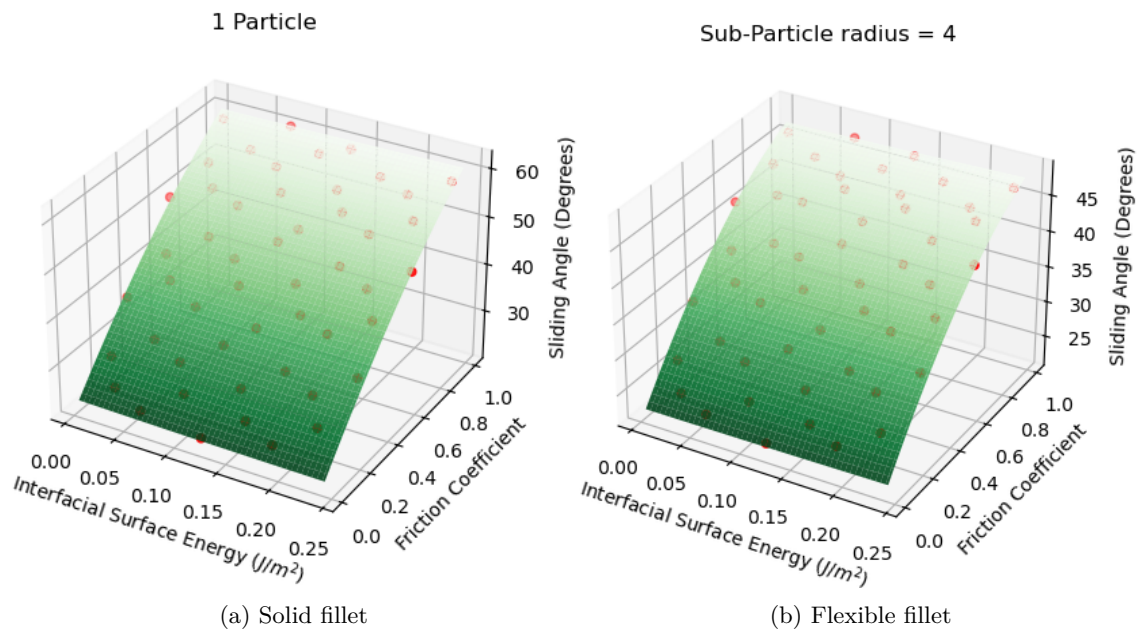


Figure 4.6: The sliding angle of different fillet models, the test was run for all sub-particle sizes mentioned in Figure 3.3, but there were no noticeable differences between the sizes.

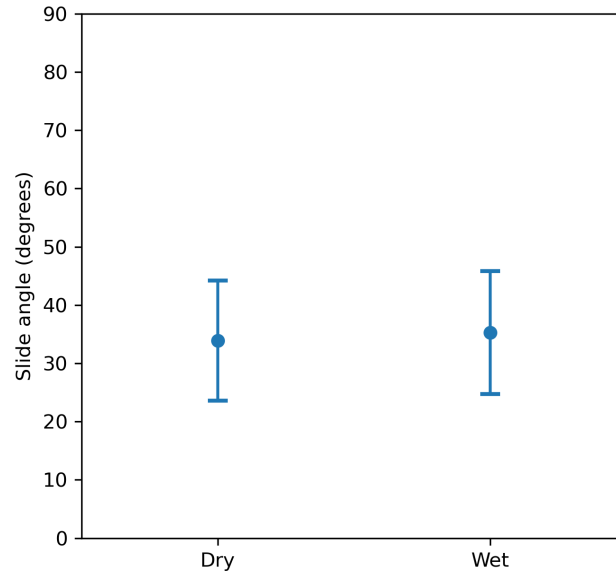


Figure 4.7: The sliding angles of a dry and wet chicken fillet on a stainless steel surface in real life.

## 4.2 Sensitivity Analysis

This section will cover the results of the different sensitivity analyses performed to test the responses of the model.

### 4.2.1 Impact Speed Stability

Figure 4.8 shows the results of the impact speed test. Figure 4.8a and 4.8c show all points in the DOE space for which more than 50% of the bonds remained intact. Figure 4.8b shows a slice of the 3D shape; in this slice, it can also be seen that lower impact velocities result in fewer broken bonds. This graph also shows that, while a stiffness combination might be very stable at low-impact velocities, it can still become unstable at higher impact velocities. The unstable region at high normal and relatively low shear stiffness values is also visible in these plots. It was expected that some stiffness combinations would be less stable than others, however, that initially stable configurations can become unstable under larger stress was surprising.

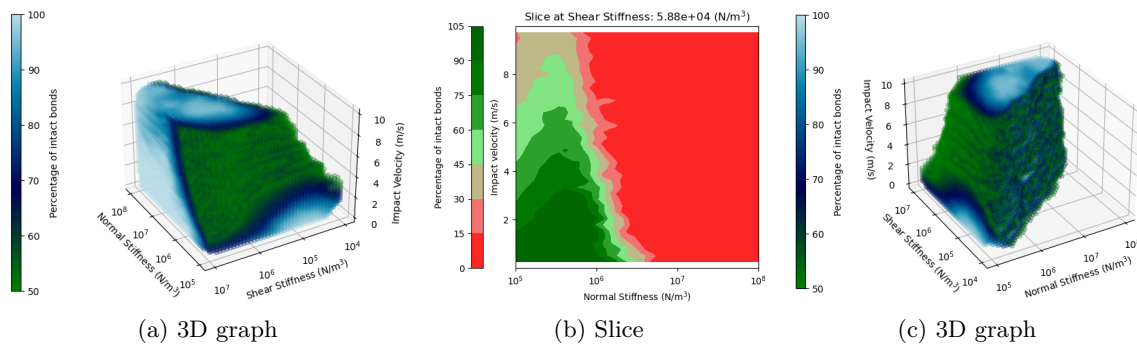


Figure 4.8: The stability of the model for different stiffness combinations under different impact velocities. The colours visualise the percentage of intact bonds for that position in the DOE space. The two 3D graphs show the same plot and contain all points for which 50% or more bonds remained intact.

### 4.2.2 Angle Stability

The angle drop test results are in Figure 4.10. Every graph shows all orientations for which the number of intact bonds at the end of the simulation is below a certain percentage. Distinct impact

orientations are less stable than others, as is evident by the growing patches in the plot as the threshold increases, culminating in a complex 3D shape. This was expected as when the fillet lands on its tip, the force is distributed across only a few particles, resulting in a higher bond stress. Figure 4.11 shows different 2D of the 75% threshold plot. To better understand the meaning of the graphs, Figure 4.9 shows the 75% threshold plot with the orientations of the fillets visualised on the different axes.

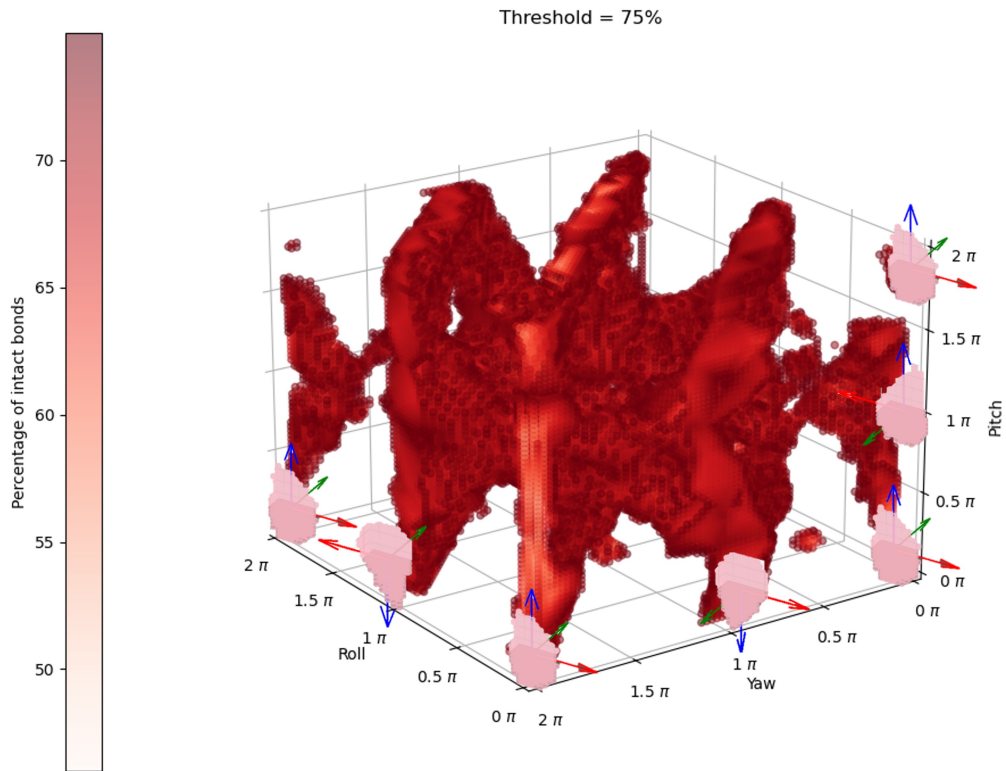


Figure 4.9: A visualisation of some of the drop orientations.

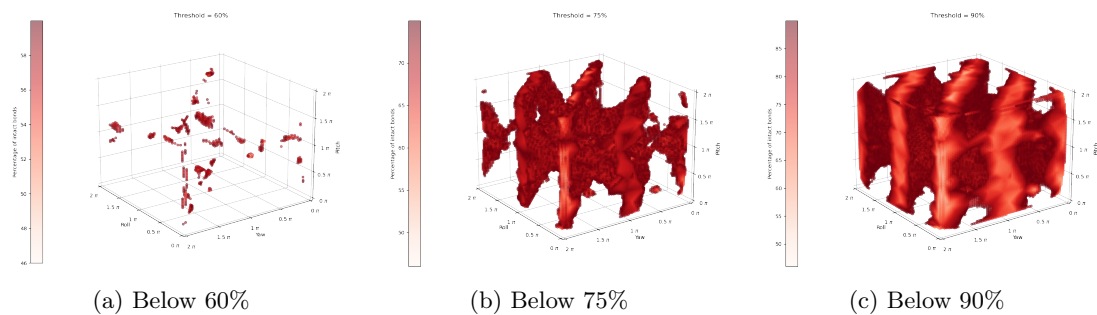


Figure 4.10: The stability of the model dropped on a floor at two m/s velocity under all possible angles. The thresholds mean that for all the plotted points, less than that percentage of the bonds are still intact.

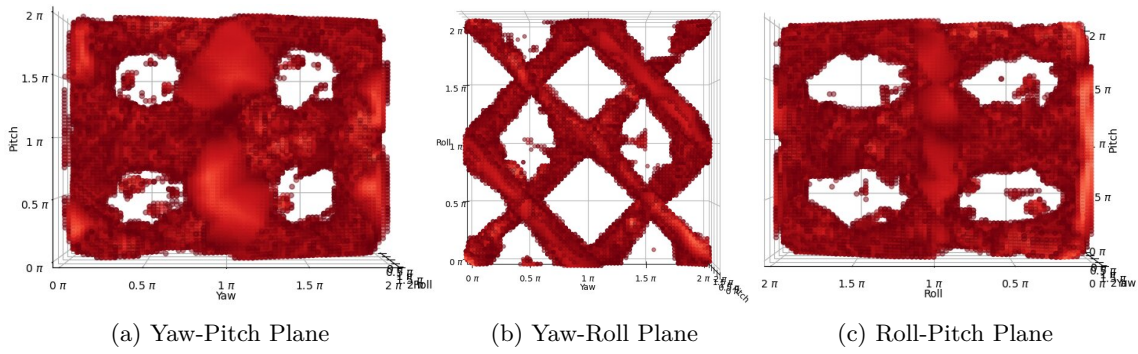


Figure 4.11: Three 2D views of the 75% threshold plot.

### 4.2.3 Scaling Stability

The results of the scaling test can be seen in Figure 4.12. The damping time gradually increases when scaling up. The damping time is very long for a scale of 0.25, but this is due to the model becoming unstable, as is evident from Figure 4.12b. Additionally, the stability of the model also drastically increases when the particles are scaled up, this was expected as scaling the model up linearly scales the bond stiffness parameters. And if these parameters were initially stable, the stability increases, as was also evident from the impact speed test of Section 4.2.1.

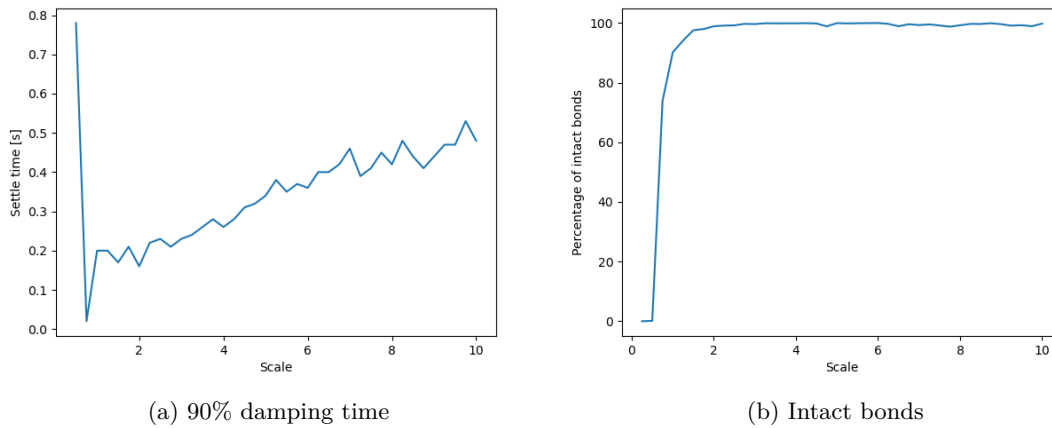


Figure 4.12: The behaviour of the model when scaling between 0.25x - 10x.

## 4.3 Compression Test

Figure 4.13 show the compression test results on the fillet block. The graph shows three consecutive tests on the same block of fillet. The second and third lines do not start at 0mm compression, indicating significant plastic strain. Overall, the material seems to show a typical visco-elastic behaviour. Additionally, when pressure was not relieved at the end of a test, the measured force started decreasing over time, which is also an indication of visco-elasticity. The resulting Young's modulus, calculated from run 1 in Figure 4.13, was 48.4 kPa.

The results of the tests on the whole fillet can be found in Figure 4.14. The 15, 1 and 0.25 mm/min lines also suggest visco-elastic material behaviour because there is a much more significant deformation if the fillet was given more time to deform. It was intuitively expected that chicken fillets would behave visco-elastically; however, applying compression at a rate of 30mm/min also resulted in a more considerable deformation, which is not consistent with that.

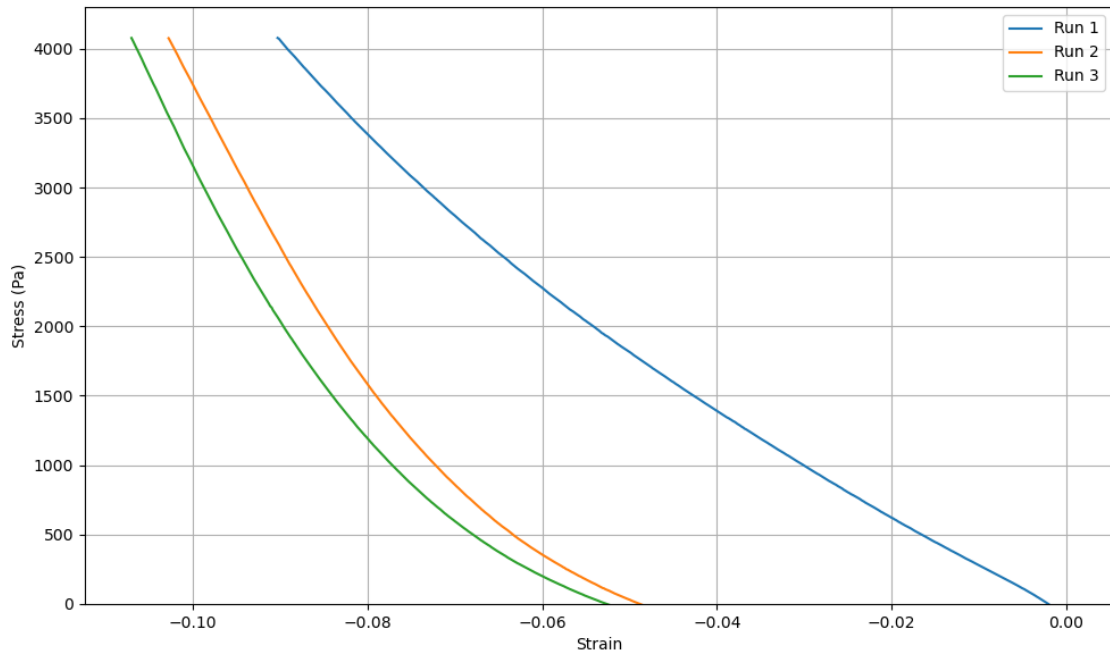


Figure 4.13: The stress strain curve resulting from the compression test.

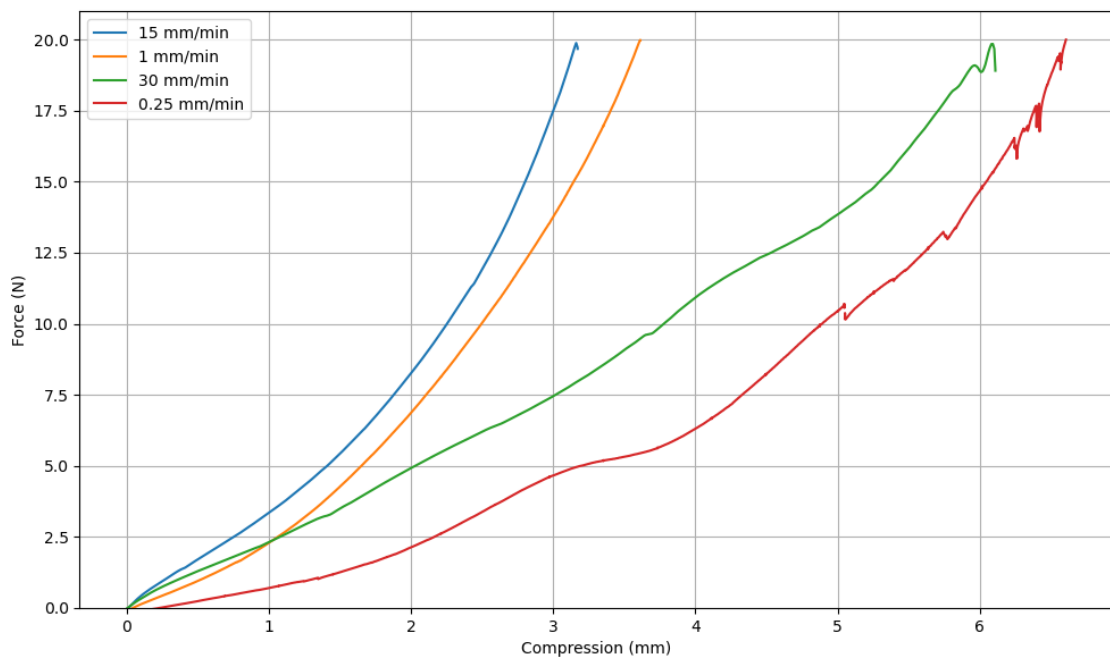


Figure 4.14: The force-displacement curves of a chicken fillet tested at different compression speeds. The tests were performed in the same order as the legend.

## 4.4 Chapter Conclusions

This chapter covered the results of the various tests performed on the DEM chicken fillet model. A sub-particle of 4mm was selected as it provides the best fillet representation while maintaining good model stability and a manageable computational time. The tests revealed that bonding stiffness parameters significantly influence the damping, flexibility and stability of the DEM model. Combinations of a high normal stiffness and a lower shear stiffness result in the fillet model becoming unstable and exploding. The real-life slide test indicated that the sliding angle does not purely depend on friction but also on adhesion. However, the adhesion model did not influence the sliding angle, so more research is required to model this. Additionally, the sensitivity analysis

revealed that model stability significantly depends on the angle and speed of impact, as well as on the scaling of the fillet. Moreover, as the results from the compression tests showed, chicken fillet exhibits complex non-elastic material behaviour. More research is required to fully understand the behaviour of this material and find modelling techniques for it. Chapter 5 will now discuss the deployment of the refined model for concept evaluation and design detailing.

# Chapter 5

## Concept Evaluation

This chapter delves into the concept design phase. DEM implementations were created of the concepts developed in Chapter 2, and their performance was evaluated, synthesising a final design that combines the best-performing sub-solutions in Section 5.1. Finally, Section 5.3 discusses creating a detailed CAD model and visualising the solution in the DEM software.

### 5.1 DEM implementations

As mentioned in Section 2.3, a preliminary model was developed for each concept and integrated into DEM to evaluate its performance and potential feasibility as a solution. These DEM implementations can be seen in Figure 5.2, 5.3 and 5.4. The performance of each concept was assessed by visually inspecting the efficacy of its sub-solutions, verifying that it fulfils its function as defined in the morphological chart.

Multiple factors influence the behaviour of the concept solutions, as depicted by Figure 5.1. The solution's performance depends on the fillet model shape, flexibility, and machine configuration, such as the dimensions and belt speed.

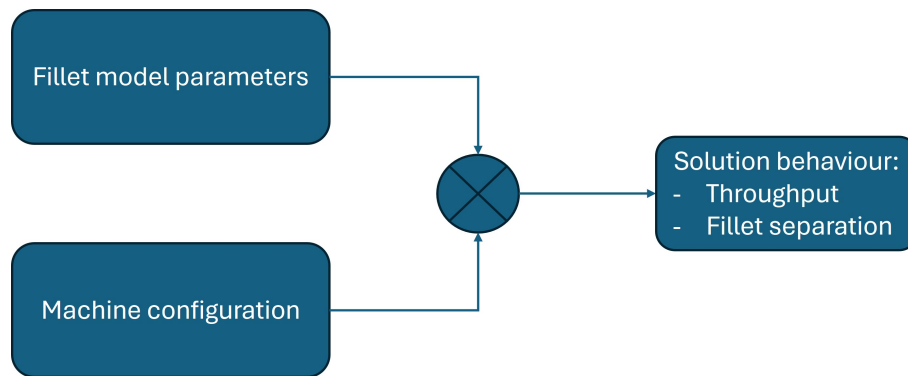


Figure 5.1: The fillet model configuration and the concept configuration influence the concept solution's behaviour.

For some of the sub-solutions in the concepts, assessing their performance together with the other parts was impossible as it would require advanced timing and control. Thus, these were tested in separate simulations. The function of removing potential air gaps was not tested in the simulations as this is impossible to evaluate with DEM using this model.

The evaluation of the three concepts' performance was conducted by visually assessing the following key performance indicators (KPIs):

- Throughput, How many fillets the solution can process per minute.
- Fillet layer height, the height of the 2D layer of fillets.
- Fillet stream width, the width of the 1D stream of fillets.
- Fillet separation, how much (if at all) the fillets get singulated.

A smaller fillet layer height and stream width are preferable, as they signify the proper formation of the 2D layer and 1D stream. Other important characteristics that will be visually compared between the solutions are:

- Flow consistency
- Subsolution cooperation
- Reliability

## 5.2 Evaluations

This section discusses the DEM evaluations of the three proposed concepts and lists each concept's main benefits and challenges. The three concepts and their specific parts can be seen in Figure 5.2, 5.3 and 5.4. Each concept should singulate the fillet in stages, from 3D to 2D to 1D to single; this is the central part of each concept. Subsequently, each concept manipulates the orientation of the fillet; this was sometimes tested in a separate simulation. The green arrows depict the direction in which the fillets should flow through the machine.

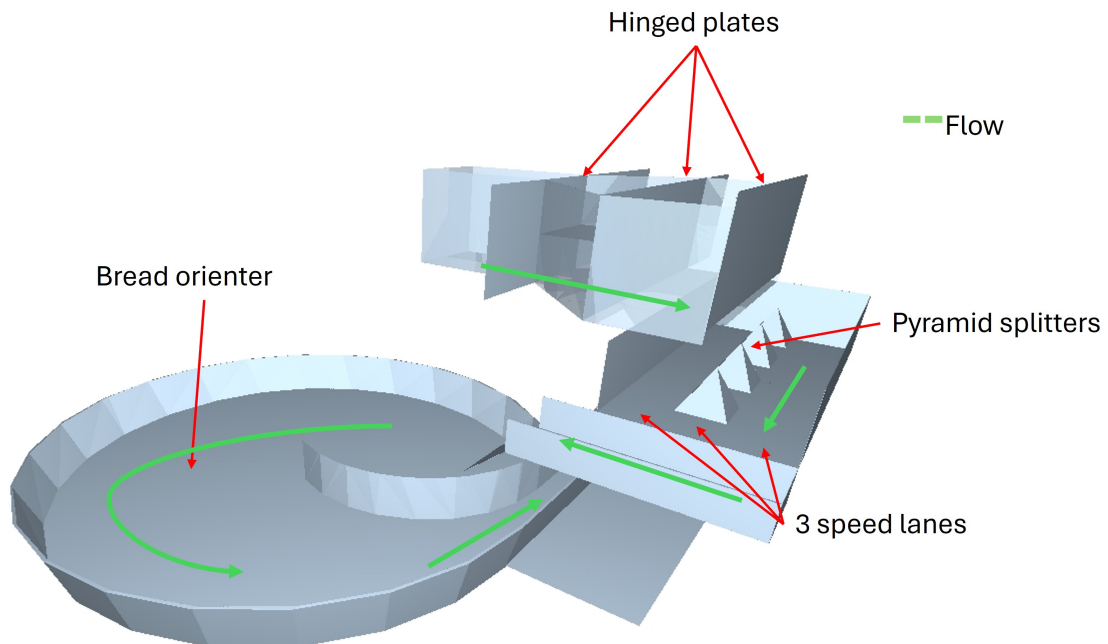


Figure 5.2: The hinged plates concept.

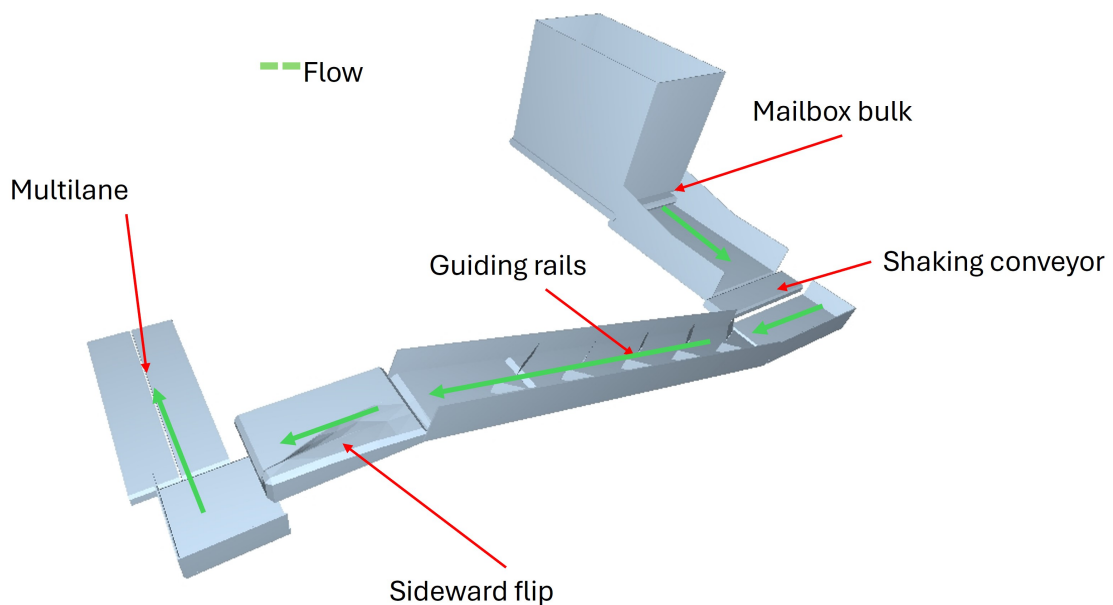


Figure 5.3: The mailbox bulk concept.

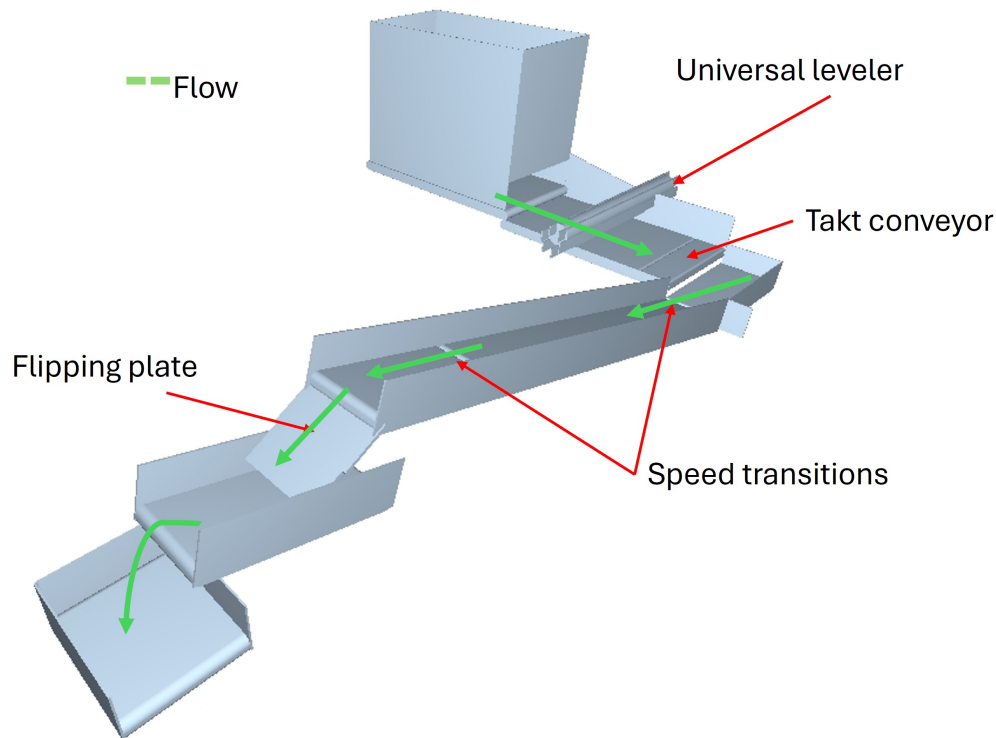


Figure 5.4: The leveller concept.

### 5.2.1 Hinged Plates Concept Evaluation

The different stages of the evaluation of the hinged plates concept can be found in Figure 5.5, 5.6 and 5.7. Altair@Motionview® was used to simulate the multibody dynamics of the hinged plates as it is a crucial part of the concept [44]. The plates successfully created the 2D layer from bulk, as seen in Figure 5.5. However, the splitters and 3-lane belt could not produce the 1D line, resulting in oversaturation of the spinning plate and bad singulation (Figure 5.6). Additionally, the fillets were pulled out of their aligned orientation by the spinning plate when leaving the disk. The scooper, seen in Figure 5.7, functioned as expected, reliably scooping up and flipping the fillets. The performance of the concept is summarised in Table 5.1.

Table 5.1: The main pros and cons of the mailbox plates concept.

Pros	Hinged plates create 2D layer reliably that is almost always 1 fillet high Outflow from bread orienter is high and consistent
Cons	No accurate fillet orientation No fillet separation

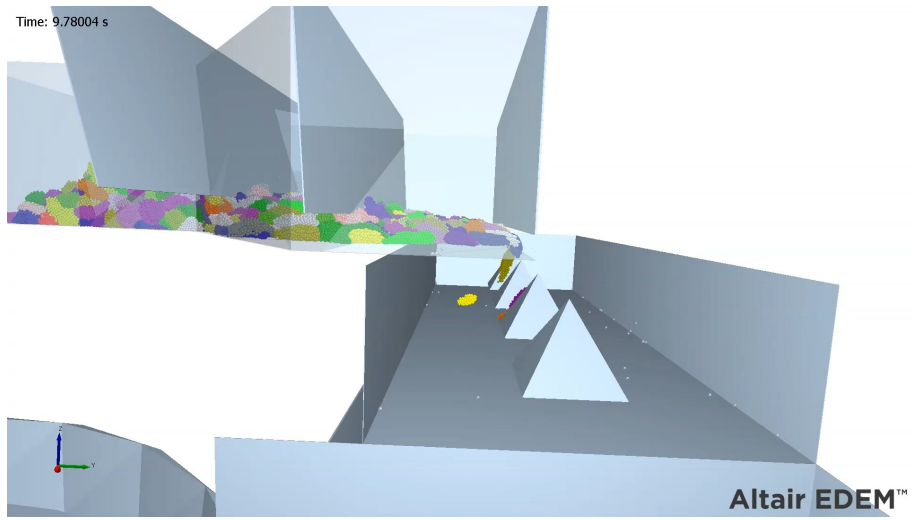


Figure 5.5: Hinged plates, pyramid splitters, and 3-lane belt.

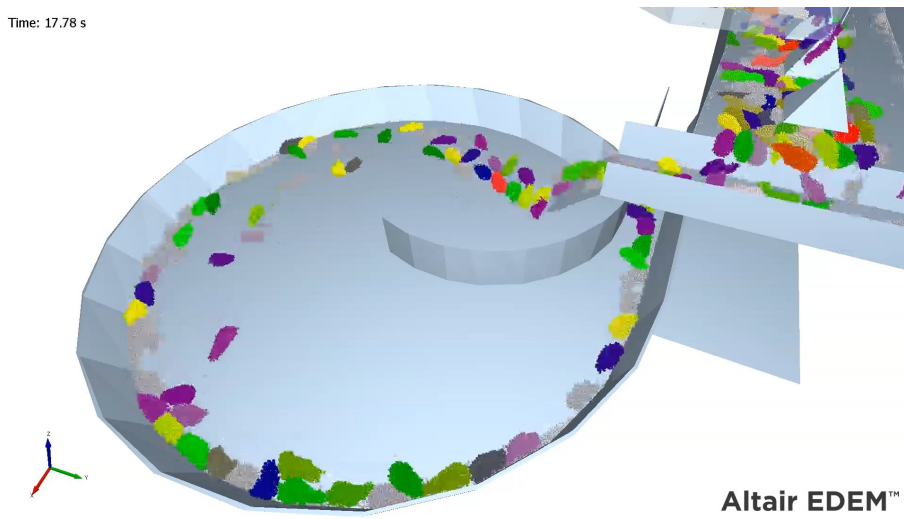


Figure 5.6: Bread orienter.

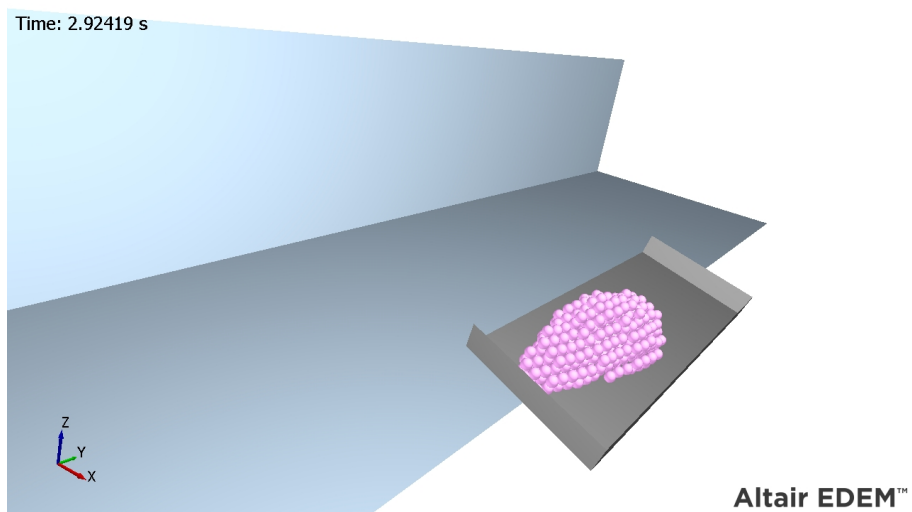


Figure 5.7: Scooper.

## 5.2.2 Mailbox Bulk Concept Evaluation

The assessment of the mailbox bulk concept is illustrated in Figure 5.8, 5.9 and 5.10. Although the mailbox exhibited potential, it failed to consistently produce a single fillet high layer without experiencing blockages. Conversely, the shaking and transverse conveyors successfully formed a one-dimensional array of fillets in conjunction with the guiding rails as seen in Figure 5.9. Nevertheless, they did not create sufficient spacing between fillets to ensure consistent singulisation. The multi-lane belt also functioned well, swiftly adjusting the orientations even when fillets were not perfectly centred but were limited to  $\pm 90$ -degree adjustments. The key takeaways from the evaluation can be found in Table 5.2.

Table 5.2: The main pros and cons of the mailbox bulk concept.

Pros	Narrow 1D array width, ensuring early orienting Precise orienting by the multilane
Cons	No consistent 2D layer flow from the bulk Multiple subsolutions needed to cover 360-degree range of rotation

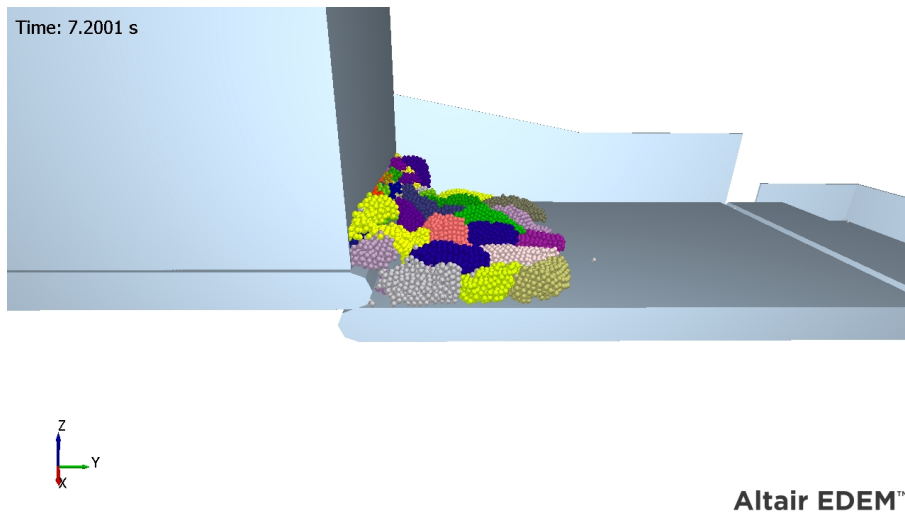


Figure 5.8: Mailbox bulk.

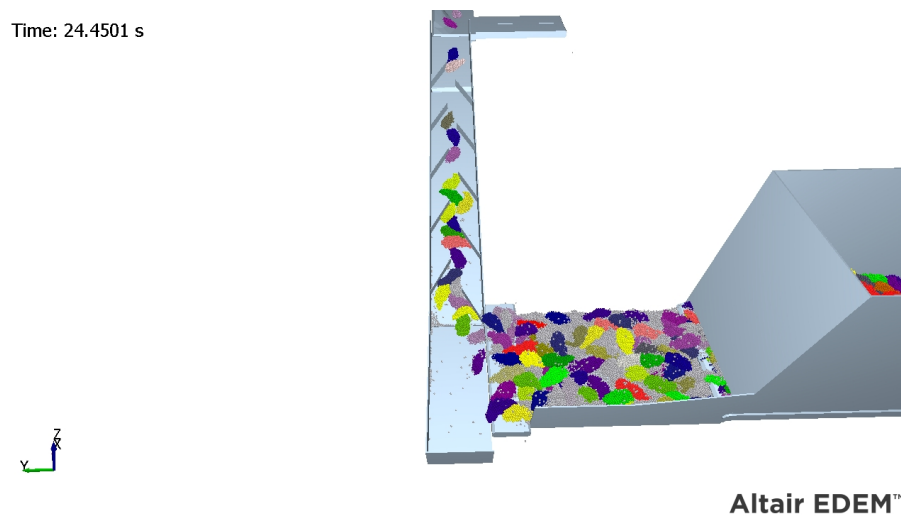


Figure 5.9: Shaker and guiding rails.

Time: 27.1801 s

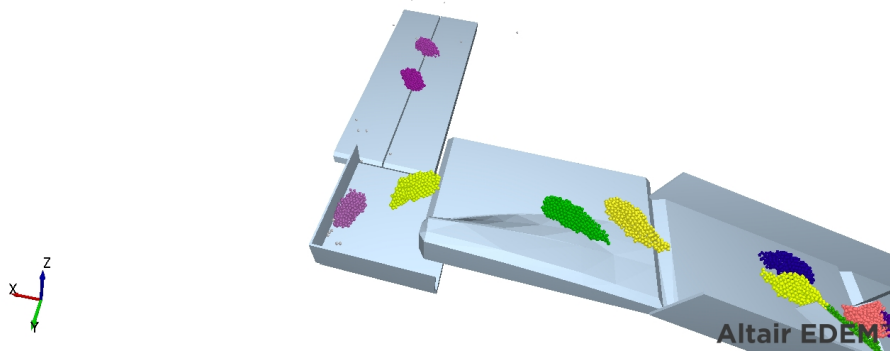


Figure 5.10: Sideflip and multilane belt.

### 5.2.3 Leveller Concept Evaluation

The evaluation of the leveller concept is illustrated in Figure 5.11, 5.12 and 5.13. The universal leveller proficiently created a fillet layer initially ; however, it became rapidly overwhelmed as additional fillets accumulated behind it, as seen in Figure 5.11. The takt conveyor performed sufficiently but failed to consistently produce a 1D array of fillets as often it is quite wide and the fillets were still a bit bunched up. Despite this, the belt speed transitions were largely effective in singulating the fillets, albeit with an inconsistent flow, evident from Figure 5.12. The subsequent flipping plate demonstrated excellent performance. Functioning as a slide, it prevented the fillets from overturning, whereas when it moved out of the way, it resulted in the fillets flipping over (Figure 5.13). This system allowed precise control over which side of the fillet, skin or bone, faces up. Overall this concept could perform very well with the addition of more subsolutions to solve the overload and wide 1D line issues. The performance of this concept is summarised in Table 5.3.

Table 5.3: The main pros and cons of the leveller concept.

Pros	Good 2D layer height Good fillet separation
Cons	1D line is quite wide Leveller gets overwhelmed requires cooperation

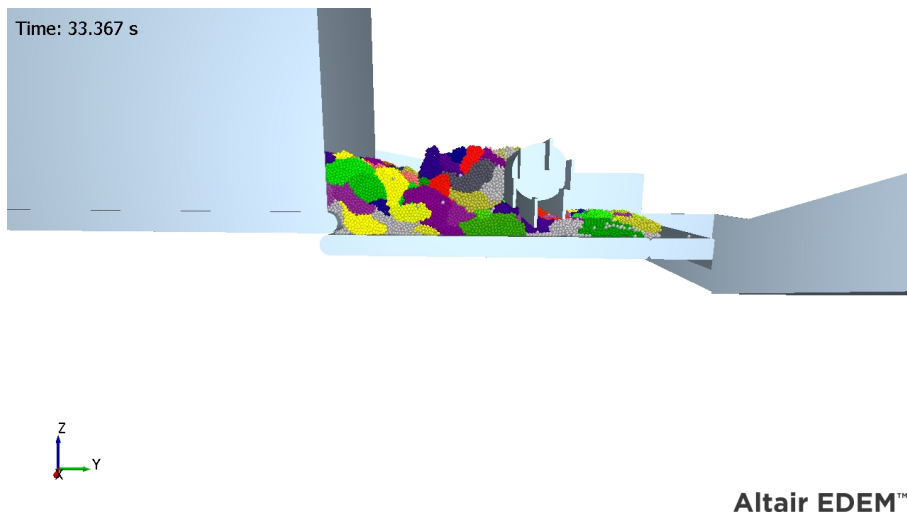


Figure 5.11: Universal leveller.

Time: 15.9601 s

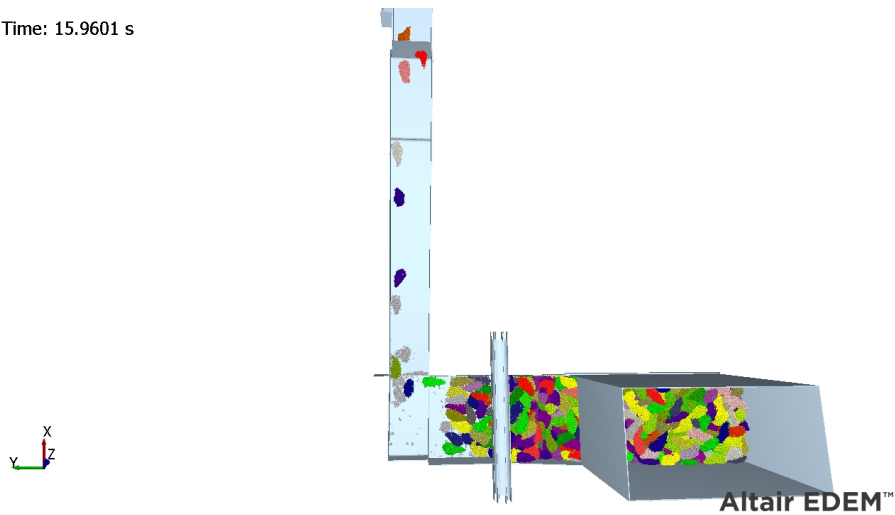


Figure 5.12: Speed transitions.

Time: 17.01 s

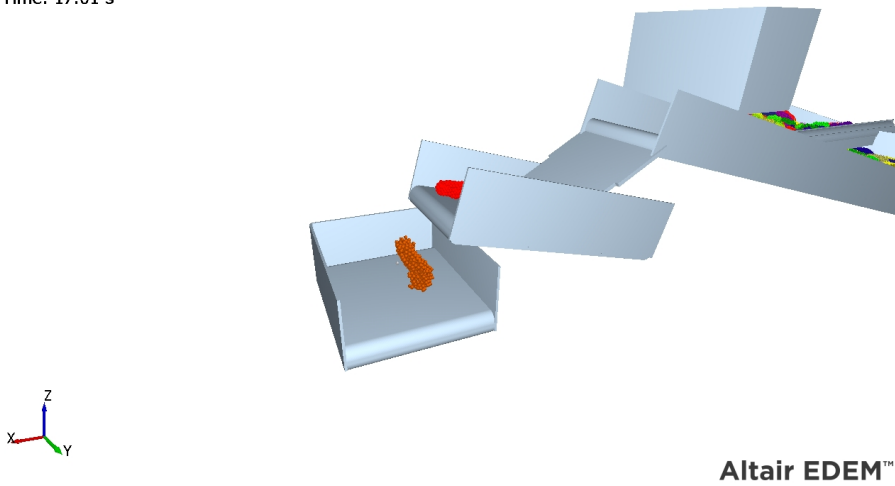


Figure 5.13: Flipping plate.

Table 5.4: The scores of the three concepts.

Concept	Create layer	Create stream	Singulate	Orient 1	Orient 2	Final Score
Hinged plates	8	4	2	9	6	5.8
Mailbox bulk	7	5	8	3	8	6.2
Leveller	7	9	7	9	7	7.8

The performance evaluation of individual components within each concept during simulations was quantified, as detailed in Table 5.4. The Leveller concept demonstrated the highest overall performance, though other concepts showed significant efficacy for various sub-solutions. Consequently, a final concept was synthesised, integrating all top-performing sub-solutions and combining sub-solutions that complement each other, such as the mailbox bulk and the leveller. This consolidated concept is illustrated in Figure 5.15. The mailbox bulk executes the initial stage of singulation, but instead of creating a single-fillet thick layer, this process produces a multi-fillet thick layer to prevent clogging and ensure a consistent flow. This smaller block of fillets is then directed to the universal leveller, forming the 1D layer while avoiding overloading. The takt conveyor, aided by guiding rails, takes a line this layer into the 1D array, with the guiding rails removing any clumps and making the flow more consistent. An additional flipping plate mechanism is incorporated to achieve the desired fillet orientation, addressing the multi-lane belt's limitation of rotating fillets by no more than  $\pm 90$  degrees. This supplementary mechanism ensures control over the direction in which the tip of each is facing.

Consequently, all eight potential states a fillet can adopt beyond the guiding rail section (Figure 5.14) are accurately managed. A speed transition finalises the singulation process, and the multi-lane belt positions the fillets at the required angle. Finally, the squeeze roller will remove potential air gaps. This solution was selected because it is the simplest and cheapest solution.

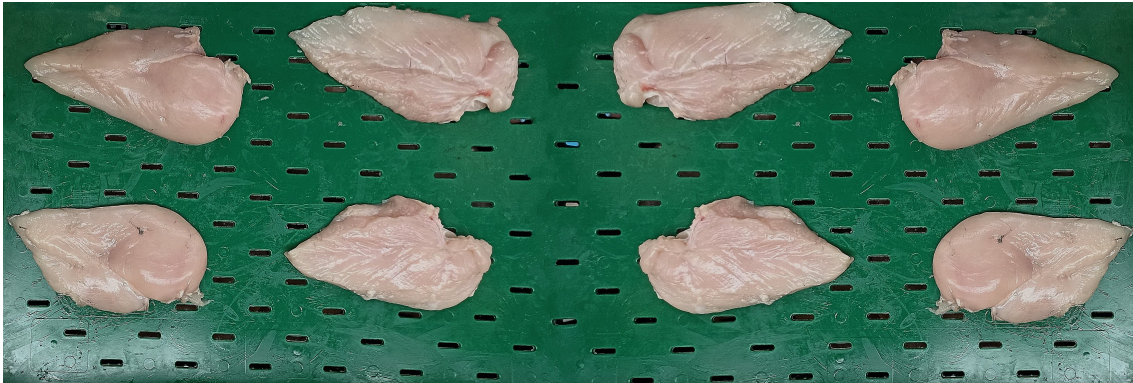


Figure 5.14: The eight possible fillet orientations when leaving the guiding rail section.

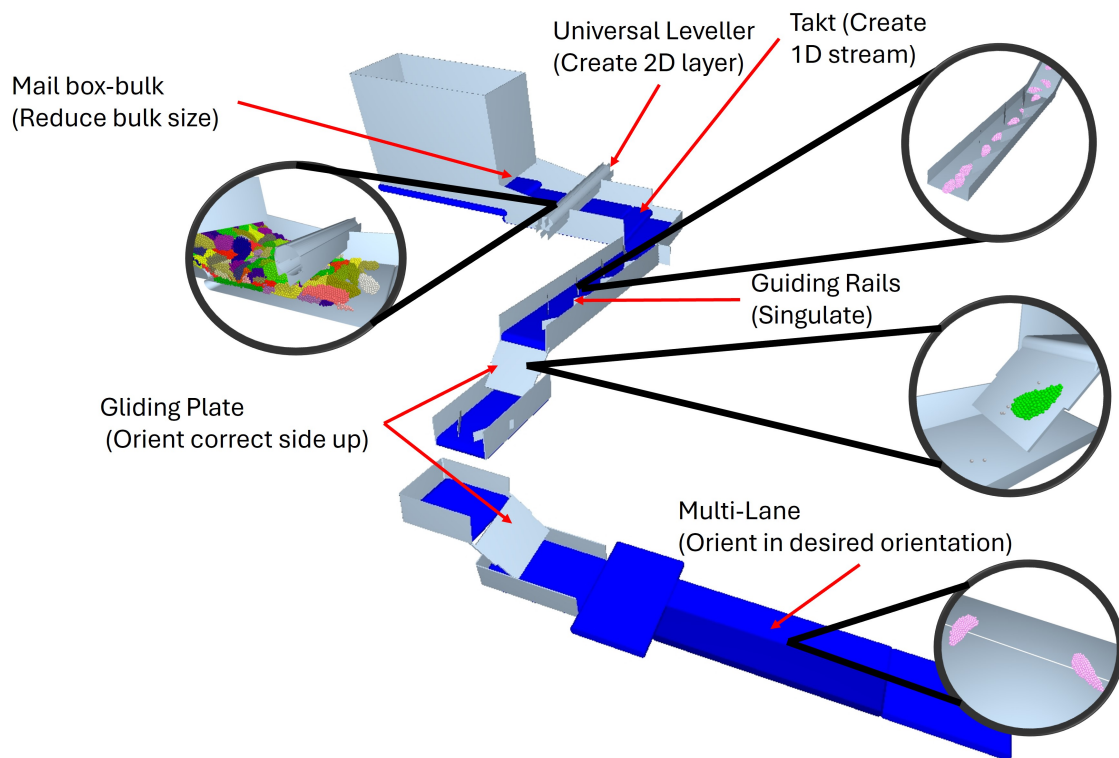


Figure 5.15: The combined concept, the blue components are conveyors.

### 5.3 Detailing the Design

The combined concept was detailed with CAD software, significantly relying on pre-existing elements from the Kortlever repository, such as conveyor belts. The derived model was subsequently imported into the DEM software for enhanced visualisation and iterative refinement. This methodology further enables a visual of the operational concept for the client, thus ensuring transparency in the design and facilitating early-stage feedback. Early intervention is advantageous, as it provides cost-effective modifications during the preliminary phases instead of incurring higher expenses in the latter stages when specific components might already be fabricated.

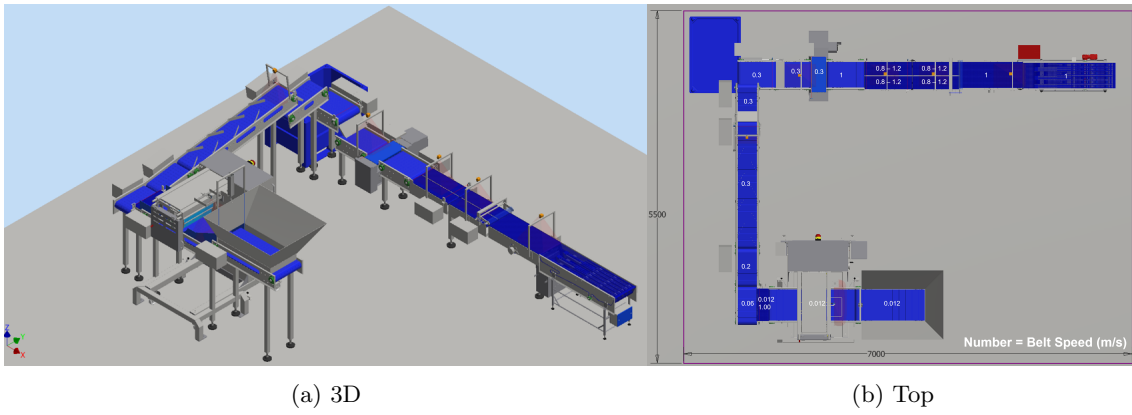


Figure 5.16: The CAD model of the concept.

Figure 5.16 provides an overview of the CAD model, while Figure 5.16b delineates the belt speeds across the various sections in meters per second. The twin speeds on the takt conveyor represent the standard and takt speeds. All these velocities were iteratively obtained using the model to ensure optimal and consistent flow, thereby establishing a benchmark for subsequent optimisation and fine-tuning during the actual construction of the setup.

The process begins with the mailbox bulk storage, as illustrated in Figure 5.17. A cylinder can adjust the height of the opening, facilitating optimal flow and mitigating obstructions. The fillets descend onto a secondary conveyor, traversing beneath the universal leveller. A level sensor situated in front of the leveller, represented by the red beam, ensures a sufficient quantity of fillets is delivered to the leveller by regulating the velocity of the bulk belt accordingly.

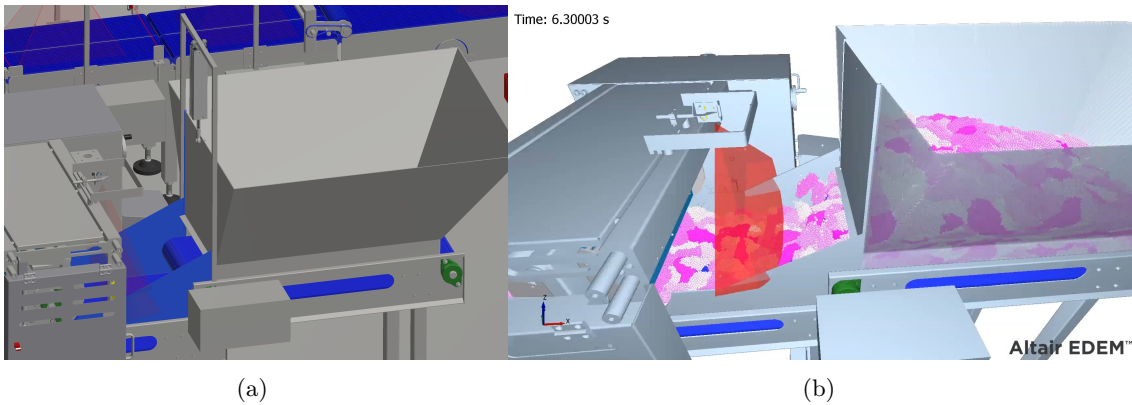


Figure 5.17: The mailbox bulk.

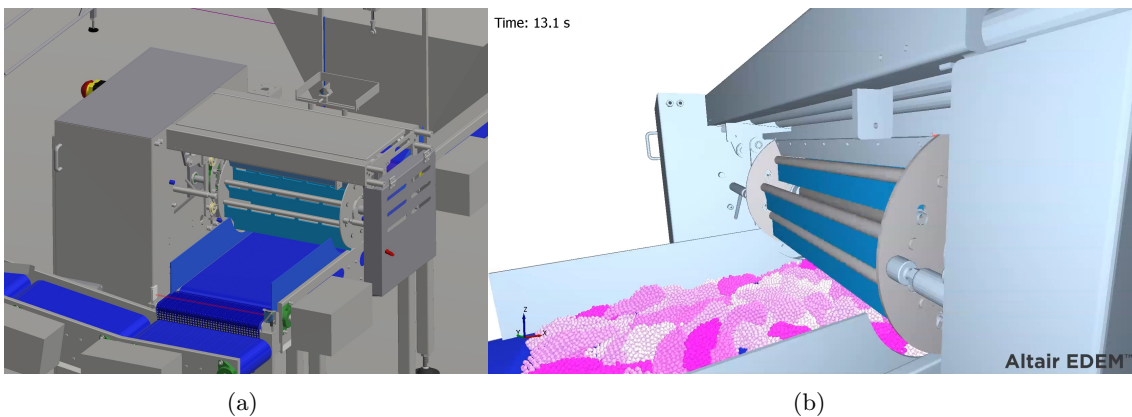


Figure 5.18: The universal leveller.

The universal leveller, Figure 5.18, ensures only a 1-fillet thick layer proceeds down the line. The leveller has eight blades that swiftly spin around and swipe the fillets back. These blades remain

vertical and are made of polyurethane (PU), a flexible and food-grade polymer that ensures hygiene and avoids damage to the fillets.

The levelled layer is subsequently conveyed onto the takt conveyor, as illustrated in Figure 5.19a. The takt is actuated when the fillets intercept the laser, triggering the extraction of a row. This row then traverses several velocity transitions, which separate the fillets, thereby singulating them. These fillets proceed to a segment equipped with guiding rails, further singulating them and aligning the fillets with the belt. This segment also exhibits an upward motion, facilitating the fillets' glide along the belt by diminished frictional forces (Figure 5.19b).

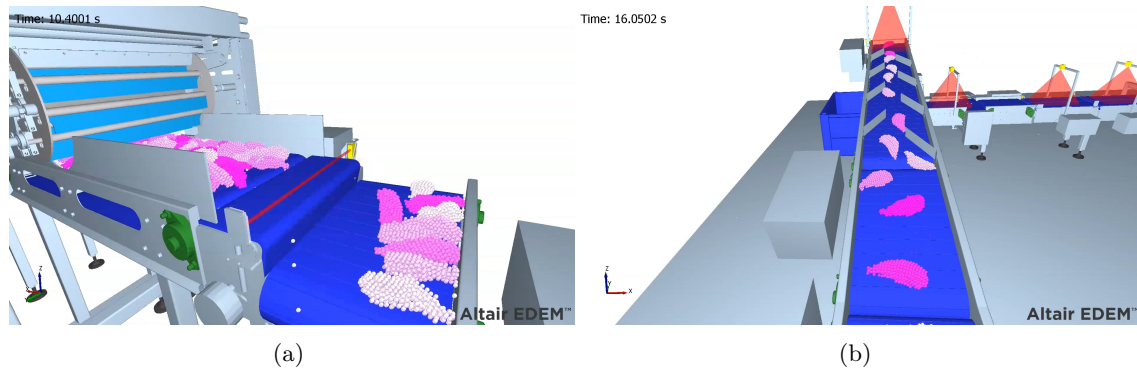


Figure 5.19: The takt and aligning section.

At the end of the guiding rail section, a camera furnished with AI vision software supplied by Vierpool is positioned [45]. This camera determines within 100 milliseconds whether the fillet is inherently left or right-oriented, whether the skin or bone side is facing upward, and what its orientation on the belt is (Figure 5.20a). Based on these determinations, the position of both flipping plates is adjusted to ensure the correct side faces upwards and the fillet's thicker portion is aligned at the rear. This configuration minimises the angle adjustment required to attain the orientation depicted in Figure 1.3a. These flipping plates are illustrated in Figure 5.20b and 5.20c. If the preceding camera finds that the fillets are not sufficiently singulated, the subsequent conveyor belt momentarily reverses to deposit them in a rejection crate (Figure 5.20d). This crate could potentially be replaced by an automated return feed mechanism to bulk storage in future implementations to enhance system autonomy.

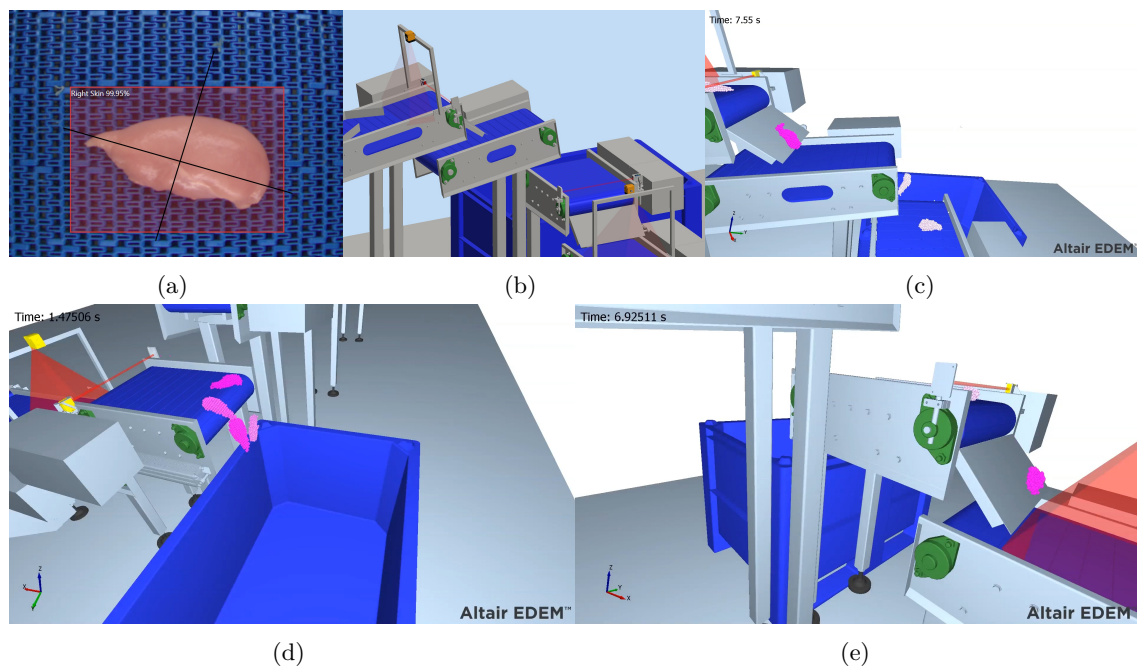


Figure 5.20: The rejection crate and flipping plates.

After the flipping plates section, an additional camera is placed to determine the position of the fillet on the conveyor belt. Should the fillet be misaligned, the subsequent unit rectifies its

horizontal position to ensure central alignment. Proper centring of the fillet is imperative for both sides of the multi-lane system to secure a grip and adjust its orientation. While on the multi-lane, another camera continuously monitors the fillet's current orientation. This real-time orientation data informs adjustments to the belt speed, occurring at approximately 25 millisecond intervals. The programmed logic computer (PLC) operates in a 10-millisecond loop, and the transmission of information to the motor frequency controller requires approximately five milliseconds, which gives the sensor system 10 ms to measure the angle, which is more than enough according to the supplier [45]. Given the requirement for the system to process approximately one fillet per second, two orienting units are used because each unit is only capable of accurately adjusting a single fillet at a time. Otherwise, there would not be enough time to reliably adjust the orientation of a fillet before the next fillet rolls on. Upon achieving the correct orientation, the fillet advances under a roller, which presses it onto the conveyor to expel any residual air underneath. After the roller verifies the fillet's orientation, a final camera is positioned, with any misaligned fillets removed from the process. The configuration of the orientation units and the squeeze roller is shown in Figure 5.21.

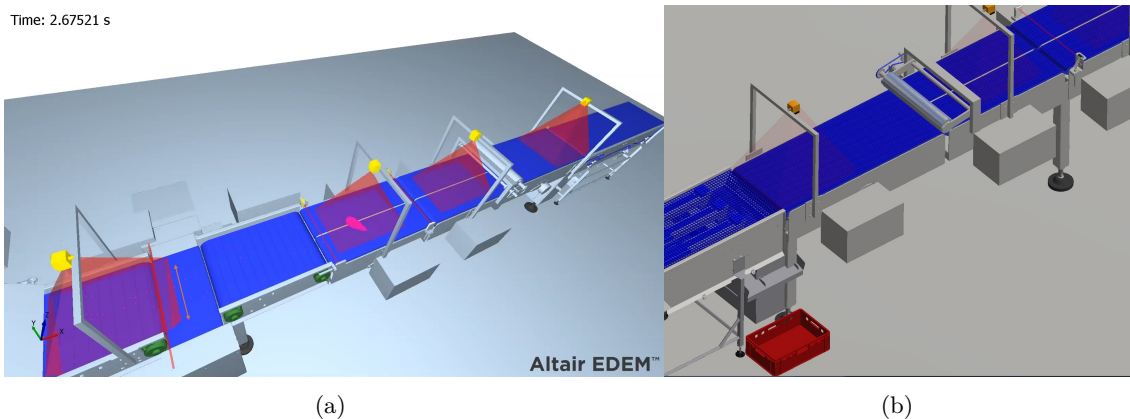


Figure 5.21: The centring and orienting units.

## 5.4 Chapter Conclusions

This chapter discussed the deployment of the refined chicken fillet DEM model. The model proved adept at predicting chicken fillet behaviour on the concept solutions, providing insights into the concepts' throughput, consistency and reliability. Using the results of the model evaluations, a combined concept was refined from the best-performing subsolutions of the different concepts. These subsolutions complement each other and ensure an optimal solution. Subsequently, the model proved valuable for detailing this combined concept, aiding in configuring belt speeds and providing a pleasing visualisation. To substantiate the model's validity and some design subsolutions, Chapter 6 will now address two empirical experiments.

# Chapter 6

## Validation Experiments

Validation experiments are a crucial step in developing and refining any simulation model. While the simulations offer a powerful tool for predicting the behaviour of chicken fillets, their results are only as reliable as the assumptions and parameters on which they are based. Without experimental validation, there is a risk that the model might oversimplify real-world dynamics or overlook critical factors, leading to inaccurate or misleading outcomes. By conducting a validation experiment, the simulated results can be compared with empirical data, discrepancies can be identified, and the model can be adjusted if necessary.

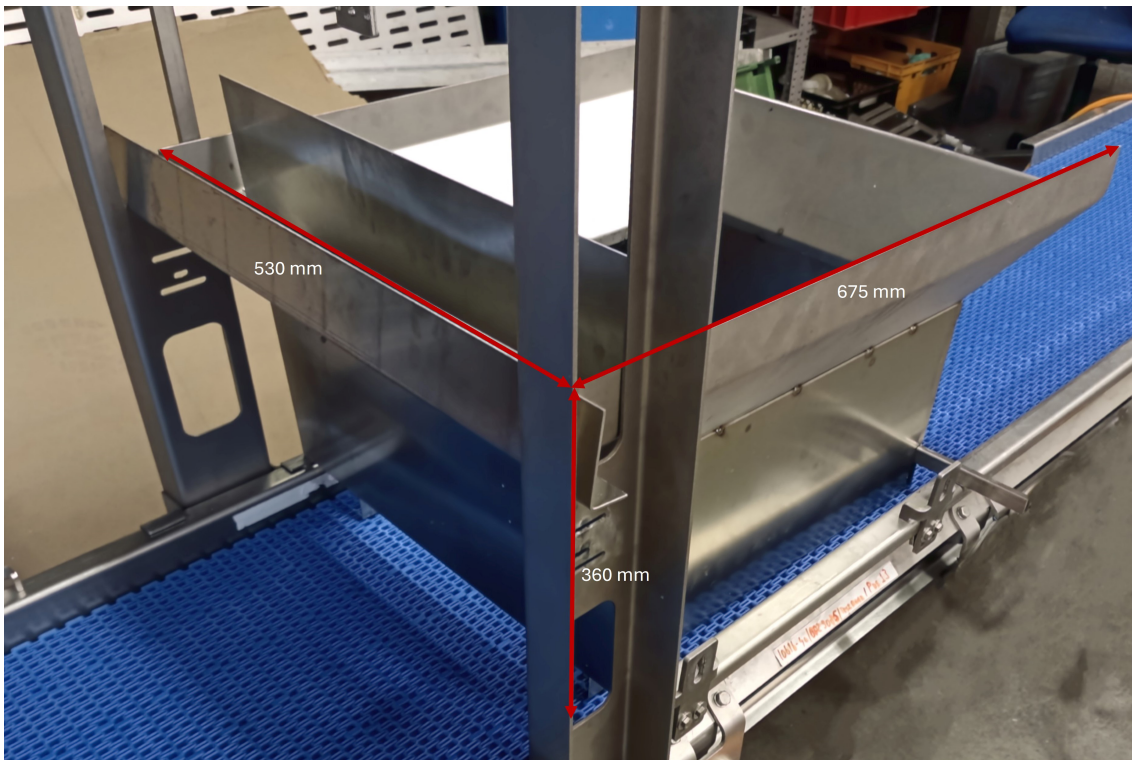
The mailbox-bulk and the squeeze roller were selected for validation experiments due to their critical role in the design and the necessity to verify their functionality. The mailbox bulk will provide a crucial insight into the bulk behaviour of chicken fillets. Moreover, the squeeze roller was selected because it is impossible to assess its performance with simulations in DEM. The experiments were conducted on a pre-existing testing conveyor at the Kortlever facility. During the tests, five crates of Plukon chicken fillets were utilised. The experimental setup is illustrated in Figure 6.1.



Figure 6.1: The experiment setup.

### 6.1 Mailbox Bulk

A miniature version of the mailbox bulk storage was created by cutting, bending, and welding several pieces of metal plates underneath an old hopper from storage. A separate metal plate was inserted in a slot and fixed with glue clamps to configure the opening height. The mailbox hopper can be seen in Figure 6.2.



(a)

Figure 6.2: The smaller version of the mailbox bulk.

During the experiments, the hopper was filled up with chicken fillets, at which point the conveyor was turned on, and the flow of fillets through the opening was observed. Additionally, in a few tests, a little water was added to the bulk to observe the effect on the flow. Some experiment images are in Figure 6.3.



(a) Flow

(b) Stuck

Figure 6.3: The mailbox bulk test with chicken fillets.

At the minimum opening height of 4.5cm, the fillets initially flowed out of the hopper. However, the flow was not constant, especially when the hopper was almost empty. Additionally, when some

water was added to the mix, the fillets got stuck, and the conveyor belt slid underneath the fillets. The belt could not pull the fillets through the opening, as seen in Figure 6.3b. Then, the opening was enlarged to around 6cm, close to the height of two fillets. A stable outflow of fillets from the hopper could be observed, even when water was added to the bulk, proving the feasibility of this concept as a first step in the singularisation process.

The experiment is compared to the model in Figure 6.4. As can be seen, the model behaviour looks pretty much identical to the experiment. In both the experiment and the simulation, the fillets curl up as they leave the hopper due to their flexibility.

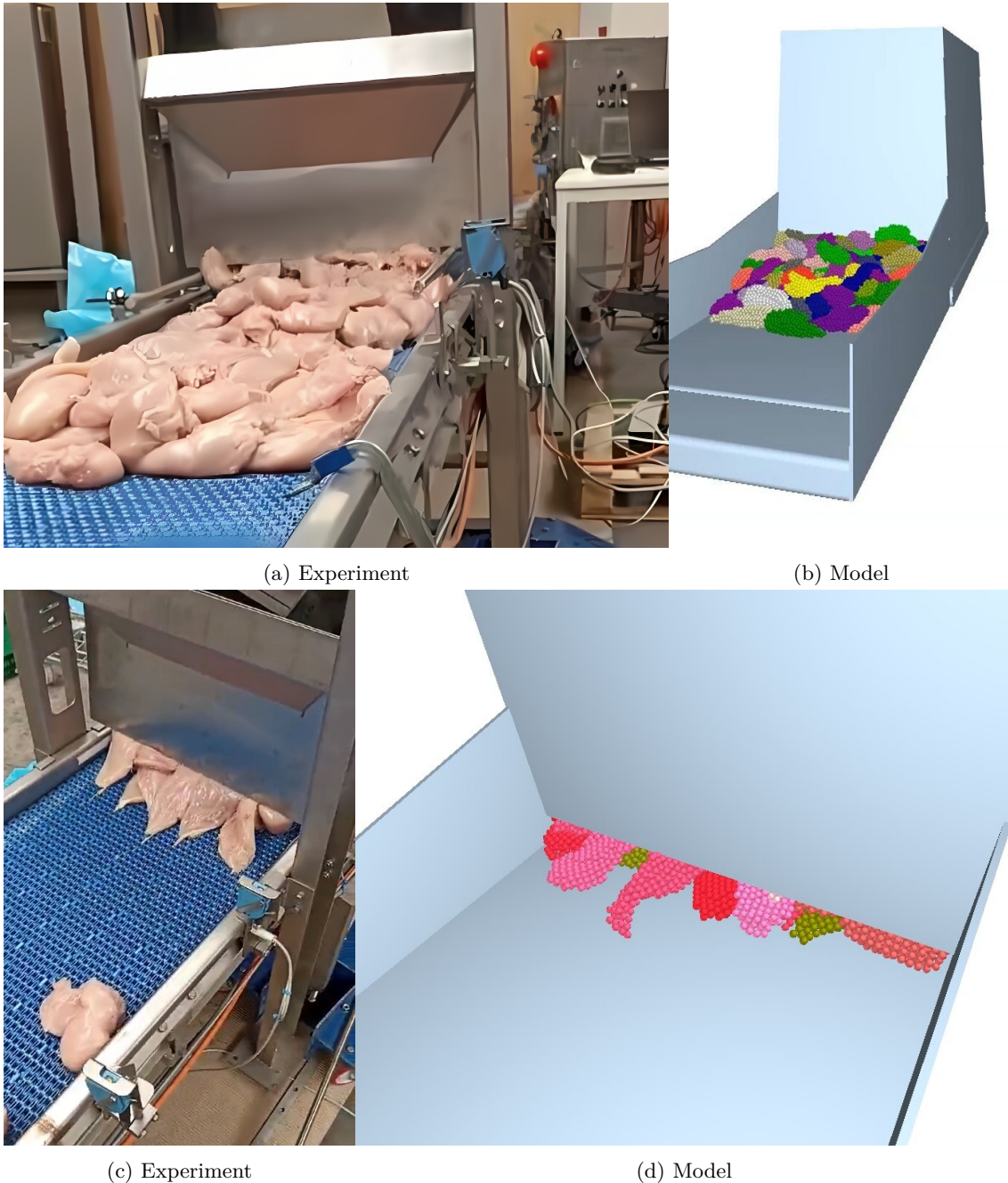


Figure 6.4: The mailbox bulk test with chicken fillets compared to the same setup in the DEM software.

## 6.2 Squeeze Roller

The other component that was tested was the squeeze roller; the height of the roller above the belt could be adjusted if needed. The image of the roller can be seen in Figure 6.5. The green arrows in Figure 6.5b show roughly the range in which the roller can move freely up and down, creating some flexibility. The red arrows show the range in which the height of the roller can be adjusted.

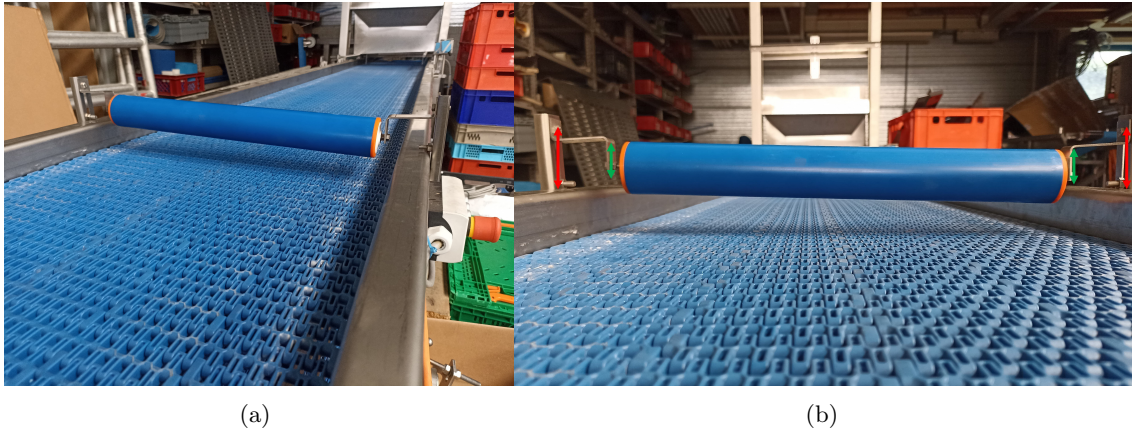


Figure 6.5: The squeeze roller assembled on the testing conveyor.

Figure 6.6 shows the squeeze roller during the test. The roller demonstrated high efficiency in flattening the fillets, provided that the tip of the fillet faced forward. Conversely, improper orientation caused the fillet to become stuck behind the roller or inadequately flattened. This is due to the gradational increase in the thickness of a chicken fillet from its tip to its base. If the roller initially encountered the fillet's thickest portion, it could not progressively flatten it, unlike when the thinner portion led. This issue could be mitigated by enlarging the roller and introducing controlled actuation. Such actuation would ensure the roller initiated pressure application only after the thickest section of the fillet was positioned beneath it. Consequently, this would prevent the fillet from becoming stuck while ensuring effective flattening to remove any air pockets underneath.

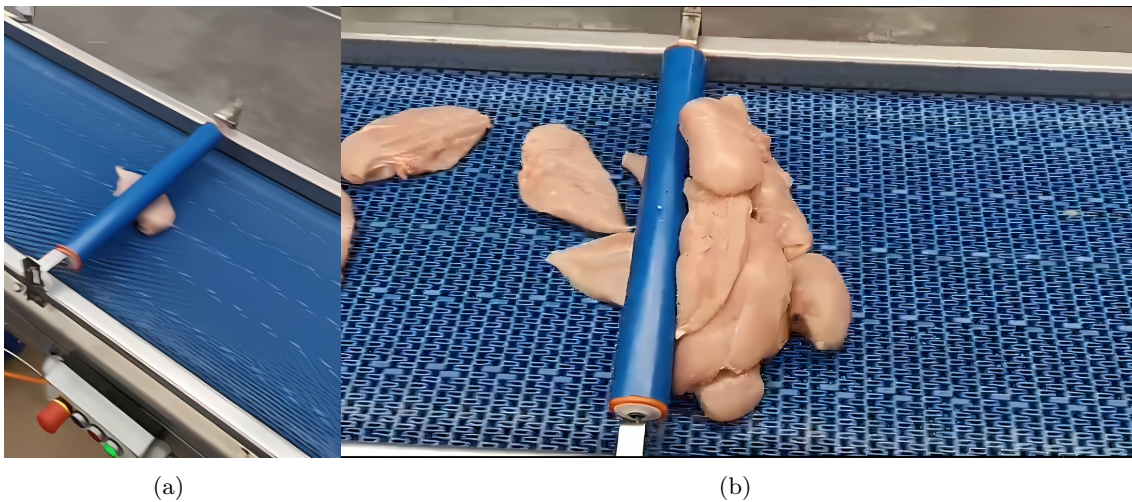


Figure 6.6: The squeeze roller interacting with chicken fillets.

## 6.3 Discussion

The results of this study provide a crucial understanding of the behaviour of chicken fillets under diverse conditions and the factors influencing the stability and dynamics of a DEM fillet model. The research proves the feasibility of constructing a DEM model of a complex product within a practicable timeframe, prioritising an adequate representation over a perfect model. This methodology significantly accelerates the design process by enabling preliminary performance assessments and assisting in the detailing of design specifics.

### 6.3.1 Insights Gained in this study

The damping tests revealed that maintaining an equal balance of low normal and shear stiffness is crucial for optimal damping and stability in this setup. Although removing tangential bond stiffness seemed to lead to better damping, it made the model unstable. This instability was surprisingly not a function of the timestep being too high, as it persisted even at a timestep of 1e-10s. Analysis of damping with full chicken fillet particle models also revealed that this instability occurred only if the normal bond stiffness was significantly higher than the shear stiffness. However, when the shear stiffness was higher than the normal stiffness, it did not cause complete instability, but the resulting model was less stable than that of balanced stiffnesses. This was unexpected because an increase in stiffness should intuitively make the model stiffer and, thus, more stable. The damping tests also showed that it is possible to achieve sufficient damping without damping terms in the bonds or introducing global damping in the simulation, as is often done in other research considering DEM models with meta-particles.

The impact speed sensitivity analysis also shows the region of unstable stiffness combinations. The test additionally reveals that more significant disturbances to the model can cause initially stable stiffness combinations to become unstable, like an exothermic reaction.

In the bending tests, the higher stiffness values expectedly resulted in lower bending angles, indicating increased rigidity, with both normal and shear stiffness influencing the bending angle equally. Achieving a large bending angle of around 130 degrees, replicating the behaviour of real fillets, required lower stiffness values. This finding is consistent with the literature on flexible materials, where material stiffness is known to significantly affect bending properties. Stability, damping, and bend angle are the three main considerations influencing the choice of bond stiffness parameters to create an accurate chicken fillet DEM model.

The sliding tests demonstrated that the coefficient of friction influenced the sliding angle linearly, while interfacial surface energy and sub-particle size did not have a significant effect. The slide test involving real fillets supports this observation, as the sliding angle of the wet fillets was not significantly different from the dry fillets. This suggests that the sliding behaviour of chicken fillets is primarily controlled by the coefficient of friction and less so by adhesion. However, the real-life slide test did show a high level of uncertainty which is not indicative of pure frictional sliding. In addition, introducing water to the bulk of the fillets significantly influenced the flow when testing the mailbox concept, as it caused the conveyor belt to slip. Thus, more research is needed to fully understand the adhesive behaviour of chicken fillets and to create modelling methods for this.

The scaling of the model exerted a significant influence on its stability. This phenomenon can be attributed to the linear relationship between the radius of the bond, the tangential stiffness, and the normal stiffness. Consequently, as a stable stiffness configuration was scaled, the overall stability improved as the stiffness increased. This observation aligns with the results of the bending, damping, and impact speed tests, where higher stiffness, if balanced, results in a more stable model. Furthermore, the elongation of the damping time with an increased scale corresponds to the findings of the damping tests, where elevated stiffness values prolonged the damping time.

The angle stability tests not only yielded an aesthetically appealing 3D shape but also highlighted that certain impact orientations exhibit markedly higher stability, as evidenced by holes and tunnels through the graph. Detailed analysis reveals that in the most stable configurations, the fillet's orientation results in a larger impact area, landing flat horizontally. This orientation distributes the impact force across a larger number of particles, thereby diminishing the stress within the bonds.

Upon deployment, the model demonstrated significant utility not only during the conceptual design phase but also in the detailing and visualisation stages. It provided critical insights into the performance metrics of the proposed solutions, thereby enabling a more substantiated and informed concept selection process and reducing the need for extensive and expensive, real-life testing. The preliminary visualisations were well-received by the customer, facilitating a comprehensive understanding of the concept's functionality and enabling informed feedback. Moreover, the small-scale real-life tests verified the feasibility of the tested sub-solutions and confirmed that the model represented chicken fillets with sufficient accuracy.

### 6.3.2 Limitations of this Study

Although this research gained valuable information about methods for modelling chicken fillets with DEM, several additional limitations of the model must be acknowledged. The model visually resembles a chicken fillet, but the particle representation induces considerable surface roughness.

In bulk form, this surface roughness can result in interlocking, which can make the bulk density unrealistically packed. While a reduction in sub-particle size can mitigate this issue, it introduces other stability challenges. Furthermore, the uniform stiffness of the fillets does not accurately represent the mechanical properties of the actual chicken fillets. Experts from Plukon have identified the tips of the modelled fillets as excessively flexible, whereas the thicker rear section was assessed as overly rigid.

Additionally, the sliding tests need to be redone in a better-controlled environment, as adhesion, which is intuitively very important for the sliding behaviour of the material, did not seem to influence it. The compression test results also require validation, as the Young's modulus value of chicken fillets that was calculated is roughly 10x lower than the value from the literature. Furthermore, these tests revealed an apparent viscoelastic material behaviour of chicken fillets that should be further investigated to better understand and predict this behaviour.

# Chapter 7

## Conclusions and Recommendations

### 7.1 Conclusions

Implementing automation in the food industry has always been a slow and challenging process due to food products' inherently complex and varying nature. The behaviour of items such as chicken fillets on machinery has always been difficult to predict, among others, due to the absence of knowledge and existing modelling techniques, hampering the process of automating. Because of this, the sector has thus far relied on extensive iterative testing for implementing new automatic solutions, which is costly and time-consuming.

This research constitutes a significant advancement within this domain. Using well-established technology from diverse sectors within the food industry and incorporating innovative yet straightforward ideas, three concept solutions were developed to automatically singulate and orient chicken fillets from bulk storage. This process traditionally requires manual pick-and-place actions.

The inherent complexity and variability of chicken fillets pose considerable challenges in evaluating the performance of conceptual solutions, thereby impeding informed decision-making. To mitigate this issue, this study adopted an innovative methodology, developing a chicken fillet model for the first time and achieving this within a practical timeframe. By concentrating on the fundamental characteristics of chicken fillets, namely their flexibility, shape, and damping, an adequate representation was attained within a few weeks.

Particle representations of chicken fillets of varying sizes were created using the discrete element method (DEM), surpassing previous research that modelled simple or relatively rigid items. By arranging multiple sub-particle types in the fillet shape, the flexibility of the chicken fillet meta-particle was significantly increased.

While there is not much research specifically on the properties of chicken fillets, a closely related value was found to speed up the model creation process for many model input parameters. Substituting these inputs, damping, bending and sliding tests were performed to configure the model's particle bonding stiffnesses and friction parameters by looking at the behaviour of real chicken fillets. Furthermore, sensitivity analyses were run to investigate the model's response to changes in scaling, bond stiffnesses, impact speed and angle. Finally, a compression test was performed on a sample to validate the Young's modulus input parameter and gain more insight into the material behaviour of chicken fillets.

With this fillet particle representation, a sub-particle with a radius of four millimetres was the optimal choice for the model. This configuration successfully balances the accuracy of the shape and the surface roughness of the meta-particle while ensuring sufficient model stability and a reasonable computational cost.

The various configuration tests demonstrated that the bond stiffness parameters substantially influence the stability and behaviour of the model. Reduced normal and shear stiffness values resulted in a more flexible model; however, instabilities occurred when normal stiffness was not adequately balanced by shear stiffness. Notably, these instabilities were not dependent on the simulation timestep, as even simulations with timesteps as small as 1e-10 seconds remained unstable. In contrast, when shear stiffness significantly exceeded normal stiffness, no instabilities occurred, and the only result was an increase in bond fractures. This underscores the necessity for equilibrium between the stiffness parameters. The requirement for balance was further underlined by the damping test, which indicated that when the stiffness parameters were imbalanced, the model exhibited unrealistic elasticity and required more time to dissipate energy post-impact.

When examining the sliding behaviour of the model, it was observed that the friction coefficient exhibited a linear influence on the sliding angle. Contrary to initial expectations, the interfacial surface energy representing adhesion did not affect this angle. However, despite real-life tests showing no significant difference between the sliding angles of dry and wet chicken fillets, the high uncertainty suggests that adhesion does play a part in sliding behaviour.

Furthermore, sensitivity analysis revealed that the stability of the model, indicated by the number of broken bonds, is significantly affected by parameters such as scaling, impact speed, and impact angle. Stiffness configurations that were initially stable can become entirely unstable under higher impact velocities. Compression testing demonstrated that chicken fillets exhibit complex non-elastic material behaviour. The accumulation of strain across different test runs and a reduction in measured force over time suggests a visco-elastic material behaviour.

The devised model demonstrated significant utility in executing concept evaluations. It successfully modelled the behaviour of chicken fillets and the interaction dynamics between the machinery and the product. Through these simulations, optimal subsolutions and complementary subsolutions were identified, culminating in a combined concept. This concept was subsequently refined and visualised with the assistance of the model, facilitating the configuration of belt speeds and dimensions.

Finally, empirical validation was achieved through two real-world experiments, which confirmed both the model and specific components of the conceptual solution. The experiments demonstrated an excellent resemblance in chicken fillet behaviour between the model and actual observations, substantiating its practical applicability.

## 7.2 Recommendations

To overcome the limitations of this research mentioned in Section 6.3.2, future research should focus on gathering knowledge about the behaviour and characteristics of chicken fillets to create a more secure base for the model input parameters. This research assumed the fillets to be fully isotropic, which, combined with the particle representation, resulted in the thick rear section of the fillets being too rigid and the tips being too flexible. Future research could create a more accurate model by establishing a non-isotropic model that separates the fillet into different stiffness sections. More research is also needed to understand the adhesion properties of chicken fillets. Additional sliding tests and a tensile adhesion test under differing moisture levels in a controlled environment could provide the insights needed. Moreover, the calculated Young's modulus did not correspond with the value from the literature, so this should be investigated further.

Ultimately, this thesis has developed a novel approach to automation. The methodology of this study should also be extended to other areas involving flexible products, not only within the food industry. This research has proven that it is possible to create a sufficiently accurate representation of a complex product like chicken fillets within a practical timeframe that can be used for concept evaluation. For example, processes that involve products like other types of meat, pasta, or wool could also be automated using this study's methods.

# Bibliography

- [1] A. Mottet and G. Tempio, "Global poultry production: current state and future outlook and challenges," *World's Poultry Science Journal*, vol. 73, no. 2, pp. 245–256, Jun. 2017, doi: <https://doi.org/10.1017/s0043933917000071>.
- [2] N. Alexandratos and J. Bruinsma, "World Agriculture Towards 2030/2050: The 2012 Revision," 2012.
- [3] R. 24/7 Staff, "World Robotics Report 2023 shows ongoing global growth in installations, finds IFR," *Robotics 24/7*, Sep. 26, 2023. [https://www.robotics247.com/article/world\\_robotics\\_report\\_2023\\_shows\\_ongoing\\_global\\_growth\\_installations\\_finds\\_ifr](https://www.robotics247.com/article/world_robotics_report_2023_shows_ongoing_global_growth_installations_finds_ifr).
- [4] DW.D.R. Daley, J.C. Wyvill, J.C. Thompson, W.D. Holcombe, G.V. McMurray, "Robotics and the poultry processing industry," in *Robotics in Meat, Fish and Poultry Processing*, K. Khodabandehloo, Ed. Boston, MA: Springer, 1993, pp. 48–69. doi: [https://doi.org/10.1007/978-1-4615-2129-7\\_3](https://doi.org/10.1007/978-1-4615-2129-7_3).
- [5] P.Y. Chua, T. Ilschner, and D.G. Caldwell, "Robotic manipulation of food products – a review," *Industrial Robot*, vol. 30, no. 4, pp. 345–354, 2003. doi: <https://doi.org/10.1108/01439910310479612>.
- [6] Lien, T.K. "Gripper Technologies for Food Industry Robots." *Robotics and Automation in the Food Industry*, 2013, pp. 143–170, doi: <https://doi.org/10.1533/9780857095763.1.143>.
- [7] Ross, S., et al. "A Review of Unilateral Grippers for Meat Industry Automation." *Trends in Food Science & Technology*, vol. 119, Jan. 2022, pp. 309–319, doi: <https://doi.org/10.1016/j.tifs.2021.12.017>.
- [8] S. Kaewkor et al., "Development of Pick and Place Delta Robot," in *The Impact of the 4th Industrial Revolution on Engineering Education*, 2020. doi: [https://doi.org/10.1007/978-3-030-40271-6\\_47](https://doi.org/10.1007/978-3-030-40271-6_47)
- [9] "RoboBatcher Flex Breast Fillets." <https://marel.com/en/products/robobatcher-flex-breast-fillets/>.
- [10] D.G. Caldwell, S. Davis, R.J. Moreno Masey, J.O. Gray, "Automation in Food Processing," in *Springer Handbook of Automation*, S. Nof, Ed. Berlin, Heidelberg: Springer, 2009, ch. 60, pp. 1041–1059. doi: [https://doi.org/10.1007/978-3-540-78831-7\\_60](https://doi.org/10.1007/978-3-540-78831-7_60).
- [11] "Portion Cutter PORTIO 1 - MARELEC." <https://www.marelec.com/industries/fish/portioning/portion-cutter-portio-1/>
- [12] Bader, Farah, and Shahin Rahimifard. "A Methodology for the Selection of Industrial Robots in Food Handling." *Innovative Food Science & Emerging Technologies*, vol. 64, 1 Aug. 2020, doi: <https://doi.org/10.1016/j.ifset.2020.102379>.
- [13] "Food Industry Struggles with Barriers to Automation," *Food Processing*, May 01, 2020. [Online]. Available: <https://www.foodprocessing.com/on-the-plant-floor/technology/article/11305668/food-industry-struggles-with-barriers-to-automation>.
- [14] M. Vink, "Chicken Fillet Processing: A review on advancements in poultry handling automation", 7, Aug. 12, 2024.
- [15] A. Massobrio, "What is Simulation-Driven Design? Main benefits explained," *Neural Concept*, Nov. 27, 2023. <https://www.neuralconcept.com/post/what-is-simulation-driven-design-main-benefits-explained>.
- [16] "SoftGrippers in Poultry Processing Factories: Improving Efficiency with High Speed Delta Robots - SoftGripping." *SoftGripping*, [Online] Available: [soft-gripping.com/discover/softgrippers-in-poultry-processing-factories-improving-efficiency-with-high-speed-delta-robots/](https://soft-gripping.com/discover/softgrippers-in-poultry-processing-factories-improving-efficiency-with-high-speed-delta-robots/). Accessed 22 Jan. 2024.

- [17] “Soft Robotics mGripAI Poultry (Chicken Breast) Automation,” [www.youtube.com. https://www.youtube.com/watch?v=uSGkCEjw5Io](https://www.youtube.com/watch?v=uSGkCEjw5Io) (accessed Feb. 12, 2024).
- [18] Koenig Group Baking Equipment. (2019, February 18). *Koenig & Dynatec @ Goman Jæren - Complete Hamburger and Hot Dog line* [Video]. YouTube. <https://www.youtube.com/watch?v=NrAalKGq7II>
- [19] Z. Guan, et al., “Flexible DEM model development and parameter calibration for Rape STEM,” *Applied Sciences*, vol. 12, no. 17, p. 8394, Aug. 2022, doi: <https://doi.org/10.3390/app12178394>.
- [20] M. W. Schramm and M. Z. Tekeste, “Wheat straw direct shear simulation using discrete element method of fibrous bonded model,” *Biosystems Engineering*, vol. 213, pp. 1–12, Jan. 2022, doi: <https://doi.org/10.1016/j.biosystemseng.2021.10.010>.
- [21] L. Zhong, et al., “A numerical study on gas-fluidized beds of wet flexible fibers,” *Powder Technology*, vol. 399, p. 117094, Feb. 2022, doi: <https://doi.org/10.1016/j.powtec.2021.117094>.
- [22] A. Patel et al., “Quantitative assessment and optimization of parallel contact model for flexible paddy straw: a definitive screening and central composite design approach using discrete element method,” *Scientific Reports*, vol. 14, no. 1, Jan. 2024, doi: <https://doi.org/10.1038/s41598-024-52388-7>.
- [23] C. Xu, et al., “Determination of characteristics and establishment of discrete element model for whole rice plant,” *Agronomy*, vol. 13, no. 8, p. 2098, Aug. 2023, doi: <https://doi.org/10.3390/agronomy13082098>.
- [24] X. Li et al., “A rapid prototyping method for crop models using the discrete element method,” *Computers and Electronics in Agriculture*, vol. 203, p. 107451, Dec. 2022, doi: <https://doi.org/10.1016/j.compag.2022.107451>.
- [25] H. Gilvari, D. J. W, and D. L. Schott, “Biomass pellet breakage: A numerical comparison between contact models,” 2019. <https://repository.tudelft.nl/islandora/object/uuid:f1f1c652-dfa4-45bc-bc9f-5fe4f41c3033?collection=research>.
- [26] A. Shafiei and F. Barthelat, “3D mechanics of scaled membranes,” *International Journal of Solids and Structures*, vol. 241, p. 111498, Apr. 2022, doi: <https://doi.org/10.1016/j.ijsolstr.2022.111498>.
- [27] L. Mathias, et al., “Packing simulation of thin flexible particles using a novel discrete element model,” *Computational Particle Mechanics*, vol. 9, no. 3, pp. 407–420, Jun. 2021, doi: <https://doi.org/10.1007/s40571-021-00419-9>.
- [28] P. A. Cundall and O. D. L. Strack, “A discrete numerical model for granular assemblies,” *Géotechnique*, vol. 29, no. 1, pp. 47–65, Mar. 1979, doi: <https://doi.org/10.1680/geot.1979.29.1.47>.
- [29] Hertz, H. (1882) On the Fixed Elastic Body Contact. *Journal für die reine und angewandte Mathematik (Crelles Journal)*, 92, 156-171. doi: <https://doi.org/10.1515/crll.1882.92.156>.
- [30] R. D. Mindlin, “Compliance of elastic bodies in contact,” *Journal of Applied Mechanics*, vol. 16, no. 3, pp. 259–268, Sep. 1949, doi: <https://doi.org/10.1115/1.4009973>.
- [31] R. D. Mindlin and H. Deresiewicz, “Elastic spheres in contact under varying oblique forces,” *Journal of Applied Mechanics*, vol. 20, no. 3, pp. 327–344, Sep. 1953, doi: <https://doi.org/10.1115/1.4010702>.
- [32] Y. Tsuji, T. Tanaka, and T. Ishida, “Lagrangian numerical simulation of plug flow of cohesionless particles in a horizontal pipe,” *Powder Technology*, vol. 71, no. 3, pp. 239–250, Sep. 1992, doi: [https://doi.org/10.1016/0032-5910\(92\)88030-l](https://doi.org/10.1016/0032-5910(92)88030-l).
- [33] G. Chen, G. Lodewijks, and D. L. Schott, “Numerical prediction on abrasive wear reduction of bulk solids handling equipment using bionic design,” *Particulate Science and Technology*, vol. 37, no. 8, pp. 964–973, Aug. 2018, doi: <https://doi.org/10.1080/02726351.2018.1480547>.
- [34] D. Schott, J. Mohajeri, J. Jovanova, S. Lommen, and W. De Kluijver, “Design framework for DEM-supported prototyping of grabs including full-scale validation,” *Journal of Terramechanics*, vol. 96, pp. 29–43, May 2021, doi: <https://doi.org/10.1016/j.jterra.2021.04.003>.

- [35] Altair. EDEM [Computer software], 2023. Available: <https://www.altair.com/edem/>
- [36] Sketchfab, “Chicken breast - Download Free 3D model by nhatminhletu195,” Sketchfab. <https://sketchfab.com/3d-models/chicken-breast-fd312cdeeac34a828b90345479d3b7f8>.
- [37] D. O. Potyondy and P. A. Cundall, “A bonded-particle model for rock,” *International Journal of Rock Mechanics and Mining Sciences*, vol. 41, no. 8, pp. 1329–1364, Dec. 2004, doi: <https://doi.org/10.1016/j.ijrmms.2004.09.011>.
- [38] C. Ko, A. Davies, and M. A. E. Auty, “Putting meat to the test: imaging and mechanical testing used to understand the properties of meat alternatives and how they mimic our typical meat sensory experience,” *Microscopy Today*, vol. 31, no. 2, pp. 21–25, Mar. 2023, doi: <https://doi.org/10.1093/mictod/qaad011>.
- [39] N. Jahanbakhshian, et al., “Measurement and prediction of the mechanical properties of a two-component food during freezing,” *International Journal of Food Properties*, vol. 20, no. sup3, pp. S3088–S3095, Dec. 2017, doi: <https://doi.org/10.1080/10942912.2016.1247856>.
- [40] H. Kosukegawa et al., “Friction of 316L stainless steel on soft-tissue-like poly(vinyl alcohol) hydrogel in physiological liquid,” *Tribology International*, vol. 82, pp. 407–414, Feb. 2015, doi: <https://doi.org/10.1016/j.triboint.2014.05.029>.
- [41] J. Silva, E. M. C. Da Silva, J. A. De Matos, L. O. De Alcântara, and B. W. S. De Souza, “The wettability of carrageenan-based edible coatings on chicken breasts,” *Ciência Agronômica/Revista Ciência Agronômica*, vol. 55, Jan. 2024, doi: <https://doi.org/10.5935/1806-6690.20240016>.
- [42] Design of Experiments | Altair HyperStudy. [Computer software], (n.d.). <https://altairone.com/Marketplace?queryText=hyperstudy&tab=Buy&app=HyperStudy>.
- [43] 3D CAD Design Software | SOLIDWORKS. [Computer software], (n.d.). <https://www.solidworks.com/>
- [44] “Multibody Simulation and Optimization | Altair MotionView,” [Computer software], <https://altair.com/motionsolve/motionview>.
- [45] Vierpool. (n.d.). *Sensoren relais besturingstechniek signaalconditionering Auto-ID input devices*. Vierpool. <https://www.vierpool.nl/>.

# Appendix A

## Scientific paper

# Advancing Poultry Processing Automation: Development of a Chicken Fillet DEM Model

Matthias Vink<sup>1</sup>, Dingena Schott<sup>1</sup>, Jovana Jovanova<sup>1</sup>, and Jan-Willem Kortlever<sup>2</sup>

<sup>1</sup>Department of Multi-Machine Engineering, Delft University of Technology

<sup>2</sup>Technisch Buro Kortlever B.V.

**Abstract**—The escalating global demand for poultry products, coupled with the challenges of labour shortages and harsh working conditions in processing plants, necessitates the automation of poultry processing. This paper presents the first development of a practice-orientated Discrete Element Method (DEM) model for simulating chicken fillets. The model’s primary objective is to be accurate enough to facilitate the evaluation of concepts and accelerate the design of automated solutions for handling chicken fillets. The research addresses the industry’s need for efficient and reliable automation by providing models and enabling simulation-aided design. The study’s findings validate the effectiveness of the DEM model in simulating fillet behaviour and its contribution to the design and optimisation of automated solutions. The developed model and methodology offer a valuable tool for advancing automation capabilities in the poultry industry.

**Keywords**—Automation, poultry, simulation, DEM

## I. INTRODUCTION

The global demand for poultry products is experiencing a substantial surge, driven by population growth and rapid development in many countries. The demand for poultry is projected to grow by over 120% in the coming decades [1], [2]. However, the poultry processing industry faces challenges in meeting this demand due to labour shortages and the demanding nature of manual tasks in processing plants. Cold operating temperatures and repetitive pick-and-place tasks contribute to harsh working conditions, making it increasingly difficult to find and retain personnel. The COVID-19 pandemic further exposed the vulnerabilities of this sector, with disease outbreaks leading to plant closures.

Although robotics has seen widespread adoption in various industries, the food industry is lagging behind, particularly in the automation of more complex operations involving products such as chicken fillets [3]. Many advances have already been made regarding packaging, shelf life extension and quality assessment, but the poultry products’ inherent variability and flexibility pose a significant challenge for automating the handling of raw products [4] [5] [6]. Chicken fillets require careful handling to avoid damage, and the high costs associated with the installation of new automated lines present additional barriers [7].

Much of the required automation technology is already in existence; however, due to the inherent properties mentioned above of chicken fillets, successful implementation remains challenging [8]. Furthermore, when automated solutions are

conceptualised, it is difficult to evaluate potential performance and predict the behaviour of chicken fillets in these systems due to the absence of knowledge and modelling methods of machine-chicken fillet interactions.

Simulation-aided design offers a promising approach to accelerate the development of solutions. Creating virtual environments to evaluate concepts and optimise designs can reduce the need for costly physical prototypes [9].

### A. Research Gap

The increasing demand for automation in the food industry highlights a technological void that demands urgent attention. Innovative solutions that are capable of handling the inherent flexibility of food products are required. Compared to other industries, this sector’s relatively slow development and implementation of automation can be partly attributed to the challenges of modelling irregular objects, such as chicken fillets, among others, due to the absence of knowledge of the engineering properties of fillets. As of now, existing research on flexible object modelling has either focused on simple beam-like objects or, when tackling more complex shapes, has yielded relatively rigid models. Additionally, no modelling methods for simulating chicken fillets and machine-fillet interactions exist. Moreover, developing an accurate model of a complex product such as chicken fillets is time-consuming, which makes it impractical to do during the design process.

This paper aims to bridge these research gaps by formulating a novel chicken fillet model within a feasible timeframe, focussing on achieving a sufficiently precise representation for concept performance assessments. This model can subsequently be utilised to facilitate simulation-aided design, thereby expediting the automation process within the industry.

## II. METHODS

### A. The discrete element method

The discrete element method (DEM) was chosen to simulate the behaviour of chicken fillets. DEM is a numerical method mainly used to analyse the behaviour of coal, soils and fibres, Equation (1) show the force equations of two colliding particles of the method [10] [11] [12] [13] [14]. Where  $E^*$  and  $G^*$  are the equivalent Youngs, shear moduli,  $R^*$  is the equivalent radius, and  $\delta_n$  and  $\delta_t$  are the normal and tangential particle overlap. These particle contacts also include damping terms, Equation (2) and (3) show how the damping forces are

calculated, here  $m^*$  is the equivalent mass,  $e$  is the coefficient of restitution and  $v^{rel}$  the relative particle velocity. DEM was selected for its ability to easily create and configure complex shapes, such as chicken fillets, and its ability to simulate bulk material behaviour [15] [16] [17]. This is important for many industrial processes that involve chicken fillets. The DEM software used in this study was Altair®*EDEM*<sup>TM</sup> [18].

$$F_n = \frac{4}{3}E^*\sqrt{R^*}\delta_n^{\frac{3}{2}} \quad \text{and} \quad F_t = -8G^*\sqrt{R^*}\delta_n\delta_t \quad (1)$$

$$F_n^d = -2\sqrt{\frac{5}{6}} \cdot \frac{-\ln(e)}{\sqrt{\ln^2(e) + \pi^2}} \cdot \sqrt{2mE^*\sqrt{R^*}\delta_n} \cdot \vec{v}_n^{rel} \quad (2)$$

$$F_t^d = -2\sqrt{\frac{5}{6}} \cdot \frac{-\ln(e)}{\sqrt{\ln^2(e) + \pi^2}} \cdot \sqrt{8mG^*\sqrt{R^*}\delta_n} \cdot \vec{v}_t^{rel} \quad (3)$$

### B. Generating a fillet shape in DEM

A key challenge was representing the irregular shapes and flexibility of the fillets since no literature was found with such a focus. An STL file of a chicken fillet was taken from the internet and modified into six different variants to represent the variety of chicken fillets, three sizes and their mirrored versions to represent left and right-sided fillets [19]. The dimensions of these size variants can be seen on Table I. An algorithm filled the mesh with sub-particles to form flexible meta-particles. A 4mm sub-particle radius was selected to balance shape accuracy, surface roughness, and computational cost. A modelled fillet can be seen next to a real chicken fillet in Figure 1.

TABLE I: The different sizes of the modeled fillets in mm

	Length	Width	Thickness
1	144	72	40
2	172	72	32
3	176	72	40

The bonded particle model (BPM) was used to connect the particles using a virtual contact radius [20]. Torque feedback in the bonds was disabled to enhance the flexibility of the meta-particle. When a bond is formed, the normal and shear forces on the particles are calculated by Equation (4). Where  $v_{n,t}$  are the normal and tangential velocities of the particle,  $S_{n,t}$  the bond stiffnesses,  $R_b$  the particle radius multiplied by the bonded disk scale and  $\delta_t$  the timestep. In particular, these equations do not include any damping terms, so another damping method was developed, as will be discussed in Section II-C. Consequently, the bonded disk scale was maintained at one since it merely scales the normal and shear stiffness values if torque feedback is off.

$$\delta F_n = v_n S_n \pi R_b^2 \delta_t \quad \text{and} \quad \delta F_t = v_t S_t \pi R_b^2 \delta_t \quad (4)$$

Sub-particles may detach from the meta-particle if the maximum bond strength is exceeded or if the bond is strained to a point where the contact radii no longer intersect. To keep the meta-particle together, the normal and shear bond strengths

were set at their maximum value (1e300 Pa). Moreover, multiple types of particles were utilised to augment the contact radius limit and improve flexibility.

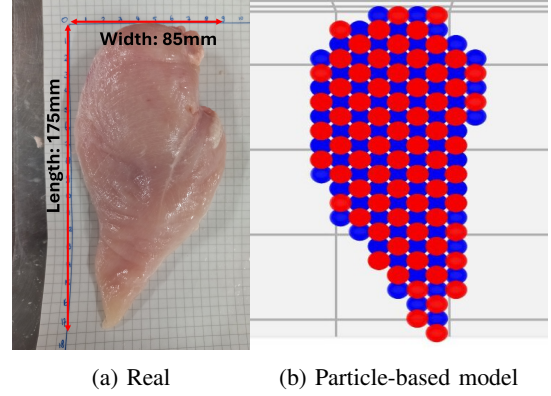


Fig. 1: A real chicken fillet (a) compared to a particle-based model (b)

The use of multiple particle types is essential, as merely increasing the contact radius would result in the formation of additional undesirable bonds. These additional diagonal bonds create a stiff truss structure which makes the meta-particle overly rigid, as can be seen in Figure 2. Furthermore, Figure 3 demonstrates that when two types are employed, and only the bonds between type red and type blue are defined, the maximum contact radius is increased to  $R\sqrt{3}$ .

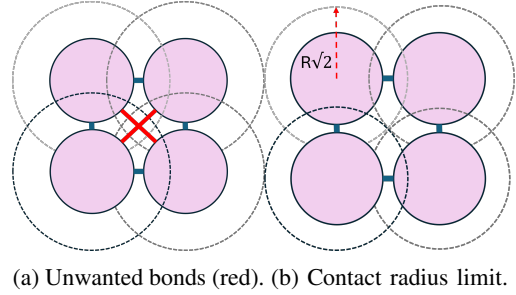


Fig. 2: Preventing undesired bonds from forming.

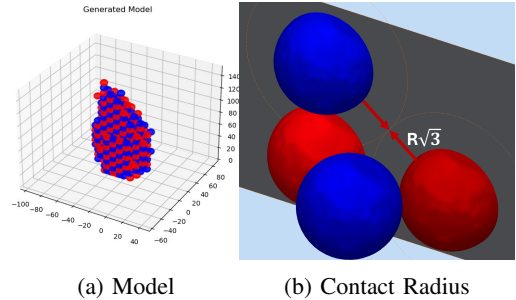


Fig. 3: 2 particle types showing the increase in contact radius.

### C. Configuring the model input parameters

The model parameters were derived from literature, controlled experiments, and iterative simulations for calibration

purposes. Due to the absence of existing knowledge on many of the input parameters required for the model, the best available alternatives were used.

Ko et al. established that the Young’s modulus of chicken breast tissue is approximately 0.37 MPa [21]. The Poisson’s ratio was adopted from the findings of Jahanbakhshian et al., who investigated the Poisson’s ratio of chicken nugget crumbs across varying temperatures. Considering that chicken nuggets partially comprise chicken fillet, their value of 0.37 at 7 degrees Celsius, which aligns with factory conditions, was employed [22]. Furthermore, the inherent stickiness of the chicken fillets was incorporated into the model using the Hertz-Mindlin contact model with JKRv2. Although the precise interfacial surface energy of chicken fillets remains undetermined, Silva et al. quantified the critical surface tension of chicken breasts to be 54.56 mN/m [23]. This measurement serves as a reasonable approximation for the purpose of this model. Given that fillets predominantly exhibit sliding rather than rolling behaviour, a rolling friction model was omitted, and the coefficients of restitution were minimised to simulate the substantial damping behaviour of fillets.

A compression test was performed on a 35x35x10mm block cut from a chicken fillet. The block was compressed and relaxed to a maximum force of 5N in three identical subsequent runs to validate the Young’s modulus of the literature and to provide insight into the material behaviour of the chicken fillet. The Hertz-Mindlin contact model assumes linear-elastic behaviour when calculating particle interactions. Therefore, the Young’s modulus was calculated from the linear section of the stress-strain curve obtained by the compression test with  $E = \frac{F \cdot L}{A \cdot \Delta L}$ .

Furthermore, several experiments were conducted to determine the coefficient of sliding friction between fillets and steel and configure particle bond stiffnesses. The bending of an actual chicken fillet rolling off a conveyor was compared with the bend of a modelled fillet to determine the values of the bond stiffness parameters that ensure a sufficient degree of flexibility (Figure 4). The stiffness values of the bond also significantly influenced the damping effects and model stability; therefore, those interrelations were also investigated because actual chicken fillets exhibit significant damping on impact.

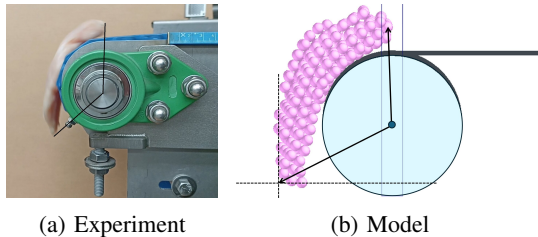


Fig. 4: The real-life bend experiment (a), compared with the model bend (b).

The coefficient of friction was determined by the sliding test, in which a metal plate was inclined until the fillet began

to slide, at which point the angle was observed (Figure 5). The sliding test was carried out with dry and wet chicken fillets to determine the influence of adhesion on the sliding angle.

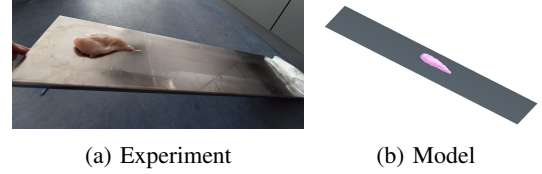


Fig. 5: The real-life sliding test (a), compared with the models sliding behaviour (b).

Several sensitivity analyses were performed, dropping fillets onto a horizontal surface to evaluate model stability under varying impact speeds and angles of impact. These tests determine the limits of the model and provide insights into how different parameters influence its behaviour and characteristics.

The simulations were run on an average laptop with an NVIDIA RTX 3070 Ti GPU and 12th generation Intel i7 CPU.

### III. RESULTS

#### A. Model configuration

The results of the compression experiments are delineated in Figure 6. The sample exhibited significant plastic deformation, evident by the initial compression of runs 2 and 3. Furthermore, successive runs required a more substantial strain of the sample before reaching identical stress levels, and once a particular strain was applied, the measured force decreased over time. The Young’s modulus, calculated from the initial run, yielded a value of 48.4 kPa.

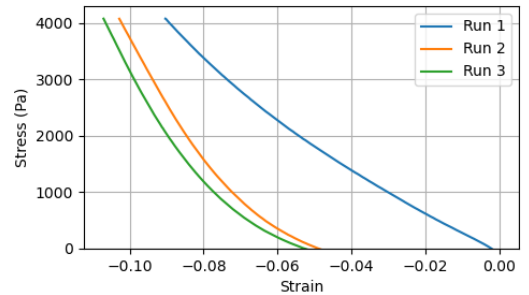


Fig. 6: The stress-strain curves resulting from the compression test.

The outcomes of the bending test are presented in Figure 7a. As anticipated, reduced stiffness values lead to greater bend angles; however, very low values are required to achieve an angle of more than 120 degrees, as measured in the real fillet. Interestingly, a high normal stiffness in relation to shear stiffness induces instabilities, which is also apparent in Figure 7b. Interestingly, this instability was not a function of the simulation timestep, occurring even at a timestep of 1e-10s. Moreover, when the shear stiffness is high in relation to the normal stiffness, these instabilities do not occur.

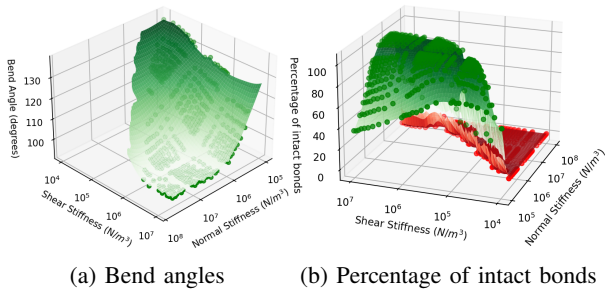


Fig. 7: The bend angles (a) and stability (b) of the model for different stiffness combinations.

The bond stiffness configuration also significantly affects the damping behaviour of the model, as is evident from Figure 8. The graphs reveal that low and balanced stiffness values result in the most damping. An unbalanced stiffness configuration can take up to five times as long to dampen 99% of the total energy, as is evident from the distinct valley shape in Figure 8b.

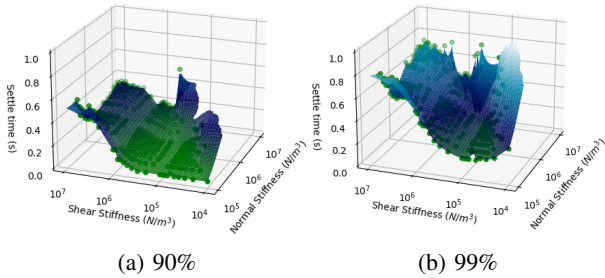


Fig. 8: The time it takes to dampen 90% (a) and 99% (b) of the total energy under different stiffness configurations.

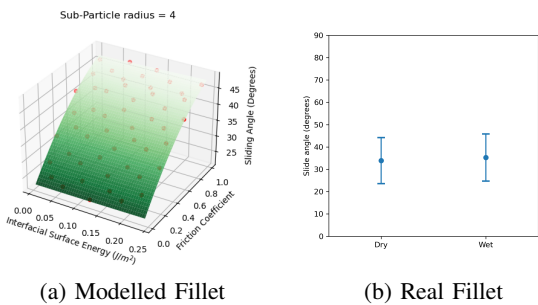


Fig. 9: The sliding angle of the fillet model (a) and the result of the real-life sliding experiment (b).

Figure 9 shows the outcomes of the sliding experiments. The coefficient of friction exhibits a linear relationship with the sliding angle in the simulations. However, unexpectedly, the interfacial surface energy in the JKRv2 model does not exert any influence on the angle in these results. Figure 9b illustrates the results of the empirical slide tests; immersion of the fillet in water prior to testing did not influence the angle, also suggesting that adhesion does not affect the sliding behaviour. However, the error bars in the plot indicate substantial

uncertainty in the angle measurements, indicating the angle is also not purely dependent on regular friction. When comparing the model data with the experimental data, a friction coefficient of 0.5 for the model yields comparable sliding angles.

### B. Model sensitivity analyses

Figure 10 demonstrates that the robustness of the model is significantly influenced by the angle of impact. The impact orientation of the fillet is also shown at several points along the axes. As expected, when the fillet impacts upon fewer particles, more bonds break as higher bond stress results in too much strain on the bonds, causing them to break due to particle separation.

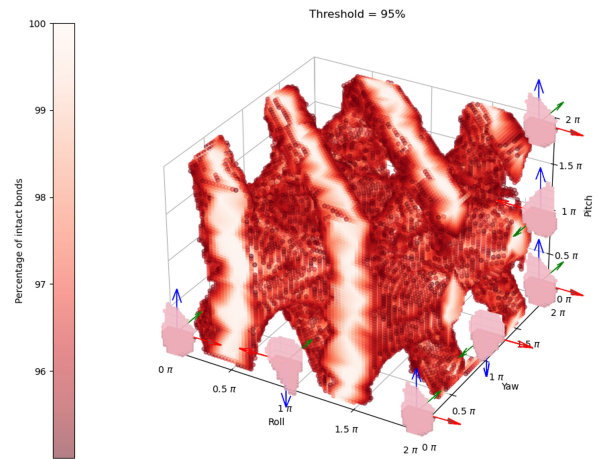


Fig. 10: All impact angles for which more than 95% of bonds remained intact.

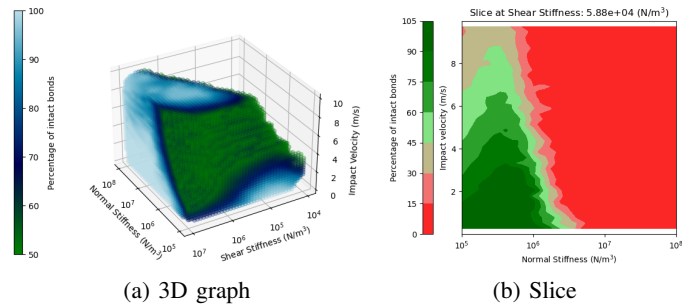


Fig. 11: The stability of the model for different stiffness combinations under different impact velocities. The 3D graph contains all points for which 50% or more bonds remained intact.

The velocity of the impact of the fillet also affects the stability of the model, as indicated in Figure 11. Moreover, Figure 11b reveals that stiffness configurations that were initially stable can become unstable with higher impact velocities.

### C. Validating the model by comparing with an experiment

To validate that the refined DEM model adequately represented chicken fillets, a real-world experiment was carried

out with a small bulk storage of fillets. The front of the bulk box has an adjustable opening from which the conveyor belt pulls the fillets. During the experiment, the bulk storage was filled with chicken fillets, the conveyor belt underneath was subsequently turned on, and the flow of fillets was observed. The opening height was adjusted multiple times during the experiment to observe changes in flow. Figure 12 delineates the experimental setup.



Fig. 12: The bulk experiment test setup, the height of the opening near the conveyor is adjustable.

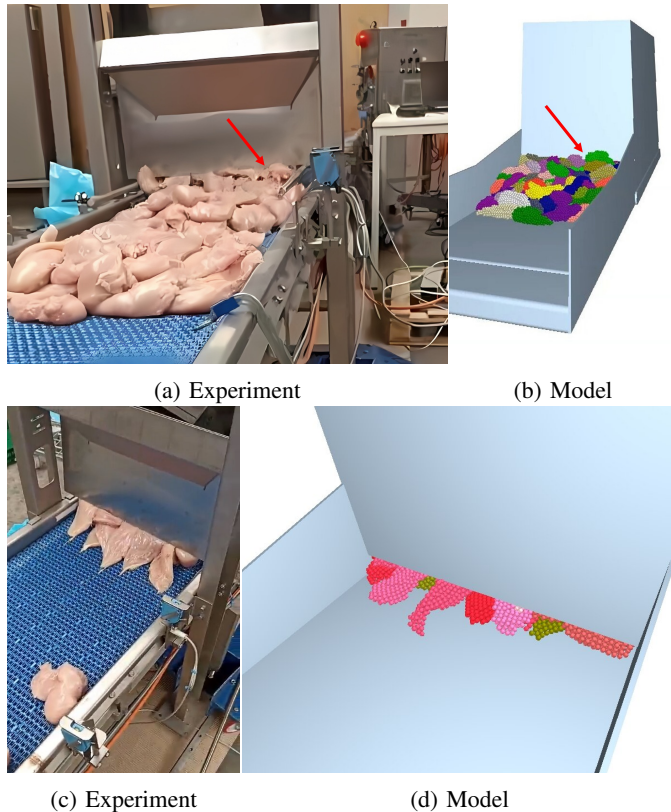


Fig. 13: Very similar behaviour can be observed comparing the bulk experiment with chicken fillets (a and c) compared to the same DEM setup (b and d).

As illustrated in both Figure 13b and Figure 13a, both the real and modelled fillets exhibit curling behaviour upon exiting the hopper, attributed to their intrinsic flexibility, thereby validating the model's representation of the actual fillet dynamics.

Introducing a nominal amount of water to the bulk resulted in a loss of traction from the conveyor, particularly when the opening of the bulk box was small, as seen in Figure 13c and 13d. Simulating this bulk test with 450 fillets, which is over 160k particles for 15 seconds, took about an hour, which is relatively fast for a DEM simulation.

#### IV. DISCUSSION

During the configuration of the model, compounding plastic strain in the compression tests on a small sample of chicken fillet suggests that chicken fillet exhibits visco-elastic material behaviour. The observation that the measured force decreases over time after applying strain also supports this assessment, as visco-elastic materials need time to deform, which relaxes the stress in the sample. More research is needed to investigate the material properties of chicken fillets and how to model them. More research is also required to verify the Young's modulus of chicken fillets, as the value found in the compression test is roughly 10x lower than the value from the literature.

Furthermore, the bending tests demonstrated that reduced stiffness values led to reduced bending angles, indicative of increased rigidity, with both normal and shear stiffness exerting equal influence on the bending angle. It was necessary to adopt lower stiffness values to achieve a substantial bending angle of over 120 degrees, which mimics the behaviour of real fillets. Additionally, a relatively high normal bond stiffness in comparison to normal stiffness rendered the model unstable, culminating in the disintegration of the meta-particles. Notably, this instability was not attributable to a large simulation timestep, as it manifested even at a timestep of  $1e-10$ s. When shear stiffness surpassed normal stiffness, it did not result in complete instability but only in a greater number of fractured bonds than when the stiffnesses were balanced. This requisite for equilibrium was unexpected, as an increase in stiffness would intuitively suggest that the model would become stiffer and, hence, more stable, which was not observed. The model's stability was maximised when there was equilibrium in both types of particle bond stiffness.

Moreover, as the damping tests revealed, maintaining an equal balance of low normal and shear stiffness is also crucial for optimal damping in this setup. A meta-particle with an unbalanced bond stiffness combination can require up to 10 times more time to dampen 99% of its energy after impacting a surface. The damping tests also proved that it is possible to achieve sufficient damping without damping terms in the bonds or introducing global damping in the simulation, as is often done in other research considering flexible DEM models [24]. In summary, stability, damping, and bend angle are the three primary considerations influencing the choice of bond stiffness parameters to create a representative DEM model of chicken fillets.

The sliding tests demonstrated that the coefficient of friction in the model influences the sliding angle linearly, while the interfacial surface energy and the sub-particle size did not have a significant effect. The slide test involving real fillets supports this observation, as the sliding angle of the wet fillets was not

significantly different from the dry fillets. This suggests that the sliding behaviour of chicken fillets is primarily controlled by the coefficient of friction and less so by the adhesion forces. However, the results of the real-world slide test showed a high uncertainty, which is not indicative of pure frictional sliding. In addition, introducing water to the bulk of the fillets significantly influenced the flow in the bulk experiment, as it caused the conveyor belt to slip. Thus, more research is needed to fully understand the adhesive behaviour of chicken fillets and to create modelling methods for this.

Furthermore, angle stability tests highlighted that specific impact orientations exhibit markedly higher stability, as evidenced by holes and tunnels through the graph. In the most stable configurations, the fillet's orientation results in a larger impact area, often positioned horizontally. This orientation distributes the impact force across a larger number of particles, thereby diminishing the stress within the bonds.

The impact speed sensitivity analysis also clearly shows the region of unstable stiffness combinations seen in the bending and damping tests. Additionally, the test reveals that more significant disturbances to the model can cause initially stable stiffness combinations to become unstable.

Although this research gained valuable information about methods for modelling chicken fillets with DEM, several additional limitations must be acknowledged. Although the model visually resembles a chicken fillet, the particle representation causes considerable surface roughness. This surface roughness can result in interlocking in bulk form, making the bulk density unrealistically packed. While reducing sub-particle size can mitigate this issue, it introduces other stability challenges. Furthermore, the uniform, homogenous stiffness of the fillets does not accurately represent the mechanical properties of the actual chicken fillets. The tips of the modelled fillets are excessively flexible, whereas the thicker rear section is overly rigid. Moreover, the size range of the different model variants is quite limited, as, in reality, even smaller and bigger chicken fillets exist. The results from the compression test also need validation, as the Young's calculated modulus value of chicken fillets is roughly 10 times lower than the value from the literature.

## V. CONCLUSION

The development of a practice-oriented chicken fillet DEM model successfully addresses the challenges of modelling flexible and complex food products. The research identified workable parameters and configurations for accurate representation in DEM simulations. This research contributes to the automation efforts in the food industry by offering a validated and practical modelling approach for handling highly flexible food products. Furthermore, the advancements in DEM modelling for chicken fillets have practical implications for the poultry processing industry, as it is the first time such a complex, flexible product has been simulated in DEM. The deployment of this model can help address the urgent need for innovative automation solutions within the poultry processing industry. By providing insights into the behaviour of chicken

fillets in potential concept solutions, thereby reducing the need for costly prototypes and speeding up the design process. The relatively short computational duration of the model on standard hardware further underscores its utility for use in the design process, as it is capable of simulating an entire automated system within a computational timeframe of merely one day.

This study demonstrates the feasibility of constructing a DEM model for a complex product with limited prior knowledge of the input parameters. This approach emphasises achieving a sufficient representation in favour of a perfect model to accelerate its development, thereby rendering it practicable to establish a model concurrently with the design process. This methodology should be used in additional areas and processes within the food industry to enhance automation in the entire sector.

To improve the model, future research should focus on improving the model's stability, as some sub-particles break off from the fillets during simulations. This could be achieved by introducing additional particle types or modifying the bond radius after the bonds have been formed. Moreover, the cause of the unstable region of stiffness combinations should be investigated. The sliding behaviour and adhesion of chicken fillets, both in simulations and in real-life scenarios, should also be further explored. Factors such as temperature, humidity, and surface texture could be examined to gain a more comprehensive understanding of this behaviour. Additionally, ways to better represent the heterogeneous stiffness of chicken fillets should be investigated to represent the flexible nature of chicken fillets more accurately. Furthermore, the influence of other model input parameters on the model's stiffness, damping and stability could be investigated to further refine the chicken fillet model.

## ACKNOWLEDGEMENTS

The author thanks Hao Shi from the Machines and Materials Interactions research group, Bart Oelen from Plukon Food Group and Jonathan Kortlever from Technisch Bureau Kortlever for their valuable insights and fruitful discussions. The author also thanks the employees of the Applied Labs at TU Delft for facilitating the compression test. An additional thanks to Plukon for providing the chicken fillets used in the bulk experiments.

## REFERENCES

- [1] A. Mottet and G. Tempio, "Global poultry production: current state and future outlook and challenges," *World's Poultry Science Journal*, vol. 73, no. 2, pp. 245–256, Jun. 2017, doi: <https://doi.org/10.1017/s0043933917000071>.
- [2] N. Alexandratos and J. Bruinsma, "World Agriculture Towards 2030/2050: The 2012 Revision," 2012.
- [3] R. 24/7 Staff, "World Robotics Report 2023 shows ongoing global growth in installations, finds IFR," *Robotics 24/7*, Sep. 26, 2023. [https://www.robotics247.com/article/world\\_robotics\\_report\\_2023\\_shows\\_ongoing\\_global\\_growth\\_installations\\_finds\\_ifr](https://www.robotics247.com/article/world_robotics_report_2023_shows_ongoing_global_growth_installations_finds_ifr).
- [4] S. Peng et al., "Characterization of carvacrol incorporated antimicrobial film based on agar/konjac glucomannan and its application in chicken preservation," *Journal of Food Engineering*, vol. 330, p. 111091, Apr. 2022, doi: <https://doi.org/10.1016/j.jfoodeng.2022.111091>.
- [5] S. A. Bhoir, M. Jhaveri, and S. P. Chawla, "Evaluation and predictive modeling of the effect of chitosan and gamma irradiation on quality of stored chilled chicken meat," *Journal of Food Process Engineering*, vol. 42, no. 7, Sep. 2019, doi: <https://doi.org/10.1111/jfpe.13254>.
- [6] Y. Yang et al., "Evaluation of broiler breast fillets with the woody breast condition using expressible fluid measurement combined with deep learning algorithm," *Journal of Food Engineering*, vol. 288, p. 110133, May 2020, doi: <https://doi.org/10.1016/j.jfoodeng.2020.110133>.
- [7] "Food Industry Struggles with Barriers to Automation," *Food Processing*, May 01, 2020. [Online]. Available: <https://www.foodprocessing.com/on-the-plant-floor/technology/article/11305668/food-industry-struggles-with-barriers-to-automation>.
- [8] M. Vink, "Chicken Fillet Processing: A review on advancements in poultry handling automation", 7, Aug. 12, 2024.
- [9] A. Massobrio, "What is Simulation-Driven Design? Main benefits explained," *Neural Concept*, Nov. 27, 2023. <https://www.neuralconcept.com/post/what-is-simulation-driven-design-main-benefits-explained>.
- [10] P. A. Cundall and O. D. L. Strack, "A discrete numerical model for granular assemblies," *Géotechnique*, vol. 29, no. 1, pp. 47–65, Mar. 1979, doi: <https://doi.org/10.1680/geot.1979.29.1.47>.
- [11] Hertz, H. (1882) On the Fixed Elastic Body Contact. *Journal für die reine und angewandte Mathematik (Crelles Journal)*, 92, 156-171. doi: <https://doi.org/10.1515/crll.1882.92.156>.
- [12] R. D. Mindlin, "Compliance of elastic bodies in contact," *Journal of Applied Mechanics*, vol. 16, no. 3, pp. 259–268, Sep. 1949, doi: <https://doi.org/10.1115/1.4009973>.
- [13] R. D. Mindlin and H. Deresiewicz, "Elastic spheres in contact under varying oblique forces," *Journal of Applied Mechanics*, vol. 20, no. 3, pp. 327–344, Sep. 1953, doi: <https://doi.org/10.1115/1.4010702>.
- [14] Y. Tsuji, T. Tanaka, and T. Ishida, "Lagrangian numerical simulation of plug flow of cohesionless particles in a horizontal pipe," *Powder Technology*, vol. 71, no. 3, pp. 239–250, Sep. 1992, doi: [https://doi.org/10.1016/0032-5910\(92\)88030-1](https://doi.org/10.1016/0032-5910(92)88030-1).
- [15] C. Xu, F. Xu, H. Tang, and J. Wang, "Determination of characteristics and establishment of discrete element model for whole rice plant," *Agronomy*, vol. 13, no. 8, p. 2098, Aug. 2023, doi: <https://doi.org/10.3390/agronomy13082098>.
- [16] G. Chen, G. Lodewijks, and D. L. Schott, "Numerical prediction on abrasive wear reduction of bulk solids handling equipment using bionic design," *Particulate Science and Technology*, vol. 37, no. 8, pp. 964–973, Aug. 2018, doi: <https://doi.org/10.1080/02726351.2018.1480547>.
- [17] D. Schott, J. Mohajeri, J. Jovanova, S. Lommen, and W. De Kluijver, "Design framework for DEM-supported prototyping of grabs including full-scale validation," *Journal of Terramechanics*, vol. 96, pp. 29–43, May 2021, doi: <https://doi.org/10.1016/j.jterra.2021.04.003>.
- [18] Altair. EDEM [Computer software], 2023. Available: <https://www.altair.com/edem/>
- [19] Sketchfab, "Chicken breast - Download Free 3D model by nhatminhletu195," Sketchfab. <https://sketchfab.com/3d-models/chicken-breast-fd312cdeeac34a828b90345479d3b7f8>.
- [20] D. O. Potyondy and P. A. Cundall, "A bonded-particle model for rock," *International Journal of Rock Mechanics and Mining Sciences*, vol. 41, no. 8, pp. 1329–1364, Dec. 2004, doi: <https://doi.org/10.1016/j.ijrmm.2004.09.011>.
- [21] C. Ko, A. Davies, and M. A. E. Auty, "Putting meat to the test: imaging and mechanical testing used to understand the properties of meat alternatives and how they mimic our typical meat sensory experience," *Microscopy Today*, vol. 31, no. 2, pp. 21–25, Mar. 2023, doi: <https://doi.org/10.1093/mictod/qaad011>.
- [22] N. Jahanbakhshian, et al., "Measurement and prediction of the mechanical properties of a two-component food during freezing," *International Journal of Food Properties*, vol. 20, no. sup3, pp. S3088–S3095, Dec. 2017, doi: <https://doi.org/10.1080/10942912.2016.1247856>.
- [23] J. Silva, E. M. C. Da Silva, J. A. De Matos, L. O. De Alcântara, and B. W. S. De Souza, "The wettability of carrageenan-based edible coatings on chicken breasts," *Ciência Agronômica/Revista Ciência Agronômica*, vol. 55, Jan. 2024, doi: <https://doi.org/10.5935/1806-6690.20240016>.
- [24] M. Schramm and M. Z. Tekeste, "Wheat straw direct shear simulation using discrete element method of fibrous bonded model," *Biosystems Engineering*, vol. 213, pp. 1–12, Nov. 2021, doi: <https://doi.org/10.1016/j.biosystemseng.2021.10.010>.

# Appendix B

## Model Parameters

### B.1 Model Testing Parameters

Table B.1: The EDEM input parameters used in this study, these are used unless mentioned otherwise.

<b>Bulk Material:</b>		
Poisson's ratio	0.37	-
Density	940	$kg/m^3$
Young's modulus	3.7e5	$Pa$
<b>Interactions</b>		
	<b>Fillets</b>	<b>Fillets</b>
Restitution	0.0001	-
Static Friction	0.1	-
<b>Interactions</b>		
	<b>Fillets</b>	<b>Equipment</b>
Restitution	0.0001	-
Static Friction	0.5	-
<b>BondingV2</b>		
Normal stiffness	1e6	$N/m^3$
Tangential stiffness	60000	$N/m^3$
Contact radius	6.928 ( $4\sqrt{3}$ )	$mm$
Normal strength	1e300	$Pa$
Shear strength	1e300	$Pa$
<b>JKRV2</b>		
	Interfacial surface energy	
Fillets - Fillets	0.055	$J/m^2$
Fillets - Equipment	0.055	$J/m^2$
<b>Simulator settings</b>		
Raleigh timestep	15	%
GPU solver precision	Hybrid	-

# Appendix C

## Design of experiments testmatrixes

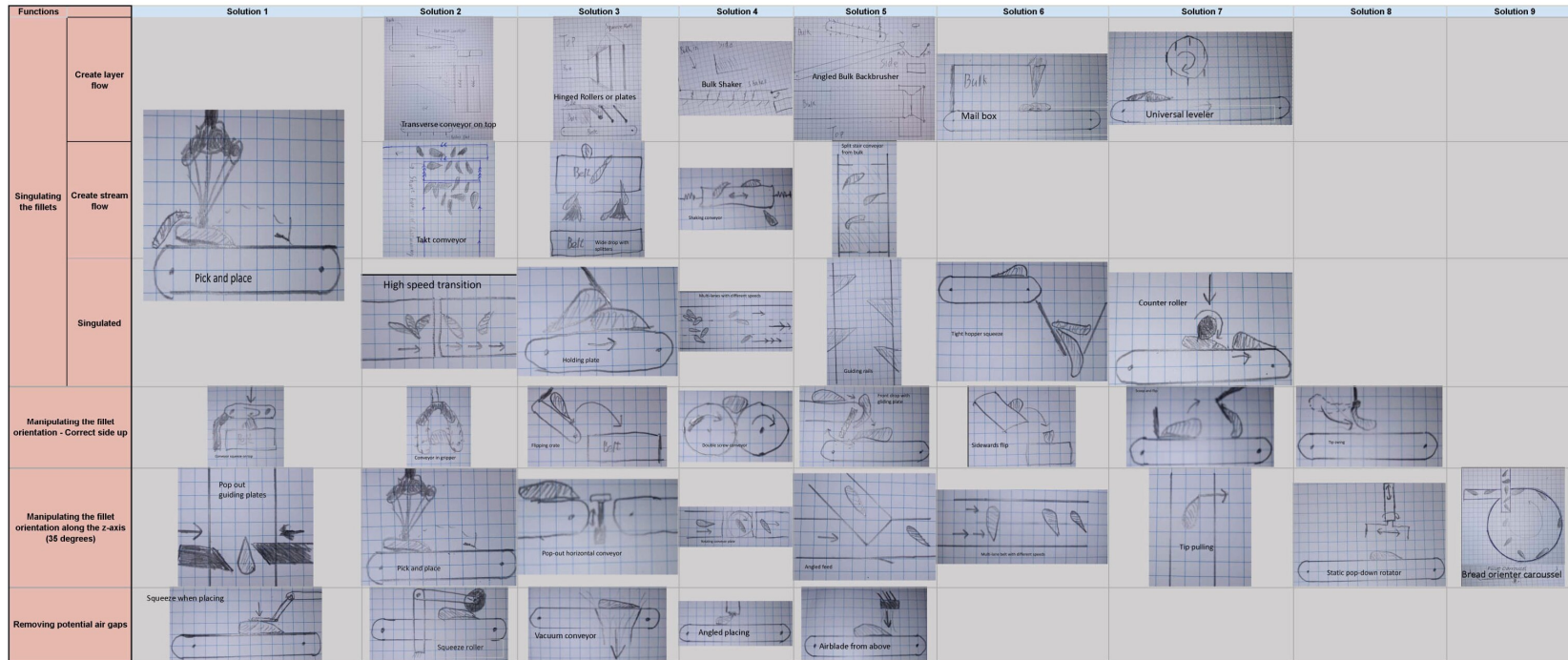
### C.1 Stiffness variations

Table C.1: The stiffness levels used in the design of experiments

Tangential stiffness	Normal stiffness
1.00E+04	1.00E+05
2.00E+04	2.00E+05
3.00E+04	3.00E+05
4.00E+04	4.00E+05
5.00E+04	5.00E+05
6.00E+04	6.00E+05
7.00E+04	7.00E+05
8.00E+04	8.00E+05
9.00E+04	9.00E+05
1.00E+05	1.00E+06
2.00E+05	2.00E+06
3.00E+05	3.00E+06
4.00E+05	4.00E+06
5.00E+05	5.00E+06
6.00E+05	6.00E+06
7.00E+05	7.00E+06
8.00E+05	8.00E+06
9.00E+05	9.00E+06
1.00E+06	1.00E+07
2.00E+06	2.00E+07
3.00E+06	3.00E+07
4.00E+06	4.00E+07
5.00E+06	5.00E+07
6.00E+06	6.00E+07
7.00E+06	7.00E+07
8.00E+06	8.00E+07
9.00E+06	9.00E+07
1.00E+07	1.00E+08

# Appendix D

## Morphological Chart



(a)

Figure D.1: The morphological chart used in the design process.

# D.1 Existing Technology Filter

Functions		Solution 1	Solution 2	Solution 3	Solution 4	Solution 5	Solution 6	Solution 7	Solution 8
Singulating the fillets	Create layer flow							Universal leveler	
	Create stream flow		Transverse conveyor on top Takt conveyor	Hinged rollers or plates	Bulk Shaker	Angled Bulk Backbrusher	Mail box		
	Singulated	Pick and place	High speed transition	Holding plate	Mail boxes with different speeds	Soft rear conveyor from bulk Guiding rails	High speed separator	Counter roller	Bread orienter carousel
Manipulating the fillet orientation - Correct side up						Feed stop with sliding plate	Sideways flip		
Manipulating the fillet orientation along the z-axis (35 degrees)		Pop out guiding plates	Pick and place	Pop-out horizontal conveyor	Horizontal plate	Angled feed	Mail box with different speeds	Tip pushing	Static pop-down rotator
Removing potential air gaps		Squeeze when placing	Squeeze roller	Vacuum conveyor	Angled placing	Airblade from above			

(a)

Figure D.2: All the existing technologies.

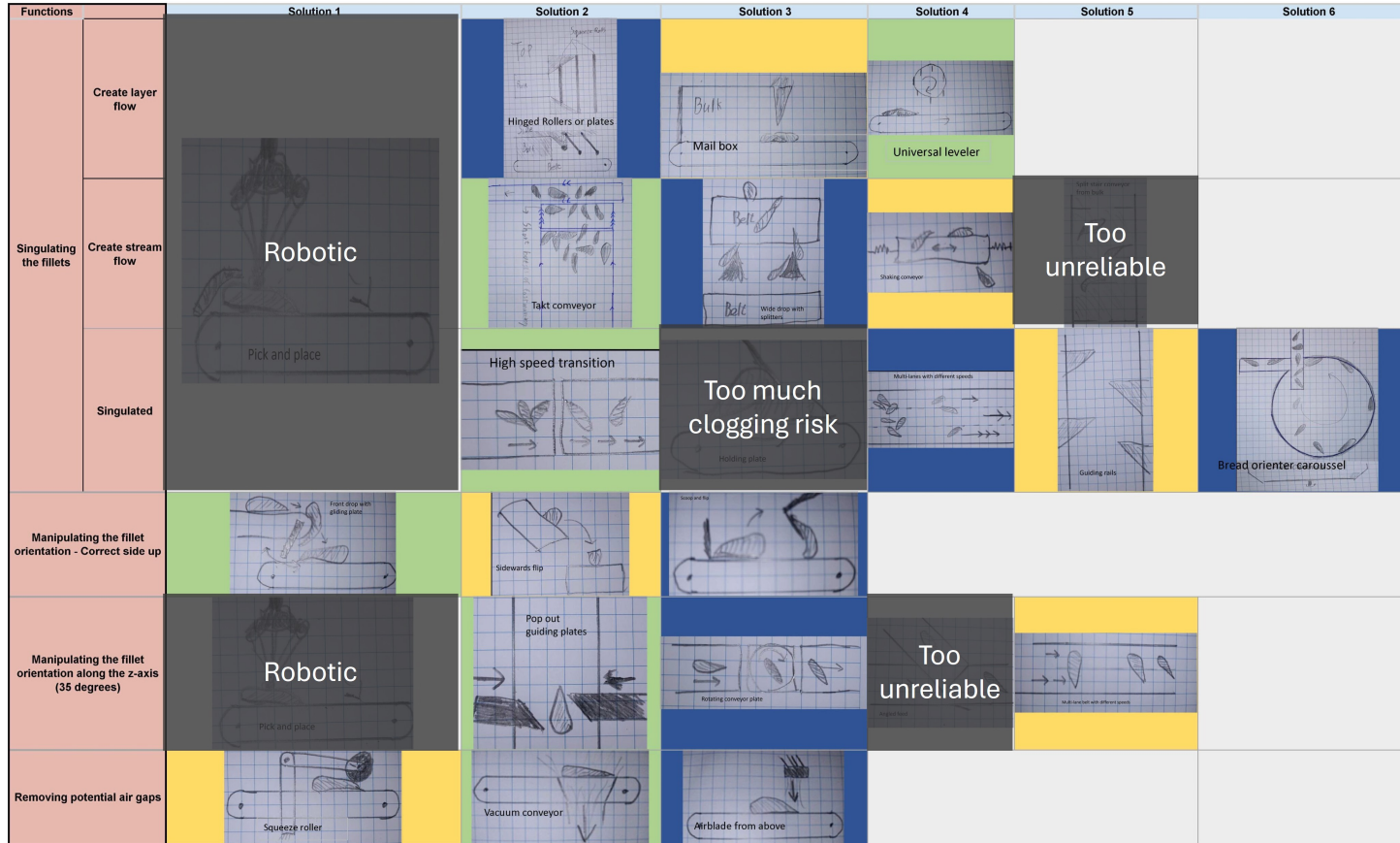
## D.2 Simple Solutions Filter

Functions		Solution 1	Solution 2	Solution 3	Solution 4	Solution 5	Solution 6	Solution 7	Solution 8
Singularizing the fillets	Create layer flow			Hinged rollers or plates	Bulk Shaker	Angled Bulk Backbrusher	Mail box	Universal leveler	
	Create stream flow		Transverse conveyor on top	Belt	Slating conveyor	Soft rear conveyor from bulk			
	Singularized	Pick and place	Tight conveyor	While enter with rollers					
Manipulating the fillet orientation - Correct side up			High speed transition	Holding plate	Wall runs with different speeds	Guiding rolls	High speed separator	Counter roller	Bread orienter carousel
	Manipulating the fillet orientation along the z-axis (35 degrees)	Pop out guiding plates	Pop out separator	Pop out horizontal conveyor				Tip pushing	Static pop down rotator
Removing potential air gaps	Squeeze when placing	Squeeze roller	Vacuum conveyor	Angled placing	Airblade from above				

(a)

Figure D.3: Some additional simple solutions.

### D.3 Chosen Concepts



(a)

Figure D.4: The three concepts highlighted on the reduced morphological chart.